Nitrogen Isotopes in the Global Ocean

Dissertation

in fulfillment of the requirements for the degree "Dr. rer. nat."

of the Faculty of Mathematics and Natural Sciences

at Kiel University

submitted by

Christopher J. Somes

Kiel, 2013

First referee:	Prof. Dr. Andreas Oschlies
Second referee:	Prof. Dr. Ralph Schneider
Date of the oral examination:	22 August 2012
Approved for publication:	22 August 2012

Signed: Prof. Dr. Wolfgang J. Duschl, Dean

Contents

Zusammenfassung

Stickstoff ist ein essentieller Nährstoff für Lebewesen. Seine geringe Abundanz in großen Teilen des euphotischen Ozeans limitiert das Wachstum von Primärproduzenten, die die Basis der Ökosysteme des Ozeans sind. Wenn Phytoplankton wächst, konsumiert es CO_2, das im Meerwasser gelöst ist. Dies beeinflusst den Partialdruck von CO_2 im Oberflächenwasser und damit den Gasaustasuch mit der Atmosphäre, wo es das Erdklima beeinflusst. Da das Gleichgewicht des bioverfügbaren Stickstoffreservoirs durch die wichtigsten Quellen und Senken, N_2-Fixierung und Denitrifizierung, kontrolliert wird und diese wiederum sensitiv gegenüber Klimabedingungen sind, erzeugen sie im Klimawandel möglicherweise eine wichtige Rückkopplung auf die atmosphärische CO_2-Konzentration. N_2-Fixierung und Denitrifizierung beeinflussen das Verhältnis der stabilen Stickstoffisotope $\delta^{15}N$, wodurch das Isotopenverhältnis ein nützlicher Tracer ist, der hilft die Verteilung und Raten von N_2-Fixierung und Denitrifizierung zu bestimmen. Diese Dissertation konzentriert sich auf die Verwendung des $\delta^{15}N$ Tracers, um wichtige Prozesse des N-Kreislaufes im Ozean besser zu verstehen und zu quantifizieren.

Der erste Teil dieser Dissertation beschäftigt sich mit der Modellentwicklung der zwei stabilen Stickstoffisotope ^{14}N and ^{15}N als prognostische Tracer in der biogeochemischen Ozeankomponente eines Erdsystemmodells. Dafür werden globale Daten von $\delta^{15}NO_3^-$ Beobachtungen aus vorausgegangenen Studien zusammengestellt und mit den Modellergebnissen verglichen. Das Modell ist in der Lage, beobachtete Strukturen wie hohe oberflächennahe Werte in Zonen mit Wassersäulendenitrifizierung, durch N_2-Fixierung produzierte niedrige Werte im Nordatlantik und durch NO_3^--Assimilation erzeugte meridionale und vertikale Gradienten im südlichen Ozean zu reproduzieren. Die Modellexperimente dieser Arbeit zeigen, dass die globalen Verteilungsstrukturen von $\delta^{15}N$ durch Isotopeneffekte erklärt werden können, die auf NO_3^--Assimilation, N_2-Fixierung und Denitrifizierung von Phytoplankton zurückgeführt werden können.

Im zweiten Teil werden Beobachtungen von Stickstoffisotopen verwendet, um die Bedeutung von atmosphärischem Eiseneintrag in den Ozean für Stickstofffixierung zu untersuchen. Das N_2-fixierende Enzym Nitrogenase, besteht in seiner Struktur zu großen Teilen aus Eisen, welches ein sehr wichtiger limitierender Faktor für Stickstofffixierer sein könnte. Daher werden Modellexperimente mit und ohne Eisenlimitierung von N_2-Fixierung mit Beobachtungen von $\delta^{15}N$ im Pazifischen Ozean verglichen. Nur das Modell mit der Eisenlimitierung von N_2-Fixierung kann die beobachteten $\delta^{15}NO_3$-Gradienten reproduzieren. Das bestätigt, dass atmosphärischer Eiseneintrag in den Ozean in der Tat ein wichtiger Faktor für die Regulierung von N_2-Fixierung im Ozean ist.

In den letzten beiden Teilen dieser Arbeit werden globale Mittelwerte von $\delta^{15}NO_3^-$ in der Wassersäule und $\delta^{15}N$ an der Sedimentoberfläche verwendet, um N_2-Fixierungsraten, Denitrifizierung in der Wassersäule und benthische Denitrifizierung im Ozean zu bestimmen. Während $\delta^{15}N$-Beobachtungen der letzten 80.000 Jahre eine direkte Beziehung zu dem physikalischen Klima aufzeigen, bleibt die Quantifizierung der Veränderungen von N_2-Fixierung und Denitrifikation aufgrund von Unsicherheiten im Stickstoffisotopenkreislauf eine Herausforderung. Daher wurden Sensitivitätsexperimente durchgeführt, um die beiden sensitivsten Prozesse zu testen, die die globalen Abschätzungen von N2-Fixierung und Denitrifizierung beeinflussen: die Reduktion von NO_3^- in suboxischen Zonen und der Netto-Fraktionierungsfaktor der benthischen Denitrifizierung. Aus dem Experiment, das die $\delta^{15}N$-Beobachtungen am besten reproduzieren konnte, wurden die Raten von N_2-Fixierung, Wassersäulendenitrifizierung und benthischer Dentrifizierung im preindustriellen Ozean mit der Annahme eines ausgeglichenen bioverfügbaren Stickstoffreservoirs zu jeweils 270–370, 70−90 und 200–280 (Tg N yr^{-1}) bestimmt. Diese Ergebnisse lassen vermuten, dass vorhergegangene Studien die marine N_2-Fixierung deutlich unterschätzt haben und dass die Residenzzeit von bioverfügbarem Stickstoff im Ozean kleiner als 1.000 Jahre ist.

Summary

Nitrogen is an essential nutrient for life. Its low abundance throughout much of the sunlit surface ocean limits the growth of primary producers that form the base of ocean ecosystems. Phytoplankton also consume surface ocean CO_2 during growth, preventing this greenhouse gas from outgassing to the atmosphere where it will influence climate. Since the source and sink processes that control the balance of the bio-available nitrogen inventory, N_2 fixation and denitrification/anammox (N-loss), respectively, are sensitive to climate, they may have an important feedback on atmospheric CO_2 during climate change. N_2 fixation and N-loss processes leave a distinguishable imprint on the ratio of stable nitrogen isotopes, $\delta^{15}N$, making it a useful tracer to constrain their patterns and rates. This dissertation incorporates $\delta^{15}N$ into an Earth System Climate Model to better understand and quantify important N-cycling processes in the ocean.

The two stable nitrogen isotopes, ^{14}N and ^{15}N, are included as prognostic tracers into the ocean biogeochemistry component of an Earth System Climate Model. A global database of $\delta^{15}NO_3^-$ observations is compiled from previous studies and compared to the model results. The model is able to qualitatively and quantitatively reproduce many of the observed patterns such as high subsurface values in water column denitrification zones, low values in the North Atlantic attributed to N_2 fixation, and the meridional and vertical gradients in the Southern Ocean caused by phytoplankton NO_3^- assimilation. Experiments show the most important isotope effects that drive the global distribution of $\delta^{15}N$ are phytoplankton NO_3^- assimilation, N_2 fixation, and denitrification/anammox.

Nitrogen isotopes trends across the Pacific Ocean support that aeolian iron deposition is an important factor regulating the distribution of N_2 fixation. N_2-fixers have high structural iron requirements in their N_2-fixing enzyme, which could restrict their growth since iron is a limiting micronutrient. Model experiments with and without Fe limitation of N_2 fixation are compared to meridional $\delta^{15}NO_3^-$ observations in the central and western Pacific Ocean. Only the model with Fe limitation of N_2 fixation could reproduce the observed trends. This

suggests that atmospheric iron deposition is important for relieving iron limitation of N_2-fixers.

Water column $\delta^{15}NO_3^-$ and seafloor $\delta^{15}N$ observations are used to constrain the rates of N_2 fixation, water column N-loss, and benthic N-loss in the ocean. Experiments investigating uncertainties associated with the isotope effects of N-loss in the water column and sediments led to estimates for N-loss that varied by a factor of 3. Two sensitive processes affecting the large range of these estimates in the model are NO_3^- utilization in suboxic zones and the net fractionation factor associated with benthic N-loss. Sensitivity experiments that best reproduce observations in the suboxic zone and seafloor sediments estimate rates of N_2 fixation, water column N-loss, and benthic N-loss are in the range 220–370, 70–90, and 150–280 Tg N yr^{-1}, respectively, assuming a balanced bio-available nitrogen budget in the pre-industrial ocean. This model result suggests rates of N_2 fixation have been previously underestimated and the residence time of bio-available nitrogen in the ocean is between 1,500 and 3,000 years.

1 Introduction

1.1 Nitrogen Cycle and Ocean Ecosystems

Nitrogen is one of the fundamental elements required for life. It is part of all living cells and plays a critical role within enzymes and metabolic processes involved in the synthesis and transfer of cellular energy that makes life possible. Nitrogen is a major component of chlorophyll, the compound that captures sunlight used for energy during growth. It also is an important part of nucleic acids such as DNA, the genetic material that allows cells to grow and reproduce. Without nitrogen, life as we know it would not exist.

Microscopic ocean plants (phytoplankton) are capable of growth in the sunlit surface ocean when nutrients are available in sufficient quantity. Phytoplankton use energy from sunlight to convert dissolved inorganic nutrients (e.g., carbon, nitrogen, phosphorus, iron) into their organic matter. They form the base of the ocean ecosystem that provides energy to organisms of higher trophic levels (Figure 1.1). The ability of phytoplankton to convert inorganic nutrients into "fixed" organic matter is a crucial step that provides these critical nutrients in a form that can be consumed by more complex organisms.

The low abundance of bio-available compared to other nutrients throughout large regions of the surface ocean suggests nitrogen is a strong limiting factor for biological production. The global bio-available nitrogen must then be lower compared to other essential nutrients for the nutritional needs of phytoplankton because it is often the first depleted nutrient. This implies that the size of global oceanic inventory of nitrogen can regulate productivity levels in the global ocean.

Any significant change to the fixed-N inventory in the ocean could very well influence the productivity level of the global ocean. Since the residence time of fixed-N ($\leq$ 3,000 years) is much smaller than other limiting nutrients (e.g., phosphate: ~10,000 years), it has the greatest potential for change and to alter marine ecosystems. The processes that control the sources and sinks of fixed-N are also sensitive to climate (See Section 1.8) suggesting that climate change could drive changes in the fixed-N inventory.

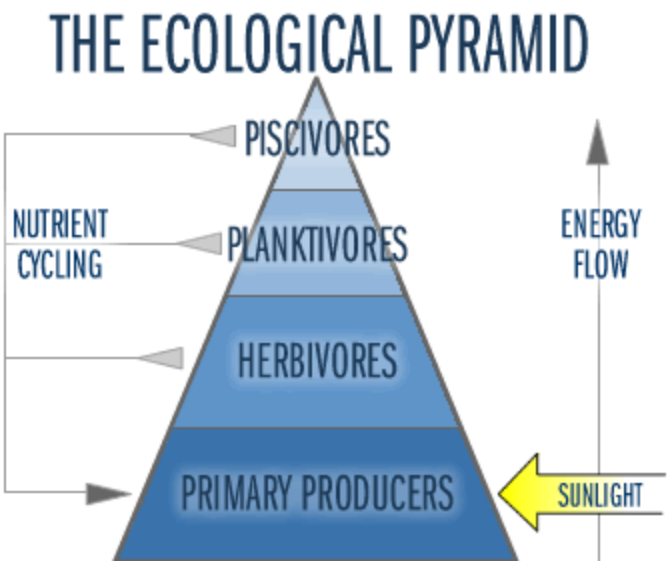

Figure 1.1: The ecological pyramid is a conceptual scheme that shows the decrease in biomass and energy towards the upper trophic levels. Figure based on *wateronthewеb.org/under/lake ecology/11_foodweb*

1.2 Forms of Nitrogen

The diversity of N species makes it one of the most complex biochemical elements in the ocean. The majority (~94%) of oceanic N exists as dissolved N_2 gas, which readily mixes in from the atmosphere into the surface ocean. It is not bio-available for most phytoplankton species. The molecular structure of N_2 consists of a strong triple-N covalent bond that requires a large amount of energy to break apart and convert into organic compounds compared to integrating other forms of dissolved inorganic nitrogen (DIN) available in seawater. Only some specialized phytoplankton (diazotrophs) are capable of "fixing" N_2 gas into their biomass that eventually cycles through other forms of "fixed-N" (e.g., NH_4^+, NO_2^-, NO_3^-, DON, PON) that become bio-available for phytoplankton. This process, which provides the ocean with most of its fixed-N, is referred to as N_2 fixation and is discussed more in following sections. Nitrate (NO_3^-) represents ~88% of the fixed-N pool, followed by DON at ~12%, while the remaining forms (NO_2^-, NH_4^+, PON) combine for less than 0.5%.

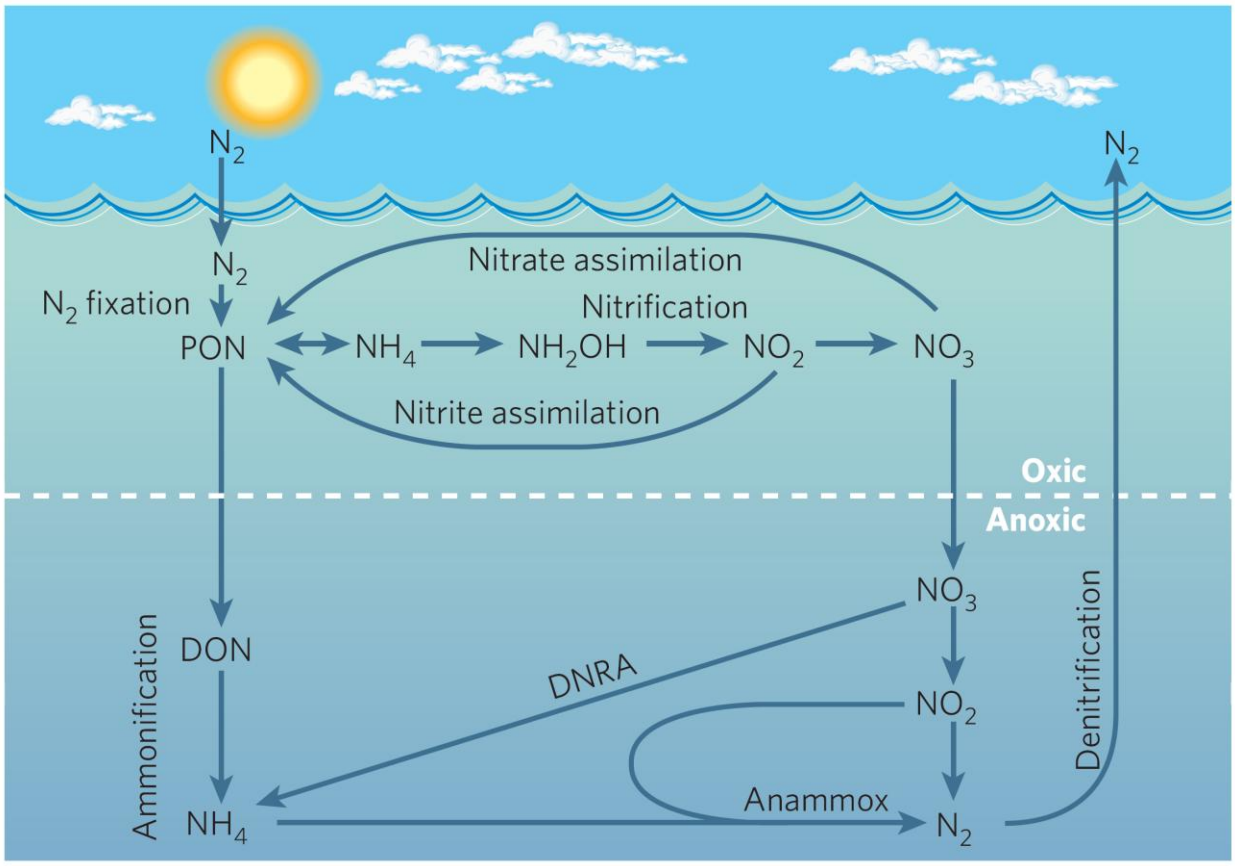

Figure 1.2: Marine Nitrogen Cycle in oxic and anoxic conditions (from Arrigo (2005)).

Many different species of N exist due to the large amount of relatively stable oxidation states of N in the marine environment. The N molecule contains 5 valence electrons, two of which occupying the 2s orbital and the remaining three in the 2p orbital, giving it a total electron configuration of $1s^2 2s^2 2p^3$. The most stable oxidation states for the nitrogen atom can be achieved when the outer shell is either completely full (oxidation state +V) or completely empty (oxidation state −III), corresponding to the fixed-N forms NO_3^- and NH_4^+, respectively.

Since most of the cycling of N is driven by biologically-mediated processes, bonding and activation energy plays an important role in the speciation of fixed-N. The ability of the valence electrons to hybridize their outer configuration to either four sp^3 orbitals or three sp^2 orbitals allows for different bonds to occur. In the sp^2 case, a π orbital can form into a high-

strength double or triple covalent bond, which yield high energy and are then costly to break down again. These high-strength bonds prevent rapid biological processing and explain the existence of the species of NO_2^-, N_2O, and N_2 in the marine environment, despite their only partially filled outer electron shell (Gruber, 2004).

1.3 Nitrogen Cycling Processes

The versatility of the nitrogen atom and its diverse speciation, as well as its importance for biological life, allows for a multitude of biologically-mediated cycling processes to occur in the marine environment. This makes N one of the most complex biogeochemical elements to understand. This section will briefly introduce the major processes that drive the cycling of N in the ocean, which will also be further discussed in the subsequent chapters.

Dissolved Inorganic Nitrogen Assimilation

The assimilation of dissolved inorganic nitrogen (DIN; e.g., NH_4^+, NO_2^-, NO_3^-) into organic N allows marine phytoplankton to meet their N requirements for growth. It is perhaps the most important N-cycling process in the ocean because of its association with phytoplankton growth and beginning the marine food chain. It is associated with photosynthesis and occurs in the forms

$$106CO_2 + 16NO_3^- + HPO_4^{2-} + 78H_2O + 18H^+ \rightarrow C_{106}H_{175}O_{42}N_{16}P + 150O_2 \quad (1.1)$$

and

$$106CO_2 + 16NH_4^+ + HPO_4^{2-} + 48H_2O + 14OH^- \rightarrow C_{106}H_{175}O_{42}N_{16}P + 118O_2 \quad (1.2)$$

when NO_3^- and NH_4^+ are being used as the nitrogen source, respectively (Gruber, 2008). Note that these stoichiometric ratios reflect average phytoplankton communities (Geider and La Roche, 2002) and any given phytoplankton stock may deviate substantially from these

ratios. NH_4^+ is the most energetically favorable species to assimilate due to its reduced form, while NO_2^- and NO_3^- require additional energy to break down (Zehr and Ward, 2002). Only phytoplankton with the specialized NO_3^- and NO_2^- reductase can break down and assimilate NO_3^-, whereas all phytoplankton are capable of assimilating NH_4^+ (Moore et al., 2002).

Remineralization

The term remineralization is generally used to describe the process of converting organic N back into forms of DIN. This conversion consists of a series of reactions that are performed by different species of bacteria. During the heterotrophic respiration of organic matter to inorganic nutrients, NH_4^+ is released via the process of ammonification, the return pathway of reaction 1.1. Most heterotrophic bacteria are capable of this transformation (Gruber, 2008).

The majority of fixed-N in the ocean is in the form of NO_3^- due to nitrification. Nitrification is the chemo-autotrophic process that converts NH_4^+ into NO_3^-, which is carried out in multiple steps. Only some specialized bacteria with the able genes are capable of performing nitrification (Teske et al., 1994). It occurs in two main steps: ammonium oxidation ($NH_4^+ \rightarrow NO_2^-$) and nitrite oxidation ($NO_2^- \rightarrow NO_3^-$). No single species has been identified that can undergo both of these process (Ward et al., 2007). Nitrification is responsible for the accumulation of NO_3^- as opposed to NH_4^+ in the deep ocean, both of which are chemically stable molecules.

N_2 fixation

N_2 fixation occurs when specialized microorganisms (diazotrophs) "fix" dissolved N_2 gas into their biomass (Karl et al., 2002). This nitrogen subsequently remineralizes into forms of "fixed-N" that are then available to general phytoplankton for uptake. This provides the ocean with most of its bio-available N because most phytoplankton do not have the biological machinery to break down the strong triple covalent bond of the N_2 molecule.

The enzyme nitrogenase carries out this process and has large structural iron (Fe) requirements. Since iron is one the limiting micronutrients in the ocean, iron limitation may

be an important factor preventing N_2 fixation (Mark Moore et al., 2009). N_2 fixation is also inhibited by the presence of O_2 so diazotrophs must undergo additional respiration to remove O_2 from the N_2-fixing compartment of the cell (Letelier and Karl, 1996). These high-energy processes contribute to diazotroph's relatively slow growth rate and preference for warm water compared to general phytoplankton. Despite this slow growth rate, diazotrophs can have an ecological advantage in regions where fixed-N is depleted at the surface, which does occur throughout most of the tropical/subtropical ocean.

The two diazotrophic microorgansims types thought to be responsible for the majority of N_2 fixation are *Trichodesmium spp.* and unicellular diazotrophs (Karl et al., 2002; Montoya et al., 2004). However, recent studies are also showing that N_2 fixation occurs not only as independent photo-autotrophs, but also as symbionts associated with diatoms (Mulholland, 2007; Foster et al., 2011), as well as heterotrophically in low oxygen environments (Hamersley et al., 2011). These new developments further complicate our understanding of N_2 fixation. However, it still remains that their largest environment is the warm tropical/subtropical surface ocean.

Denitrification

Once O_2 is consumed below suboxic concentrations (<~10 μM) in the marine environment (Codispoti and Christensen, 1985), the next energetically favorable electron acceptor to use during respiration is NO_3^-, which then replaces O_2 and is reduced into N_2:

$$C_{106}H_{175}O_{42}N_{16}P + 104NO_3^- \rightarrow 106CO_2 + 60N_2 + H_3PO_4 + 138H_2O \qquad (1.3)$$

assuming the stoichiometry of organic matter is consistent with Equation 1.1. It converts fixed-N into N_2 that can mix back into the atmosphere, closing the N cycle that begins with diazotrophs fixing atmospheric N_2 into the ocean. Most heterotrophic bacteria can switch to respiration via denitrification suggesting it should be ubiquitous in suboxic waters where organic matter remineralizes. The seafloor sediments is another area where denitrification occurs in significant quantity once pore-water becomes oxygen deficient. While the partitioning of between denitrification occuring in the water column or sediments is

uncertain, total denitrification is considered to be the largest sink the oceanic fixed-N budget (Codispoti, 2007; Gruber, 2008).

Anaerobic Ammonium Oxidation

A relatively recent discovery is the significance of anaerobic ammonium oxidation (anammox) in nature (Thamdrup and Dalsgaard, 2002). It, similarly to denitrification, converts forms of fixed-N into N_2 gas:

$$NO_2^- + NH_4^+ \rightarrow 2N_2 + 2H_2O \quad (1.4)$$

Anammox, however, it is a chemo-autotrophic process used to gain energy for growth and is not associated with the respiration of organic matter. These bacteria can also remain dormant in the water column until conditions favor their growth (i.e., low O_2 event). While anammox occurs in similar environmental conditions as denitrification (i.e., high organic matter cycling in OMZs), it has been suggested that it may have a better tolerance for slightly higher O_2 concentrations (O_2 ~ 10–15 μM) compared to denitrification (O_2 < 10 μM) (Lam et al., 2009), which could give anammox bacteria a bigger environment to grow in compared to canonical denitrifiers.

Dissimilatory Nitrate Reduction to Ammonium

Another recent development in the marine nitrogen cycle is the significance of dissimilatory nitrate reduction to ammomium (DNRA) in OMZs. It reduces NO_3^-, similarly to denitrification, but the end-product is NH_4^+, which is still a form of fixed-N so it is not a N-loss process. Although the potential free energy for total denitrification is larger than DNRA (Gottschalk, 1986), the potential free energy per mole of NO_3^- is greater for DNRA (Strohm et al., 2007). This suggests that DNRA bacteria can compete with heterotrophic denitrifiers, especially when NO_3^- becomes limiting in the system (Tiedje, 1988; Rütting et al., 2011). DNRA could also be an important source of NH_4^+ and NO_2^- in OMZs that could fuel anammox.

1.4 Distribution of fixed nitrogen

The most prevalent feature of the global distribution of fixed-N is its general depletion at the surface and repletion in the deep ocean. This trend occurs due to biological uptake of fixed-N in the sunlit surface waters and remineralization at depth due to gravity-induced sinking of particulate organic matter. Physical circulation patterns then determine where NO_3^- that accumulates in the deep ocean gets transported back to the surface where phytoplankton can once again consume it during photosynthesis. The strongest upwelling zones tend to occur near continental shelves, at the equator, and mid-latitude frontal zones.

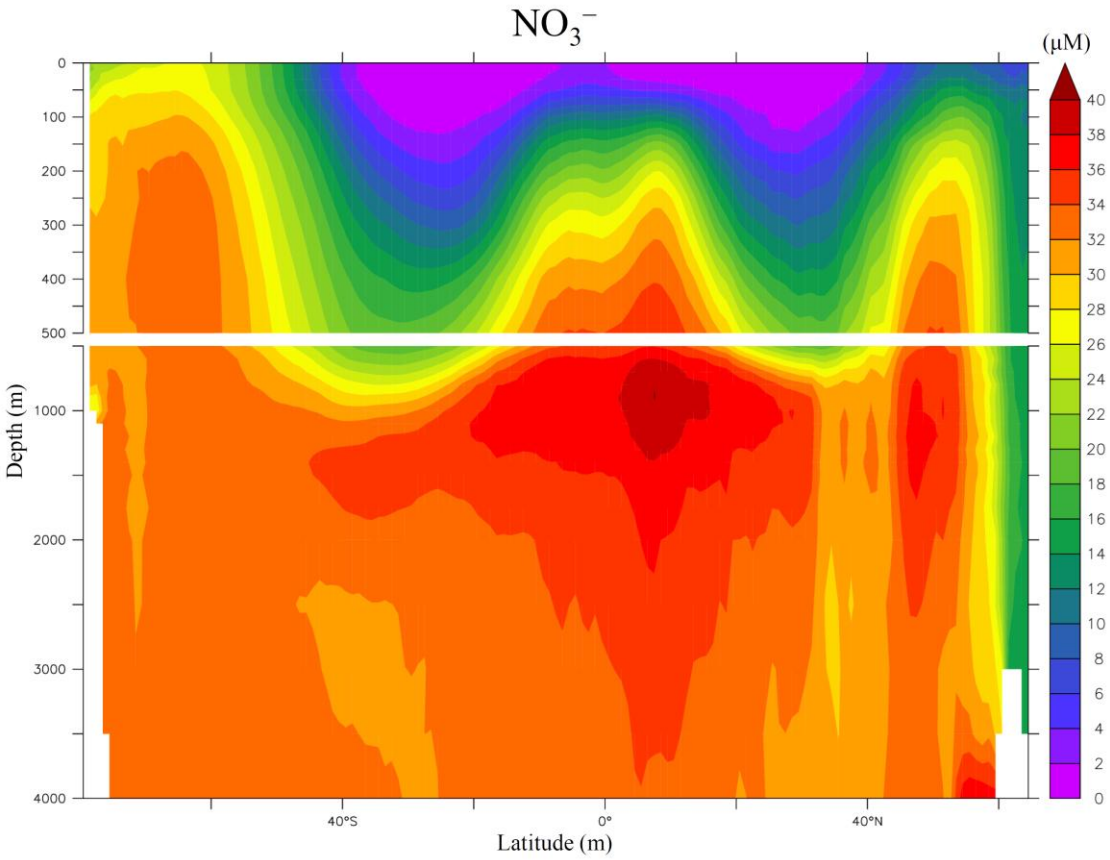

Figure 1.3: Annual zonally averaged NO_3^- concentrations (μM) (Garcia et al., 2010b).

There are regions that contain significant concentrations of fixed-N at the surface and with relatively low productivity. These High Nutrient Low Chlorophyll (HNLC) regions exist in three main areas: the Southern Ocean, the North Pacific, and the Eastern Equatorial Pacific (Figure 1.4). The micronutrient iron (Fe) is the main limiting nutrient regions that prevents

productivity in these regions. This shows the potential for limitation from other nutrients than nitrogen. The presence of HNLC regions also suggests that the main limiting nutrient can switch depending on environmental conditions. A significant inventory change in one of the important limiting nutrients could result in a fundamental ocean ecosystem shift where it is the main limiting nutrient. Since many of the processes that control the inventory of Fe and fixed-N are influenced by the physical climate, it has been suggested that changes may have occurred during past climate changes that significantly affected global rates of primary production and export production (Falkowski, 1997).

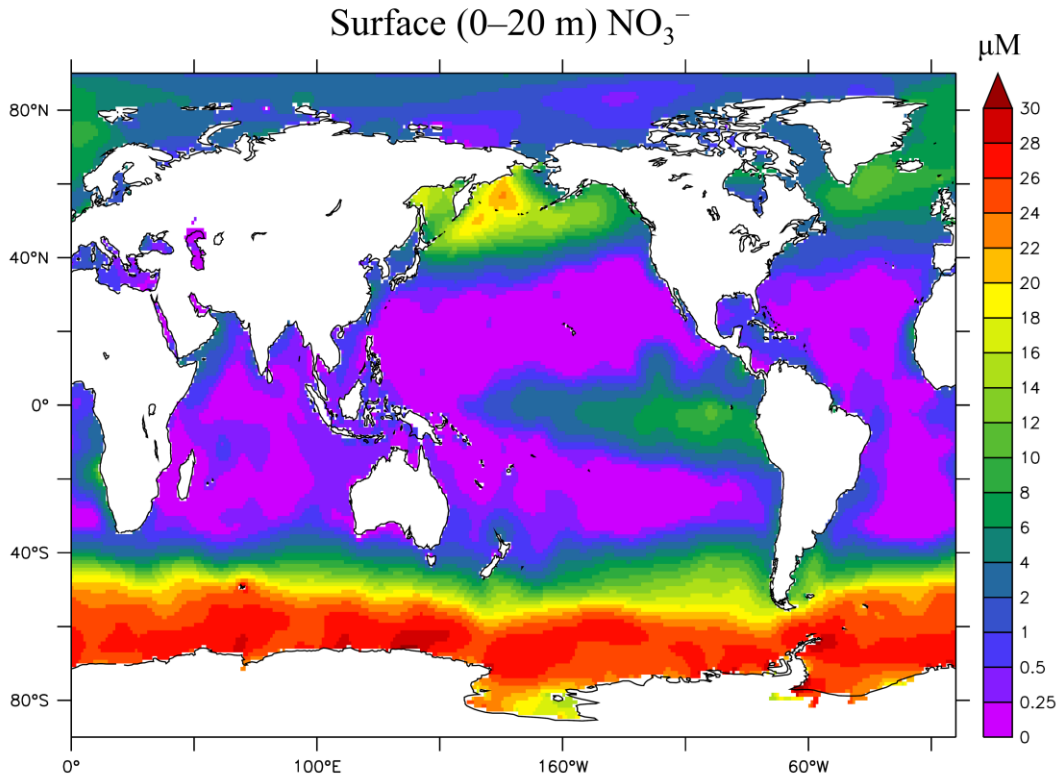

Figure 1.4: Annual surface NO_3^- concentrations (µM) (Garcia et al., 2010b).

Oligotrophic ocean environments sustain low levels of productivity. They are typically fueled by the fast-recycling of nutrients from organic matter rather than advection of NO_3^--replete deep water. The center of the subtropical ocean gyres are sometimes referred to as "ocean deserts" due to the low level of productivity that results from the lack of new nutrients transported to the surface. The largest abundance of fixed-N in these regions is typically

DON, the result from the first step of the fast-recycling process from particulate organic nitrogen. Phytoplankton typically consume the fast-recycling end-product NH_4^+ before nitrifying bacteria oxidize it to NO_2^- and NO_3^-, This makes oligotrophic oceans one of the few places where NH_4^+ can be more abundant than NO_3^-.

Under low oxygen conditions, many specific N-cycling transformations alter the speciation of fixed-N that is unique in these relatively small (< 3% of total ocean volume), but important zones. These areas are crucial of the fixed-N cycle because both significant fixed-N-loss processes, denitrification and anammox, occur in these areas. N-loss processes remove fixed-N in these subsurface waters by converting it to N_2 and N_2O gas. This removal of fixed-N contributes to the N-limitation in throughout much of the surface ocean.

1.5 Fixed Nitrogen Budget

The different processes that add (source) or remove (sink) fixed-N from the ocean determine the global inventory. Since fixed-N limits productivity in much of the surface ocean, a significant change to these source or sink processes can have ramifications for global ocean productivity. Understanding the rates and sensitivity to change of the major processes that control the fixed-N inventory becomes a crucial component of N cycling in the ocean. Here we outline the most important known source/sink processes of the fixed-N budget and briefly discuss uncertainties associated with them.

1.5.1 Fixed Nitrogen Sources

N_2 Fixation

Due to the large spatial and temporal variability, as well as new species and environments for N_2 fixation that are still being investigated, the estimates for the global rate of N_2 fixation contains considerable uncertainty. It has been shown that a methodological underestimation has existed in the majority of previous measurements by a factor of 2–10 suggesting there could be much more N_2 fixation occurring than previously thought (Mohr et al., 2010; Großkopf et al., 2012, in review). Inorganic N:P ratios in conjunction with physical circulation models have also been used to estimate N_2 fixation in a global budget. These models have estimated large ranges from 100–300 Tg N yr^{-1} and can be very sensitive to

biological parameters that are not well constrained (Gruber and Sarmiento, 1997; Deutsch et al., 2001; Deutsch et al., 2007; Moore and Doney, 2007b). New forms of N_2 fixation are still being discovered such as N_2 fixation occurring in oxygen minimum zones (Hamersley et al., 2011) as well as diatom-diazotroph symbiosis (Carpenter and Foster, 2003; Foster et al., 2011) that could provide further environments where N_2 fixation can significantly occur.

Process	**Modern Estimate (ca. 1990-2000)**
Sources	(Tg N yr^{-1})
N_2 fixation	100 – 260
River input	43 – 48
Atmospheric deposition	40 – 80
TOTAL	183–388 (263)
Sinks	
Water column N-loss	57 – 163
Benthic N-loss	102 – 300
Sediment burial	16 – 25
TOTAL	175–488 (329)
Balance	−324–+233 (−66)

Table 1.1: Estimates of fixed-N budget from 11 selected studies in the literature (see below). Totals were calculated using all low-end and high-end estimates for each process and the average from all estimates is given in parenthesis (Middelburg et al., 1996; Brandes and Devol, 2002; Karl et al., 2002; Deutsch et al., 2004; Galloway et al., 2004; Gruber, 2004; Mahaffey et al., 2005; Codispoti, 2007; Deutsch et al., 2007; Seitzinger et al., 2010; Bohlen et al., 2012, in review).

Atmospheric N deposition

Nitrogen is deposited into the ocean through the atmosphere in both dry and wet inorganic forms. The primary sources are in dust (Duce et al., 2008b), emissions from combustion engines, power plants and emissions from fertilized soils (Nevison et al., 1995; Asner et al., 2001). While pre-industrial estimates coming primarily from dust deposition are relatively

low (< 20 Tg N yr), increased anthropogenic influence from combustion engines and fertilizer soils in the coming decades are estimated to increase total N deposition to ≥100 Tg N yr^{-1} in the coming decades (Galloway et al., 2004).

River input

Nitrogen in the dissolved and particulate forms in rivers contribute to fixed-N in the ocean. Although the exact contribution to river N is not well quantified, the sources are known to be from fertilizers, manure, N_2 fixation, and deposition (Galloway et al., 2004; Seitzinger et al., 2010). The estimate for river N input has also increased from 36 Tg N yr^{-1} to 43 Tg N yr^{-1} over the last 3 decades mainly due to fertilizer and manure, but is estimated to remain more steady in future decades (Seitzinger et al., 2010).

1.5.2 Fixed Nitrogen Sinks

Water column N-loss

Specialized bacteria convert forms of fixed-N to biotically unavailable forms of N gas under suboxic water column conditions (O_2 < ~10 μM) (Codispoti and Christensen, 1985). This occurs in three predominant locations in the global ocean (i.e., ETNP, ETSP, Arabian Sea), while other areas, typically located near productive coastal zones (e.g., Benguella Coast), have also observed intermittent denitrification events (Kuypers et al., 2005) along the shelf.

The two processes that undergo N-loss, canonical denitrification and anammox, require similar environmental conditions so they often occur within close proximity to each other. This makes it difficult to distinguish the relative strength of denitrification and anammox in OMZs. Denitrification may be required to provide much of the NO_2^- needed for anammox that otherwise exists in very low concentrations. This suggesting a co-occurrence where water column denitrification could be responsible for the first step of reduction ($NO_3^- \rightarrow NO_2^-$), while anammox finishes the reduction to N_2 gas (Lam et al., 2009). Another possibility is that DNRA or AOA (described above) produces enough NO_2^- to drive anammox (Lam et al., 2009). Recent studies suggest that water column denitrification is the dominant form of N-loss in the Arabian Sea (Ward et al.), while anammox removes most of the fixed-N in the ETSP (Lam et al., 2009), but actual biogeochemical mechanisms that

cause these differences remains uncertain. Global estimates of water column N-loss range between 50–150 Tg N yr^{-1} (Gruber, 2004; Codispoti, 2007).

Benthic N-loss

Suboxic environments exist in the seafloor sediments where N-loss can occur. Large rain rates of particulate organic carbon into the seafloor are found to drive benthic community production that consumes oxygen (Middelburg et al., 1996). While early estimates were relatively low (< 100 Tg N yr^{-1} (Codispoti and Christensen, 1985)), some recent estimates have suggested much higher rates (> 300 Tg N yr^{-1}) (Middelburg et al., 1996; Codispoti, 2007). The uncertainty about the relative amount of benthic N-loss that occurs on the continental shelf, shelf-slope, and deep-sea sediments contributes to the large range of estimates that vary by a factor of ~3 (Brandes and Devol, 2002; Bohlen et al., 2012, in review).

Sediment burial

Particulate organic nitrogen that sinks and becomes buried into the seafloor removes fixed-N from the ocean. This sink is estimated to be ~25 Tg N yr^{-1} (Gruber, 2008), which is about an order of magnitude lower than total benthic N-loss. It is determined by global particulate carbon rain rate into the sediment estimates (Hedges et al., 2002), then converted to nitrogen assuming constant Redfield stoichiometry (Gruber, 2008)

1.5.3 Balance of the fixed-N budget

The large uncertainty in the main fixed-N source/sink processes make it difficult to determine if the fixed-N budget is in balance. The source/sink terms with the most uncertainty are N_2 fixation and benthic N-loss. Recent upwards revision of the rate of benthic denitrification by an order of 2–3 over recent decades have led to the debate whether the ocean is rapidly losing nitrogen (Middelburg et al., 1996; Brandes and Devol, 2002; Codispoti, 2007). However, it has been shown the method for measuring N_2 fixation has been underestimating its rate by a factor of 2–10 suggesting N_2 fixation may be much higher (Mohr et al., 2010). Monteiro et al. (2011) also found that N*-based geochemical estimates likely also underestimate N_2 fixation. Given the relative stability of the climate during the

late Holocene, as well as records of $\delta^{15}N$ (Altabet, 2007), the global fixed-N budget was likely in balance during pre-industrial times.

1.6 Nitrogen Isotopes

Nitrogen exists in two stable isotopic forms in the natural environment: ^{14}N and ^{15}N. The ^{15}N isotope contains one extra neutron within its nucleus, making it the heavier isotope. ^{14}N is the more abundant isotope accounting for 99.3667% of the global fixed-N pool (Nier, 1950). It is common to refer to the ratio of $^{15}N/^{14}N$ in the delta (δ) notation

$$\delta^{15}N = \left(\frac{^{15}N/^{14}N_{sample}}{^{15}N/^{14}N_{standard}} - 1 \right) \times 1000 \qquad (1.5)$$

where the $^{15}N/^{14}N$ ratio of a sample is reported as deviations from a standard $^{15}N/^{14}N$ ratio commonly chosen as atmospheric N_2. Since the range of deviation from the atmospheric ratio is relatively small, the per mil (‰) (i.e., ×1000) convention is used.

The lighter ^{14}N isotope is more thermodynamically reactive and preferentially incorporated into the product of most biological processes. Heavier isotopes generally have lower vibrational frequencies and require more energy to break down their molecular bonds. This is defined in quantum mechanics as having lower zero-point energies that determine the statistical probability that one isotope will be favored over the other (Bigeleisen, 1952).

In practice, the N isotope ratio of the substrate and product are measured for each process then assigned an associated fractionation factor, $\alpha = {}^{15}k/{}^{14}k$, where k is the specific reaction rate for each isotope. It can also be expressed in the delta notation, where $\varepsilon = (1 - \alpha) \times 1000$. The fractionation factor can be quantified using Rayleigh fractionation assuming an accumulated product (i.e., closed system; $\delta^{15}N_{pro} = \delta^{15}N_{sub} + R_{sub}/R_{std} \cdot \varepsilon \cdot (1-u)/u \cdot \ln(1-u)$), where u is the fraction of the substrate consumed, or an instantaneous product (i.e., $\delta^{15}N_{pro} = \delta^{15}N_{sub} + R_{sub}/R_{std} \cdot \varepsilon$) depending on the conditions of the experiment or natural environment (Altabet, 2007). The accumulated product equation requires mass balance between the

substrate and product and is generally used when a reaction consumes the substrate faster than it is replenished by the environment.

Table 1.2: Nitrogen Isotope Fractionation Factors

Process	Symbol	Field Estimates (‰)
NO_3^- Assimilation	ε_{ASSIM}	4 – 15
N_2 Fixation	ε_{NFIX}	0 – 2
Excretion	ε_{EXCR}	3 – 6
Water Column N-loss	$\varepsilon_{WCN\text{-}l}$	20 – 30
Benthic N-loss	$\varepsilon_{BN\text{-}l}$	0 – 8

The variability of $\delta^{15}N$ in the ocean is a complex pattern driven mainly by the isotope effects phytoplankton DIN assimilation, N-loss, N_2 fixation, and excretion (Table 1.2). The uncertainty involved in the isotope effects of each process alone make it a difficult task to determine which processes are the most important in affecting $\delta^{15}N$ patterns. For example, DIN assimilation and water column N-loss both increase the $\delta^{15}NO_3^-$ of the remaining ocean NO_3^-, while N_2 fixation and excretion add relatively low $\delta^{15}NO_3^-$ into the water column. This makes the interpretation of $\delta^{15}N$ at any one point in space and time very complex. Chapter 2 of this thesis focuses more on the processes that drive the spatial distribution of $\delta^{15}N$.

1.7 Nitrogen Cycle and Climate

Marine phytoplankton sequester surface ocean CO_2, an important greenhouse gas, into their biomass during growth via photosynthesis. This prevents CO_2 from releasing back into the atmosphere, where it will trap heat and warm the Earth. Much of the resulting detrital organic matter from phytoplankton sinks towards the deep ocean before it eventually remineralizes back into dissolved inorganic carbon. Any remineralization that takes place at depth in the

ocean affects the partitioning of CO_2 between the atmosphere and ocean because this remineralized carbon can remain in the deep ocean for several hundreds of years, a mechanism known as the "biological carbon pump". Since fixed-N is one of the major limiting nutrients for marine phytoplankton, its global inventory can influence the strength of the biological carbon pump and have an impact on climate.

Since N-loss processes (denitrification/anammox) remove fixed-N from the ocean, it creates an ecological niche from diazotrophs because they are not N-limited. It has been suggested that this negative-feedback should keep the fixed-N inventory balanced. Since NO_3^-:PO_4^- ratios are rarely observed above 16:1, it suggests diazotrophs restore fixed-N back to ratios needed by general phytoplankton, but not much more. General phytoplankton will likely outcompete diazotrophs once fixed-N is restored to their required stoichiometric conditions (i.e., "canonical" Redfield ratio N:P=16 (Redfield, 1958)). If this feedback does indeed operate this way in nature, it would represent a stabilizing effect that would prevent major fluctuations of the oceanic fixed-N inventory.

The most critical feature of this feedback on the oceanic fixed-N inventory will the spatial and temporal coupling between N_2 fixation and N-loss processes. For example, if N_2 fixation is able to restore all fixed-N loss from N-loss within the ocean basin, the feedback timescale (10–50 years) would be much shorter than the residence time of fixed-N (1,000–3,000 years). This would prevent large fluctuations in the fixed-N inventory from occurring. However, it has been suggested that aeolian Fe input regulates where N_2 fixation is able to occur (Falkowski, 1997). If N-deficient water from N-loss in the Fe-limited Southern Hemisphere had to travel all the way to the North Atlantic, where sufficient Fe exists, it could represent a decoupling timescale between denitrification and N_2 fixation nearing the large-scale ocean circulation (~1,000 years). Then the oceanic fixed-N inventory could undergo a significant change (McElroy, 1983; Falkowski, 1997; Galbraith et al., 2004).

Since the fixed-N source/sink processes are sensitive to climate, it has been suggested that a climate change could result in large changes in the global fixed-N inventory (McElroy; Falkowski). This would then have implications on the strength of the biological pump with a

feedback on atmospheric CO_2 during this transient climate change. While there would likely be a balance during a stable climate period, any transient climate change could produce changes to N_2 fixation and N-loss. If this transient change led to a significant decoupling between these source and sink processes, a change to the fixed-N inventory may occur, which could alter the strength of the biological pump and influence atmospheric CO_2 concentrations.

1.8 Chapter synopsis and author contributions

Chapter 2 focuses on the implementation of a new prognostic nitrogen isotope module within an existing global coupled three-dimensional circulation-biogeochemistry model. A new global database of $\delta^{15}NO_3^-$ is constructed to validate the model results. Experiments that isolate each individual isotope effect show that NO_3^- assimilation by phytoplankton, water column denitrification, and N_2 fixation are the most important processes that drive the global patterns of $\delta^{15}NO_3^-$. This chapter is from the published manuscript: Somes, C. J., A. Schmittner, E. D. Galbraith, M. F. Lehmann, M. A. Altabet, J. P. Montoya, R. M. Letelier, A. C. Mix, A. Bourbonnais, and M. Eby (2010), Simulating the global distribution of nitrogen isotopes in the ocean, *Global Biogeochem. Cycles*, *24*, GB4019, doi:10.1029/2009GB003767. Somes developed the nitrogen isotope module from scratch and performed all experiments. Somes collected published $\delta^{15}NO_3^-$ data and created the $\delta^{15}NO_3^-$ database from scratch. Somes wrote the manuscript with comments provided by all co-authors.

Chapter 3 uses observed nitrogen isotope patterns to determine the importance of atmospheric iron deposition on N_2 fixation in the Pacific Ocean. This study finds that only experiments including iron limitation of N_2 fixation can reproduce observed meridional $\delta^{15}NO_3^-$ trends in the central and western tropical Pacific, which suggests that atmospheric iron deposition is an important limiting factor for N_2 fixation in the Pacific Ocean. This chapter is from the published manuscript: Somes, C. J., A. Schmittner, and M. A. Altabet (2010), Nitrogen isotope simulations show the importance of atmospheric iron deposition for nitrogen fixation across the Pacific Ocean, *Geophys. Res. Lett.*, *37*, L23605, doi:10.1029/2010GL044537. Somes developed the iron limitation parameterization and

performed all experiments. Somes wrote the manuscript with comments provided by all co-authors.

Chapter 4 investigates how the oceanic nitrogen cycle responds to climate change using a new global seafloor $\delta^{15}N$ database. The large-scale patterns can be explained by the interplay between N_2 fixation, denitrification and the cycling of nitrate, as confirmed by a good agreement with an ocean-biogeochemistry-isotope model. Down-core measurements reveal that changes in the nitrogen cycle have paralleled known changes in ocean circulation and climate during the last 80,000 years. This chapter is from the manuscript: Galbraith, E. D., M. Kienast, and the NICOPP working group including J.-E. Tesdal, C. J. Somes et al. (2012), Coherent climate-driven changes in the global marine nitrogen cycle during the past 80,000 years, *Nature Geosciences*, in review. Tesdal created the seafloor $\delta^{15}N$ database from scratch. Somes performed the model experiments and made Figure 1. Galbraith wrote the manuscript and made the other figures with comments from the co-authors.

Chapter 5 uses $\delta^{15}N$ observations in the water column and sediments to constrain the rates of N_2 fixation, water column N-loss, and benthic N-loss in the pre-industrial ocean. Experiments were performed to test how sensitive estimates for N_2 fixation and N-loss are within the range of uncertainty for the isotope effects of these processes. The ratio of benthic N-loss to water column N-loss varied by over a factor of 3 in the sensitivity experiments. $\delta^{15}N$ observations were used to determine which model experiments give the most realistic estimates of N_2 fixation, water column N-loss, and benthic N-loss. This chapter is based on the manuscript: Somes, C. J., A. Oschlies, and A. Schmittner, Isotopic constraints on the pre-industrial oceanic fixed nitrogen budget (2012), Biogeosciences, in preparation. Somes performed all model experiments. Somes wrote the manuscript with comments from all co-authors.

2 Simulating the Global Distribution of Nitrogen Isotopes in the Ocean

This chapter is based on the manuscript from Christopher J. Somes, Andreas Schmittner, Eric D. Galbraith, Moritz F. Lehmann, Mark A. Altabet, Joseph P. Montoya, Ricardo M. Letelier, Alan C. Mix, Annie Bourbonnais, and Michael Eby

Abstract

We present a new nitrogen isotope model incorporated into the three-dimensional ocean component of a global Earth System Climate Model designed for millennial timescale simulations. The model includes prognostic tracers for the two stable nitrogen isotopes, ^{14}N and ^{15}N, in the nitrate (NO_3^-), phytoplankton, zooplankton, and detritus variables of the marine ecosystem model. The isotope effects of algal NO_3^- uptake, nitrogen fixation, water column denitrification, and zooplankton excretion are considered as well as the removal of NO_3^- by sedimentary denitrification. A global database of $\delta^{15}NO_3^-$ observations is compiled from previous studies and compared to the model results on a regional basis where sufficient observations exist. The model is able to qualitatively and quantitatively reproduce many of the observed patterns such as high subsurface values in water column denitrification zones and the meridional and vertical gradients in the Southern Ocean. The observed pronounced subsurface minimum in the Atlantic is underestimated by the model presumably owing to too little simulated nitrogen fixation there. Sensitivity experiments reveal that algal NO_3^- uptake, nitrogen fixation and water column denitrification have the strongest effects on the simulated distribution of nitrogen isotopes, whereas the effect from zooplankton excretion is weaker. Both water column and sedimentary denitrification also have important indirect effects on the nitrogen isotope distribution by reducing the fixed nitrogen inventory, which creates an ecological niche for nitrogen fixers and, thus, stimulates additional N_2 fixation in the model. Important model deficiencies are identified, and strategies for future improvement and possibilities for model application are outlined.

2.1 Introduction

Bioavailable nitrogen (fixed-N) is one of the major limiting nutrients for algal photosynthesis, which drives the sequestration of CO_2 from the surface ocean and atmosphere into the deep ocean via the sinking of organic matter. Changes in this so-called "biological pump" have been hypothesized to account for a significant amount of the glacial-interglacial fluctuations in atmospheric CO_2 (McElroy; Falkowski). However, the relative contributions of the biological and physical carbon pumps to CO_2 variations remain controversial. The size of the oceanic fixed-N inventory, which regulates the strength of the biological pump, is controlled by different biogeochemical processes that are difficult to constrain quantitatively in a global budget (Codispoti, 2007). Nitrogen isotopes (both in dissolved and organic N species) in the water column and sea floor sediments are sensitive indicators of those processes (Altabet, 2007).

Many N-transformational processes alter the ratio of the two stable forms of the nitrogen isotopes, ^{14}N and ^{15}N, differently, a process referred to as fractionation. Resulting variations in N isotopic composition can be described as deviations in $^{15}N/^{14}N$ ratio from an accepted standard

$$\delta^{15}N = [(^{15}N/^{14}N) / R_{std} - 1] \times 1000 , \qquad (2.1)$$

where R_{std} is the $^{15}N/^{14}N$ ratio of atmospheric N_2 gas. Isotope fractionation can occur due to kinetic processes (i.e., different reaction rates for isotopes in a reactant-product stream). It generally results in the enrichment of the heavier ^{15}N isotope in the reaction substrate, and its depletion in the product. For example, preferential discrimination against ^{15}N relative to ^{14}N during algal NO_3^- assimilation results in net enrichment of ^{15}N in the residual NO_3^- and net depletion of ^{15}N in organic matter. The degree of isotopic discrimination, or fractionation, for each process can be quantified with an enrichment factor, $\varepsilon = (^{14}k/^{15}k - 1) \bullet 1000$, where k is the specific reaction rate for each isotope (Mariotti et al.).

The predominant source and sink terms of the oceanic fixed-N inventory, N_2 fixation and denitrification, respectively, have their own distinct effects on the signature of the N isotopes in the ocean. N_2-fixing prokaryotes (diazotrophs) introduce bioavailable N into the ocean close to that of atmospheric N_2 ($\delta^{15}N \approx -2 - 0‰$) (Delwiche and Steyn, 1970; Minagawa and Wada, 1986; Macko et al., 1987; Carpenter et al., 1997). *Trichodesmium*, one of the most important and best studied diazotrophs, bloom more frequently and extensively in warm (>25°C) surface water where rates of aeolian Fe deposition are high such as the North Atlantic, Indian, and North Pacific compared to areas of low Fe deposition such as the South Pacific where the abundance of *Trichodesmium* appears to be much lower (Karl et al., 2002; Carpenter and Capone, 2008). However, other unicellular diazotrophs have been observed to grow in cooler water near 20°C (Needoba et al., 2007), and it has been suggested that they also may significantly contribute to the global N_2 fixation rate (Zehr et al., 2001; Montoya et al., 2004).

Denitrification occurs under suboxic conditions ($O_2 < 5$ μmol/kg) in the water column and in the sea floor sediments. Here, microbes use NO_3^- instead of O_2 as the electron acceptor during respiration and convert it to gaseous forms of N (N_2O and N_2), which can then escape to the atmosphere (Codispoti and Richards, 1976). The volume and distribution of suboxic water is affected by the temperature-dependent solubility of O_2 at the surface and the rate of subduction of oxygen-saturated water masses to greater depths, as well as the amount of organic matter that remineralizes in the ocean interior, both of which are sensitive to changes in climate. Anammox is another important process that occurs in anaerobic conditions and eliminates forms of fixed-N (NO_2^-, NH_4^+) in the water column by converting them into N_2 gas (Mulder et al., 1995; Thamdrup and Dalsgaard, 2002; Kuypers et al., 2003). It has been suggested that anammox may even eliminate more fixed-N than water column denitrification in some oxygen minimum zones (Kuypers et al., 2005; Lam et al., 2009), but just how important of a role anammox plays in the global fixed-N inventory has yet to be determined.

Denitrifiers preferentially consume $^{14}NO_3^-$ leaving the residual oceanic NO_3^- pool strongly enriched in the heavier ^{15}N, with N isotope enrichment factors between 20 – 30‰ (Cline and Kaplan, 1975; Liu and Kaplan, 1989; Brandes et al., 1998; Altabet et al., 1999b; Voss et al.,

2001b). Sedimentary denitrification is generally limited by the amount of NO_3^- that diffuses into the reactive zones within the sediments. Therefore, it consumes nearly all of the influxing NO_3^- available, leaving nearly unaltered $\delta^{15}N$ values in the overlying waters (Brandes and Devol, 1997; Brandes and Devol, 2002; Sigman et al., 2003). The average oceanic $\delta^{15}NO_3^-$ value near 5‰ (Sigman et al., 1997; Sigman et al., 1999) can be interpreted as the balance between the isotope effects of water column denitrification, sedimentary denitrification, and N_2 fixation (Brandes and Devol, 2002; Deutsch et al., 2004; Galbraith et al., 2004; Altabet, 2007).

The $\delta^{15}N$ signal in the water column and sea floor sediments is also affected by fractionation processes within the food chain. Marine algae preferentially assimilate the lighter ^{14}N into their biomass with a range of enrichment factors estimated in the field between 4 – 15‰ (Wada, 1980; Altabet et al., 1991; Altabet et al., 1999b; Sigman et al., 1999; Altabet and Francois, 2001; Karsh et al., 2003; DiFiore et al., 2006). Nitrogen is not lost or gained from the ocean during algal NO_3^- assimilation, but the spatial separation between net assimilation and remineralization can cause a trend of decreasing $\delta^{15}NO_3^-$ with depth. Distinguishing between the different isotope effects remains a challenge, especially in regions where multiple N-transformational processes are occurring within close proximity.

This study, for the first time to our knowledge, includes a dynamic nitrogen isotope module embedded within an existing global ocean-atmosphere-sea ice-biogeochemical model. This allows a direct comparison with nitrogen isotope observations, whereas previous box model studies could only be used more qualitatively (Giraud et al.; Deutsch et al., 2004). We provide a detailed description of the nitrogen isotope model and an assessment of its skill in reproducing present-day $\delta^{15}NO_3^-$ observations. Comparison of model results with $\delta^{15}N$ observations will also be used to help to quantify processes that affect the global oceanic distribution of $\delta^{15}N$. Sensitivity experiments illustrate the individual isotope effects of different processes on the spatial distribution of the N isotopes. In combination with measurements in ocean sediments and in the water column, the model can be a tool to better understand variations of $\delta^{15}N$ and the nitrogen cycle in the past and present.

2.2 Model Description

2.2.1 Physical Model

The physical model is based on the University of Victoria Earth System Climate Model (Weaver et al.), version 2.8. It includes a global, three-dimensional general circulation model of the ocean (Modular Ocean Model 2) with physical parameterizations such as diffusive mixing along and across isopycnals, eddy induced tracer advection (Gent and Mcwilliams, 1990) and a scheme for the computation of tidally induced diapycnal mixing over rough topography (Simmons et al., 2004). Nineteen vertical levels are used with a horizontal resolution of 1.8ºx3.6º. To improve the simulation of equatorial currents, we have increased the meridional resolution in the tropics to 0.9º (between 10ºS and 10ºN and smoothly transitioning to 1.8º at 20ºN/S) and added an anisotropic viscosity scheme (Large et al., 2001). A more detailed description of this parameterization and its effect on the equatorial circulation is provided in Supplementary Material 1. To account for the overestimated ventilation in the North Pacific, an artificial stratifying force equal to 0.04 Sv of freshwater is applied over the surface north of 55° in the Pacific and compensated elsewhere. A two dimensional, single level energy-moisture balance model of the atmosphere and a state-of-the-art dynamic-thermodynamic sea ice model are used, forced with prescribed NCEP/NCAR monthly climatological winds.

2.2.2 Marine Ecosystem Model

The marine ecosystem model is an improved version of the NPZD (Nutrient, Phytoplankton, Zooplankton, Detritus) ecosystem model of (Schmittner et al., 2008) (Figure 2.1). The organic variables include two classes of phytoplankton, N_2-fixing diazotrophs (P_D) and a "general" NO_3^- assimilating phytoplankton class (P_G), as well as zooplankton (Z) and organic detritus (D). The inorganic variables include dissolved oxygen (O_2) and two nutrients, nitrate (NO_3^-) and phosphate (PO_4^{3-}), both of which are consumed by phytoplankton and remineralized in fixed elemental ratios ($R_{N:P}$ = 16, $R_{O:P}$ = 170). We note, though, that most diazotrophs have been found to have a $R_{N:P}$ of 50:1 and sometimes higher (e.g., (Letelier and Karl, 1996, 1998b)). This simplification is one of the reasons why the nitrogen surplus N'= $NO_3^- - 16PO_4^{3-}$ is generally underestimated in surface waters in the model (Figure 2.10). In

addition to water column denitrification and N_2 fixation, we now include a parameterization for sedimentary denitrification (see equation 2.? and Figure 2.2), based on the flux of organic carbon into the sea floor sediments (Middelburg et al., 1996). Since the model underestimates coastal upwelling, which drives large fluxes of organic carbon to the sea floor sediments, this parameterization is tuned to fit the global mean $\delta^{15}NO_3^-$ of 5‰ by multiplying the sedimentary denitrification equation by a constant factor (α_{SD} = 4.5). The complete marine ecosystem model description is provided in Section 2.8. A comparison of the global distribution of NO_3^-, O_2, and N' with World Ocean Atlas 2005 (WOA05) observations is shown in Figure 2.10.

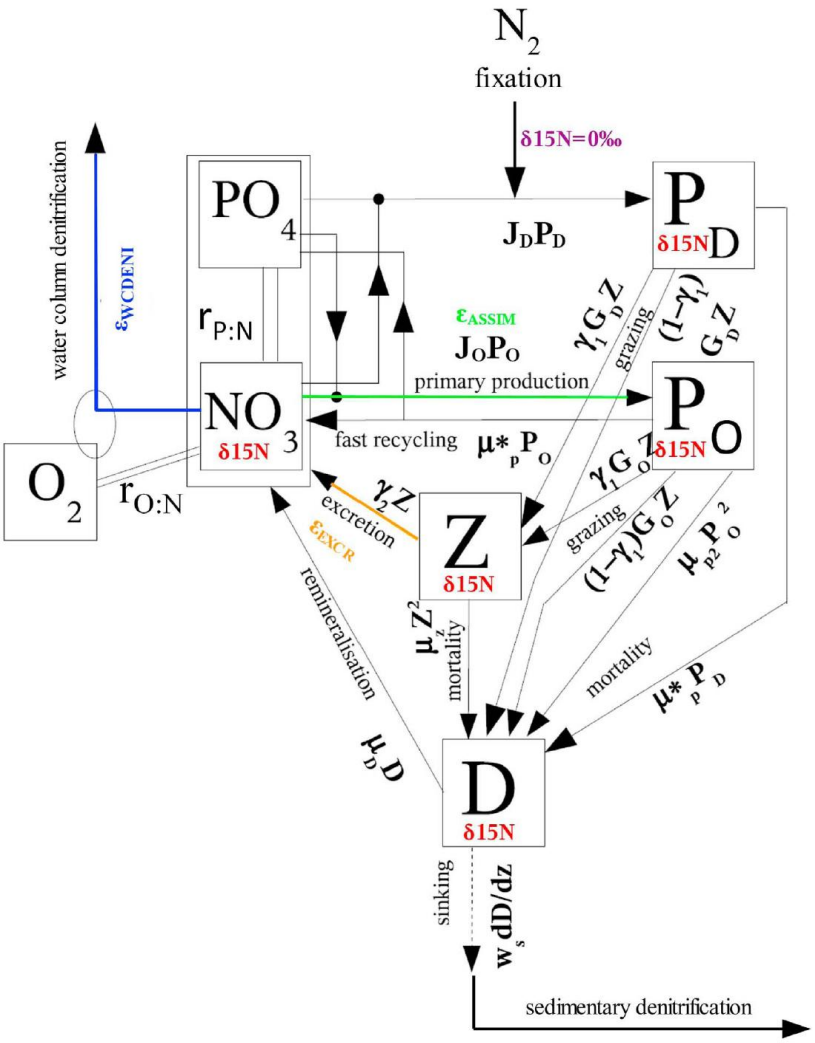

Figure 2.1. Schematic of the marine ecosystem model with the nitrogen isotope model parameters in color.

Global rates of model N_2 fixation, water column denitrification, and sedimentary denitrification are 107, 72.0, and 35.4 Tg N yr^{-1}, respectively. The relatively low model sedimentary to water column denitrification ratio of ~1:2 compared to other estimates from one-box models ranging from ~1:1 to ~4:1 (Brandes and Devol, 2002; Altabet, 2007) is mostly due to the "dilution effect" (see (Deutsch et al., 2004)), which reduces the actual isotope effect of water column denitrification as NO_3^- is locally consumed, an effect not incorporated in one-box models (see also Section 2.4.2). This results in a lower sedimentary to water column denitrification ratio needed to set the global mean $\delta^{15}NO_3^-$ to 5‰ (Altabet, 2007). We note that N' is still too high in the Bering Sea (Figure 2.10), where sedimentary denitrification is known to occur (Lehmann et al., 2005), suggesting that our simulated rate of sedimentary denitrification is too small.

Suboxic water, where water column denitrification occurs, is present in three main locations of the present-day oceans: the Eastern Tropical North Pacific (ETNP), the Eastern Tropical South Pacific (ETSP) and the Arabian Sea (Figure 2.10). Deficiencies in the physical circulation model simulate suboxic water in only one of these locations, the ETNP. The physical circulation model integrates coastal upwelling over a horizontal extent that is too large (due to its coarse resolution), which results in the underestimation of upwelling, export production, and the remineralization of organic matter at depth. This bias leads to too high O_2 concentrations, larger than required for water column denitrification, in the ETSP and the Arabian Sea. Suboxia in the so-called "shadow zone" of the ETNP is simulated better and investigated more in Section 2.4.2. In the model, some water column denitrification also occurs in the Bay of Bengal and off SW Africa (Figure 2.2c), which has not been observed in the real ocean. However, the anammox reaction, which also eliminates fixed-N in the water column, has been found to occur off SW Africa (Kuypers et al., 2005). Naqvi (2008) measured low decomposition rates in the Bay of Bengal. Effective ballasting and scavenging of organic matter by the massive riverine input of terrestrial matter, an effect not included in the model, may prevent water column denitrification in the Bay of Bengal, which is close to suboxic.

Diazotrophs grow according to the same principles as algal phytoplankton in the model (see Section 2.8), but we also account for some of their different characteristics. N_2 fixation breaks down of the triple N bond of N_2, which is energetically more costly than assimilating fixed-N (Holl and Montoya, 2005). Therefore, in the model, the growth rate of diazotrophs is lower than that of general phytoplankton. It is zero in waters cooler than 15°C and increases 40% slower with temperature than the growth rate of general phytoplankton. Diazotrophs are not limited by NO_3^- and will thrive in waters that are N-deficient (i.e., low N' as a result of denitrification) in which sufficient P and Fe are available. Denitrification and the propagation of N-deficient waters into the shallow thermocline by physical transport processes creates an ecological niche for diazotrophs in the model, which stimulates N_2 fixation (Tyrrell, 1999a).

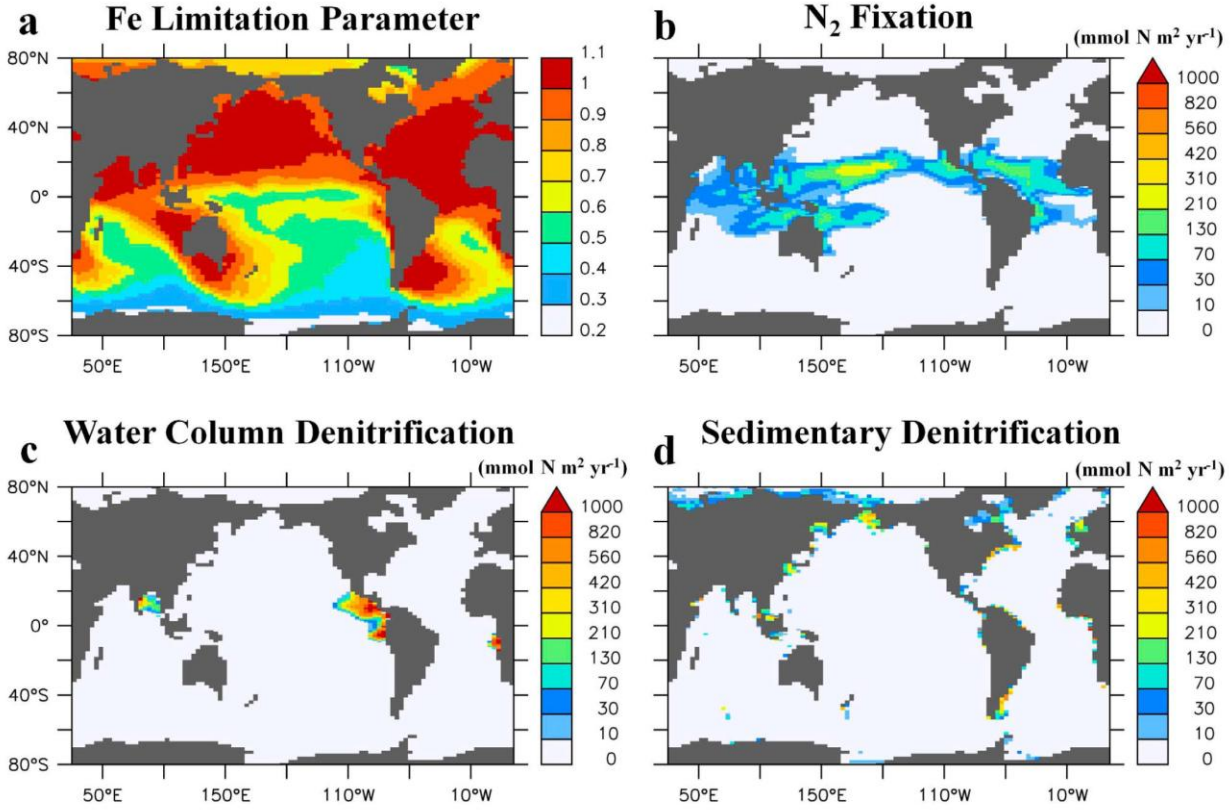

Figure 2.2. (a) Fe Limitation parameter based on an estimate of aeolian dust deposition (Mahowald et al., 2005b) which is multiplied to the maximum growth rate of diazotrophs (see text). Annual vertically integrated rates of (b) N_2 Fixation, (c) water column denitrification, and (d) sedimentary denitrification.

One of the most important and best studied diazotrophs, *Trichodesmium*, also has large iron (Fe) requirements for growth (Sanudo-Wilhelmy et al., 2001). Diazotrophs may depend on aeolian Fe in oligotrophic waters because deep pycnocline inhibits upward mixing of subsurface Fe-replete waters into the euphotic zone (Falkowski; Karl et al., 2002). Therefore, their growth rate is further reduced according to the *Fe Limitation* parameter (Figure 2.2a), where an estimate of aeolian dust deposition (Mahowald et al., 2005b) is scaled between 0 – 1 by multiplying it by a constant factor and setting the maximum value to 1. This is a simple parameterization of Fe limitation of diazotrophy and its full effects are described elsewhere (Somes et al., 2010a). The majority of N_2 fixation in the model occurs in oligotrophic waters "downstream" of denitrification zones where sufficient Fe exists (i.e., via aeolian Fe deposition) (Figure 2.2b). The pattern of N_2 fixation—such as high values in the tropical/subtropical North Pacific, the western tropical/subtropical South Pacific, the western tropical/subtropical South Atlantic, the tropical/subtropical North Atlantic and the Indian Ocean—is mostly consistent with direct observations (e.g., (Karl et al., 2002; Carpenter and Capone, 2008)), with estimates based on the observed NO_3^- deficit and simulated circulation (Deutsch et al., 2007), as well as with results from a more complex ecosystem model (Moore and Doney, 2007a). However, N_2 fixation in our model does not extend northward of 25–30°N in the North Pacific and North Atlantic, whereas some observations show N_2 fixation as far north as 35–40°N (Church et al., 2008; Kitajima et al., 2009).

2.2.3 Nitrogen Isotope Model

The nitrogen isotope model simulates the distribution of the two stable nitrogen isotopes, ^{14}N and ^{15}N, in all N species throughout the global ocean that are included in the marine ecosystem model. Five prognostic variables of $\delta^{15}N$ are embedded within the marine ecosystem model for all species containing nitrogen: NO_3^-, diazotrophs, algal phytoplankton, zooplankton and organic detritus (Figure 2.1). The 'isotope effect' is referred to in the following as the effect that each process has on the respective oceanic isotopic N pool, which depends on the $\delta^{15}N$ value of the substrate, the process-specific enrichment factor (ε), and the degree of utilization ($u_{substrate}$) of the substrate during the reaction:

$$\delta^{15}N_{product} = \delta^{15}N_{substrate} - \varepsilon(1 - u_{substrate}) \quad (2.2)$$

where $u_{substrate}$ is the fraction of the initial substrate used in the reaction. For example, if all of the available substrate is consumed in the reaction (i.e., $u_{substrate} = 1$), the product will incorporate the $\delta^{15}N$ value of the substrate, nullifying any potential fractionation. However, if the rate of utilization is low (i.e., $u_{substrate} \sim 0$), the product will incorporate a relatively light $\delta^{15}N$ value compared to the substrate by the designated enrichment factor (Table 2.1).

Table 2.1: Nitrogen Isotope Model Enrichment Factors

Process	***Symbol***	***Model Enrichment Factor (‰)***	***Field Estimates (‰)*** [a]
Algal NO_3 Assimilation	ε_{ASSIM}	5	4 – 15
N_2 Fixation	ε_{NFIX}	1.5	0 – 2
Excretion	ε_{EXCR}	6	3 – 6
Water Column Denitrification	ε_{WCD}	25	22 – 30
Sedimentary Denitrification	ε_{SD}	0	0 – 4

[a] see Appendix A for references

The processes in the model that fractionate nitrogen isotopes are algal NO_3^- assimilation (ε_{ASSIM} = 5‰), zooplankton excretion (ε_{EXCR} = 6‰), and water column denitrification (ε_{WCD} = 25‰) (Table 2.1). Fractionation results in the isotopic enrichment of the more reactive, thermodynamically preferred, light ^{14}N into the product of each reaction by a process-specific fractionation factor. For a detailed discussion of nitrogen isotope fractionation dynamics see (Mariotti et al., 1981). Although little fractionation occurs during N_2 fixation in the model, it has an important effect on $\delta^{15}N$ by introducing relatively light atmospheric N_2 ($\delta^{15}N$ = 0‰) into the oceanic fixed-N inventory. Sedimentary denitrification also has

been observed to have little effect on the oceanic isotopic N pool because denitrifiers consume nearly all NO_3^- diffusing into the sediments (Brandes and Devol, 1997; Brandes and Devol, 2002; Lehmann et al., 2004). In the model, there is no fractionation during sedimentary denitrification (ε_{SD} = 0 ‰), although this is a simplification of observations . Fractionation during the remineralization of organic matter is not included in the model. The complete nitrogen isotope model description is provided in Section 2.6.

2.3 Nitrogen Isotope Model Results

The model simulates complex spatial patterns of $\delta^{15}NO_3^-$ and δ^{15}N-particulate organic matter (POM) throughout the global ocean (top panels of Figure 2.3). Patterns of surface $\delta^{15}NO_3^-$ and subsurface δ^{15}N-POM are very similar but values are offset by two processes. First, as much as 5‰ offset due to fractionation during NO_3^- uptake by phytoplankton and second, by fractionation during zooplankton excretion, which increases the δ^{15}N-POM through zooplankton mortality (Figure 2.1). High $\delta^{15}NO_3^-$ values (>15‰) are simulated in the eastern subtropical gyres, where surface NO_3^- is depleted, and in regions in close proximity to simulated suboxic zones in the Eastern Pacific, Bay of Bengal, and Eastern Atlantic (again, note that water column denitrification has not been actually observed in the Bay of Bengal and Eastern Atlantic). A clear inter-hemispheric asymmetry appears between the subtropical gyres of the Pacific and Atlantic with higher values of 14-20‰ simulated in the southern hemisphere and smaller values of 10-14‰ in the northern hemisphere. More intermediate δ^{15}N values of 4 − 8‰ are found at high latitudes and near the equator where nutrient utilization is incomplete. δ^{15}N minima (<4‰) are located in the western tropical/subtropical ocean basins, where N_2 fixation occurs in the

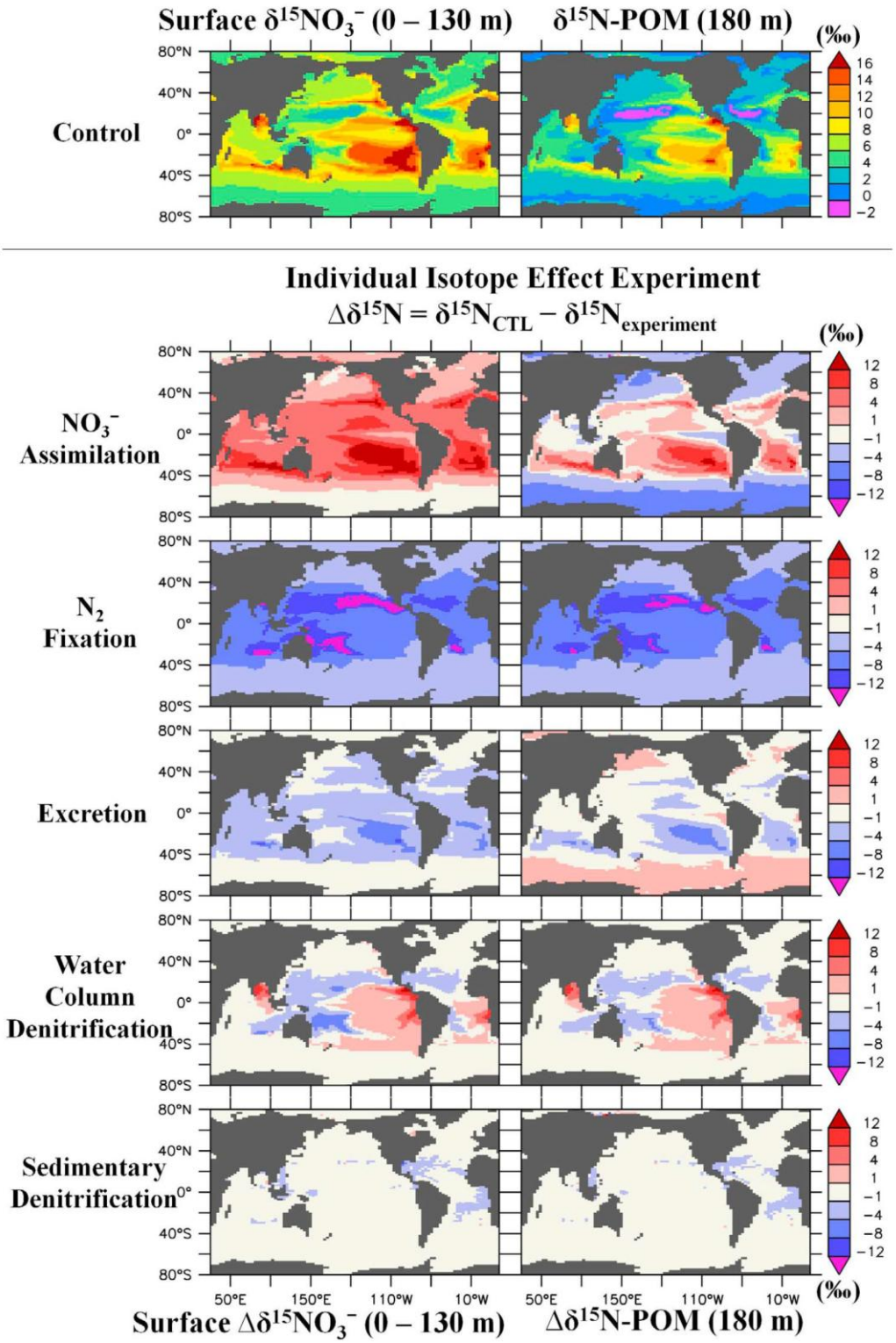

Figure 2.3. Top Panel: Surface $\delta^{15}NO_3^-$ and $\delta^{15}N$ of particulate organic matter (POM) in the model. Bottom Panel: Isotope effect sensitivity experiments where one isotope effect is neglected per simulation and its difference with CTL is shown to illustrate its individual effect on the CTL simulation.

model (Figure 2.2b). The remainder of this section presents a more quantitative description of the contributions of individual processes to these relatively complex spatial patterns of $\delta^{15}NO_3^-$ and δ^{15}N-POM.

Figure 2.3 illustrates results from the full model (CTL) that includes all isotope effects (top panels) together with results from sensitivity experiments designed to isolate the effects of individual processes (bottom panels) on the global δ^{15}N distribution . This is accomplished by removing the isotope effect of one process per experiment and then calculating the difference ($\Delta\delta^{15}$N) with CTL. In the "NO_3^- Assimilation" and "Excretion" experiments, the enrichment factors ε_{ASSIM} and ε_{EXCR}, respectively, are set to zero. In the "N_2 fixation" experiment the diazotroph's N isotope ratio is set equal to that of other phytoplankton at each location. In the "Water Column Denitrification" and "Sedimentary Denitrification" experiments, the entire process is switched off (thereby changing the global N inventory). These latter experiments also show the indirect effect that both denitrification processes have on δ^{15}N through the stimulation of N_2 fixation. In all other isotope effect experiments, the total N inventory does not change.

2.3.1 Algal NO_3^- Assimilation

As phytoplankton preferentially assimilate $^{14}NO_3^-$ into organic matter, they leave the residual inorganic N pool enriched in $^{15}NO_3^-$. This creates an offset between surface $\delta^{15}NO_3^-$ and δ^{15}N-POM that sinks towards the sea floor, which is set by the enrichment factor for NO_3^- assimilation (ε_{ASSIM} = 5‰) ("NO_3^- Assimilation" experiment, Figure 2.3). The surface NO_3^- utilization effect is also affected by the extent to which NO_3^- is depleted. When NO_3^- utilization is low (i.e., NO_3^--replete water exists), which occurs in High Nitrate Low Chlorophyll (HNLC) regions such as the Southern Ocean, the subarctic North Pacific, and the eastern equatorial Pacific, surface $\delta^{15}NO_3^-$ is determined by the source of $\delta^{15}NO_3^-$ being supplied to the surface. Algae will fractionate this NO_3^- during assimilation near the full extent set by the designated enrichment factor because of the abundance of available NO_3^-. In this oceanographic setting, the expected 5‰ difference between $\delta^{15}NO_3^-$ and δ^{15}N-POM is almost fully expressed (i.e., $\delta^{15}P_O = \delta^{15}NO_3^- - \varepsilon_{ASSIM}$ with $u_{ASSIM} \approx 0$ in Equation 2.2). Thus, surface NO_3^- utilization in HNLC regions has a small influence on the surface $\delta^{15}NO_3^-$

signature, but play an important role for δ^{15}N-POM that sinks out of the euphotic zone. This is perhaps most obvious in the Southern Ocean and in the subarctic North Pacific where $\Delta\delta^{15}NO_3^-$ is small, whereas $\Delta\delta^{15}$N-POM is strongly negative ("NO_3^- Assimilation" experiment, Figure 2.3).

A different response is observed in oligotrophic regions where surface NO_3^- is depleted. Once the algae consume nearly all available NO_3^- (which itself becomes enriched in ^{15}N), they acquire the same N isotope signature from the source NO_3^- (i.e., $\delta^{15}P_O = \delta^{15}NO_3^-$ with u_{ASSIM} approaching 1). This drives the high δ^{15}N values in both NO_3^- and POM in the subtropics with maxima in the eastern poleward edges of the gyres (Figure 2.3). Although $\delta^{15}NO_3^-$ values are very high there, they have a small effect on δ^{15}N elsewhere because NO_3^- concentrations are very low. For instance, when low NO_3^- water mixes with nearby water with significantly higher NO_3^-, the resulting $\delta^{15}NO_3^-$ value will be weighted towards the water parcel containing more NO_3^- (see also (Deutsch et al., 2004)). This 'dilution effect' prevents high $\delta^{15}NO_3^-$ values in regions with high surface NO_3^- utilization from having a large impact on the $\delta^{15}NO_3^-$ signature across the nitracline.

2.3.2 Denitrification

Denitrification only occurs at depth but its isotope effect can reach the surface due to upwelling and vertical mixing. Water column denitrification has a large enrichment factor and displays a very strong N isotope effect in close proximity to the simulated suboxic zones in the Eastern Pacific, Bay of Bengal, and Eastern Atlantic ("Water Column Denitrification" experiment in Figure 2.3). The unresolved poleward undercurrents along the western continental margin of the Americas—which could, in the real world, propagate high $\delta^{15}NO_3^-$ away from the subsurface suboxic zones (Kienast et al., 2002)—may restrict the simulated water column denitrification isotope effect too much to regions proximal to the suboxic zones. Both water column and sedimentary denitrification also indirectly lead to lower $\delta^{15}NO_3^-$ values "downstream" of denitrification zones because they create N-deficient water that stimulates additional N_2 fixation, which introduces low δ^{15}N into the ocean. This negative feedback also decreases the horizontal extension of high $\delta^{15}NO_3^-$ signature

originating from suboxic zones, because N_2 fixation introduces much lower $\delta^{15}N$ into the ocean.

2.3.3 N_2 Fixation

The addition of newly fixed, isotopically light atmospheric N_2 ($\delta^{15}N_2 = 0$) by diazotrophs is the reason for the low $\delta^{15}N$ values in the western tropical/subtropical ocean basins. Since denitrification is the only process in the model that creates N-deficient water, and therefore an ecological niche for diazotrophs, the majority of N_2 fixation in the model occurs "downstream" of denitrification zones after phytoplankton have consumed all remaining surface NO_3^- and where sufficient aeolian Fe deposition exists. This low $\delta^{15}NO_3^-$ signature is evident in the subtropical North/South Pacific, the subtropical North/South Atlantic, and the Bay of Bengal ("N_2 Fixation" experiment, Figure 2.3).

2.3.4 Excretion

According to our model results, the N isotope effect of excretion has a smaller influence on the simulated distribution of $\delta^{15}N$ in the global ocean ("Excretion" experiment, Figure 2.3) compared to the other processes discussed above. Its strongest effect is observed in the subtropical South Pacific, where NO_3^- is very low and excretion significantly contributes to the NO_3^- pool by introducing relatively low $\delta^{15}NO_3^-$. Low latitude surface waters elsewhere are generally about 1-4‰ lighter due to fractionation during excretion, with little spatial gradients. At high latitudes the effect on $\delta^{15}NO_3^-$ is very small. We note that this N isotope effect is sensitive to the parameterization for excretion used in this marine ecosystem model version. The excretion rate was tuned so that $\delta^{15}N$-zooplankton is enriched by ~3.4‰ relative to phytoplankton (Minagawa and Wada, 1984).

4. Model Evaluation

The relatively small number of $\delta^{15}N$ observations and the sparse spatial and temporal coverage make a full global model assessment difficult. However, certain regions have been sampled sufficiently to provide a meaningful comparison with the model results. All observations presented here are interpolated horizontally onto a 0.9° x 1.8° grid using a

Gaussian weighted algorithm. The 33 depth levels are consistent with WOA05 and a linear interpolation is used for depths of missing data if nearby data exist. A global database of $\delta^{15}NO_3^-$ measurements has thus been constructed and is available for download (http://mgg.coas.oregonstate.edu/~andreas/Nitrogen/data.html). Figure 2.4 shows the annually averaged global distribution of measured $\delta^{15}NO_3^-$, averaged over 200 – 300 m depth to illustrate the spatial coverage. Seasonal sampling biases exist depending on the region. More details on the data sets can be found in the respective ocean-region subsections that follow. Comparisons are presented for the Southern Ocean (Indian-Pacific sector), the Eastern Tropical North Pacific, the Central Equatorial Pacifc and the Subtropical North Atlantic. Other regions with available $\delta^{15}NO_3^-$ observations included in the dataset but not discussed in the text are the Bering Sea (Lehmann et al., 2005), the Northeast Pacific (Galbraith, 2006), the Arabian Sea (Altabet et al., 1999a) and the eastern Pacific sector of the Southern Ocean (Sigman et al., 1999).

Global measures of model performance for $\delta^{15}NO_3^-$ are presented in Table 2.2. These measures should be interpreted taken into account the highly localized nature of some of the processes as well as the limited regions covered by the database. A displacement in the location of denitrification, for example, will lead to a large decrease in the correlation coefficient and a large increase in the *RMS* errors. The CTL model has a correlation coefficient of 0.68, implying that the model explains 46% of the variance in the observations. The decrease of the correlation coefficient and the increase of the *RMS* error due to the neglection of a particular process can be regarded as the importance that this process plays in explaining the global $\delta^{15}NO_3^-$ observations of the database. The correlation coefficient measures the pattern of variability and neglects the absolute values, whereas the *RMS* error considers the deviation of the model from the observations in absolute values. Neglecting water column denitrification leads to the largest decrease in the correlation coefficient to 0.29 and to the second largest increase in the *RMS* error after N_2 fixation. Neglecting N_2 fixation and algal NO_3^- assimilation lead to the next largest decrease in the correlation coefficient. If sedimentary denitrification or excretion is not included, then the correlation coefficients decrease similarly, with both having relatively weaker effects on the distribution of $\delta^{15}NO_3^-$. Then, according to these measures, water column denitrification is the most important

process determining the global $\delta^{15}NO_3^-$ distribution of available observations in the database, followed by N_2 fixation and algal NO_3^- assimilation, respectively. Finally, sedimentary denitrification and excretion are the least important.

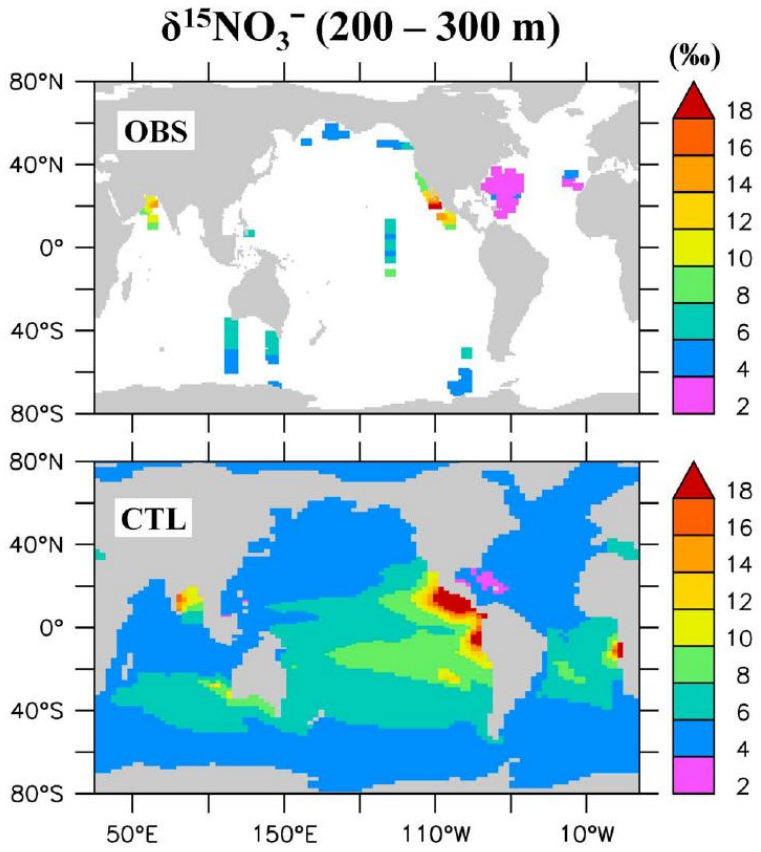

Figure 2.4. Comparison of annual $\delta^{15}NO_3^-$ (‰) averaged between 200 m – 300 m of available observations (OBS) and CTL. Due to the incomplete temporal coverage, seasonal biases in the annually averaged data exist depending on the region.

Table 2.2: Global measures of $\delta^{15}NO_3^-$ model performance: correlation coefficient (*r*), correlation significance (*P*), and root mean squared (*RMS*) error normalized by the standard deviation of the observations.

Model	***r***	***P***	***RMS***
Control	0.68	<0.0001	0.73
Algal NO_3 Assimilation	0.60	0.00046	0.85
N_2 Fixation	0.52	0.0026	2.1
Excretion	0.65	0.00010	0.80
Water Column Denitrification	0.29	0.12	1.1
Sedimentary Denitrification	0.64	0.00010	0.82

2.4.1 Southern Indian-Pacific Ocean

The Southern Ocean represents a critical region of biogeochemical cycling in the ocean because it is the largest open ocean region with incomplete drawdown of the major nutrients. This results in an excess amount of CO_2 at the surface, which is released to the atmosphere (under pre-industrial conditions). The degree to which surface nutrients are utilized here may have profound impacts on ocean-atmosphere exchanges of CO_2. Figure 2.5 shows a comparison with observations recorded in the region (Sigman et al., 1999; Altabet and Francois, 2001; DiFiore et al., 2006). This data sub-set compiles observations from 8 cruises covering various seasons. Since all cruises do not cover the same location, some seasonal biases can be expected, yet, we still decided to use annual averages for maximum spatial coverage. The model does not simulate interannual variability due to the prescribed monthly climatological winds and temporally constant biogeochemical parameters.

Qualitatively, the inverse trend of increasing $\delta^{15}NO_3^-$ with decreasing NO_3^- (Figure 2.5a) is reproduced by the model. However, the slope is underestimated suggesting that the

enrichment factor for algal NO_3^- assimilation used in the model (ε_{ASSIM} = 5‰) is too low, in agreement with (DiFiore et al., 2006) that suggests at least 7‰. The simulated vertical gradient is in good agreement with the observations. Deep water $\delta^{15}NO_3^-$ at 2000 m depth is around 5‰ and slowly increasing throughout the lower pycnocline to around 6‰ at 500 m depth. The model slightly overestimates $\delta^{15}NO_3^-$ between 200 m and 400 m depth, whereas near surface values are slightly underestimated.

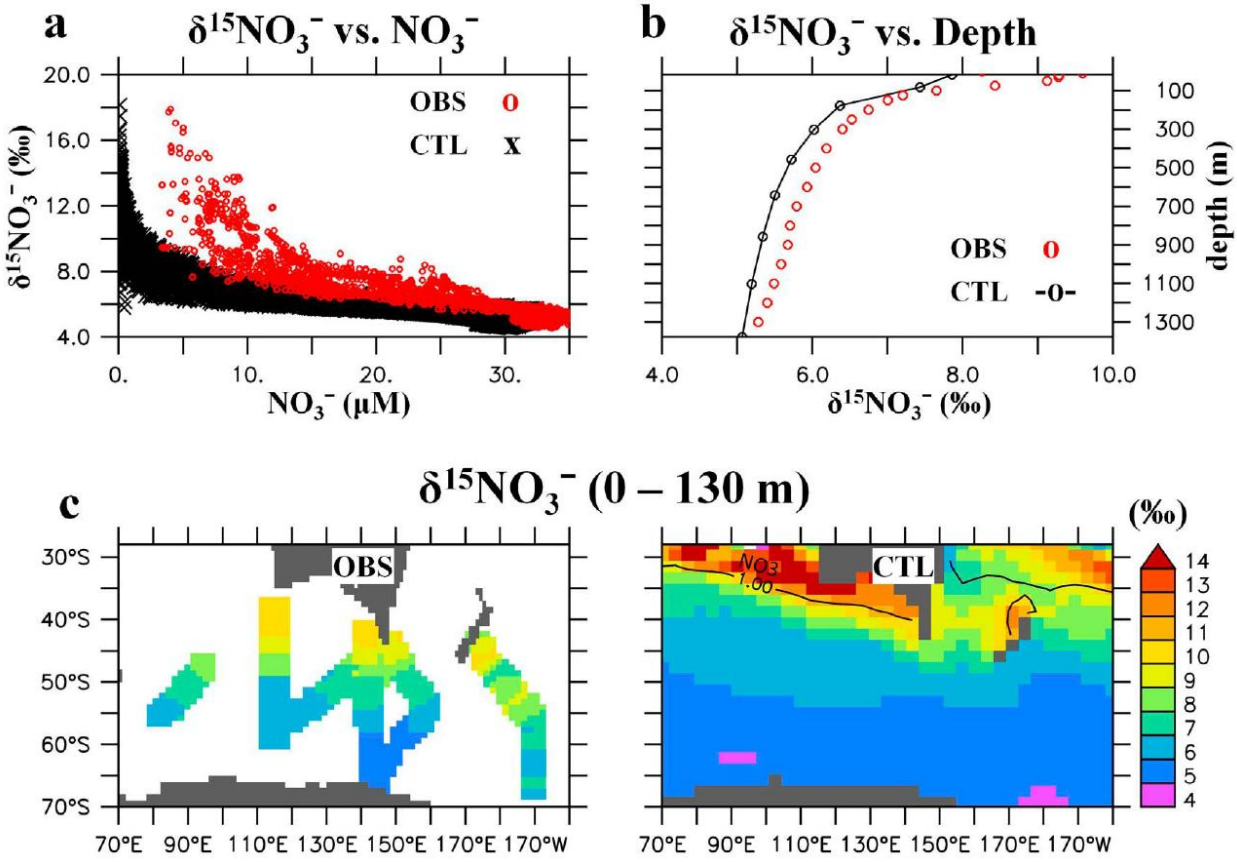

Figure 2.5. Comparison of the Indian-Pacific sector of the Southern Ocean with the δ15NO_3^- database and CTL. (a) $\delta^{15}NO_3^-$ vs. NO_3^-; (b) horizontally averaged (over available data) depth $\delta^{15}NO_3^-$ profiles; (c) surface $\delta^{15}NO_3^-$ and with a 1µM NO_3^- contour line.

A large discrepancy between simulated and observational $\delta^{15}NO_3^-$ is apparent in surface waters north of 40°S off the southern coast of Australia (Figure 2.5c). This bias is due to the fact that the model overestimates the utilization of surface NO_3^- relative to observations there (Figure 2.5c). Where the simulated NO_3^- is almost completely consumed (i.e., $NO_3^- < 1$ µM)

(see Figure 2.5c-contour line), the remaining $\delta^{15}NO_3^-$ values become as high as 18‰. Since none of the existing $\delta^{15}NO_3^-$ observations was collected in such low NO_3^- concentrations (Figure 2.5a), it impossible, at this time, to falsify this aspect of the N isotope model response. We note this heavy $\delta^{15}NO_3^-$ signature in these low NO_3^- waters has little effect on $\delta^{15}NO_3^-$ across the nitracline in the model because the $\delta^{15}N$ signature of very low NO_3^- water becomes diluted out as it mixes with much higher NO_3^- water (see Section 2.3.1).

2.4.2 Eastern Tropical North Pacific

The ETNP contains the largest suboxic zone in the ocean, where water column denitrification occurs. The relatively small spatial scale of suboxic zones makes them difficult for the model to simulate accurately and deficiencies in the coarse resolution physical model prevent it from fully resolving some important physical processes, especially in coastal regions. Underestimating coastal upwelling (due to coarse resolution) results in corresponding underestimation of primary production, organic matter remineralization, and O_2 consumption at depth. This is a major reason for overestimated dissolved O_2 at depth in areas with significant coastal upwelling (e.g., off Peru and NW Mexico) (Figure 2.10), too large for water column denitrification to occur. Preliminary experiments suggest that increased vertical resolution can improve the simulation of productivity and suboxia in the Eastern Tropical South Pacific (not shown).

The ability to reproduce the equatorial undercurrents that transport relatively oxygen-rich water from the western basin is also important for the simulation of the Eastern Pacific suboxic zones. The anisotropic viscosity scheme (Large et al., 2001) improves equatorial dynamics considerably (Section 2.7). The Pacific Equatorial Undercurrent increases from 0.15 m/s to nearly 0.8 m/s, just slightly weaker than observations, which show velocities near 1 m/s (Figure 2.9). The North Equatorial Countercurrent in the model also displays lower current velocities than observed, and does not deliver enough oxygen-rich water directly to the ETNP suboxic zone. This is likely the main reason why the simulated suboxic zone is too large and located too far south (by ~5°) relative to observations (Figure 2.10). This results in higher rates of water column denitrification and higher $\delta^{15}NO_3^-$ values, as well as more N-deficient water in the suboxic zone compared to observations (Figure 2.6).

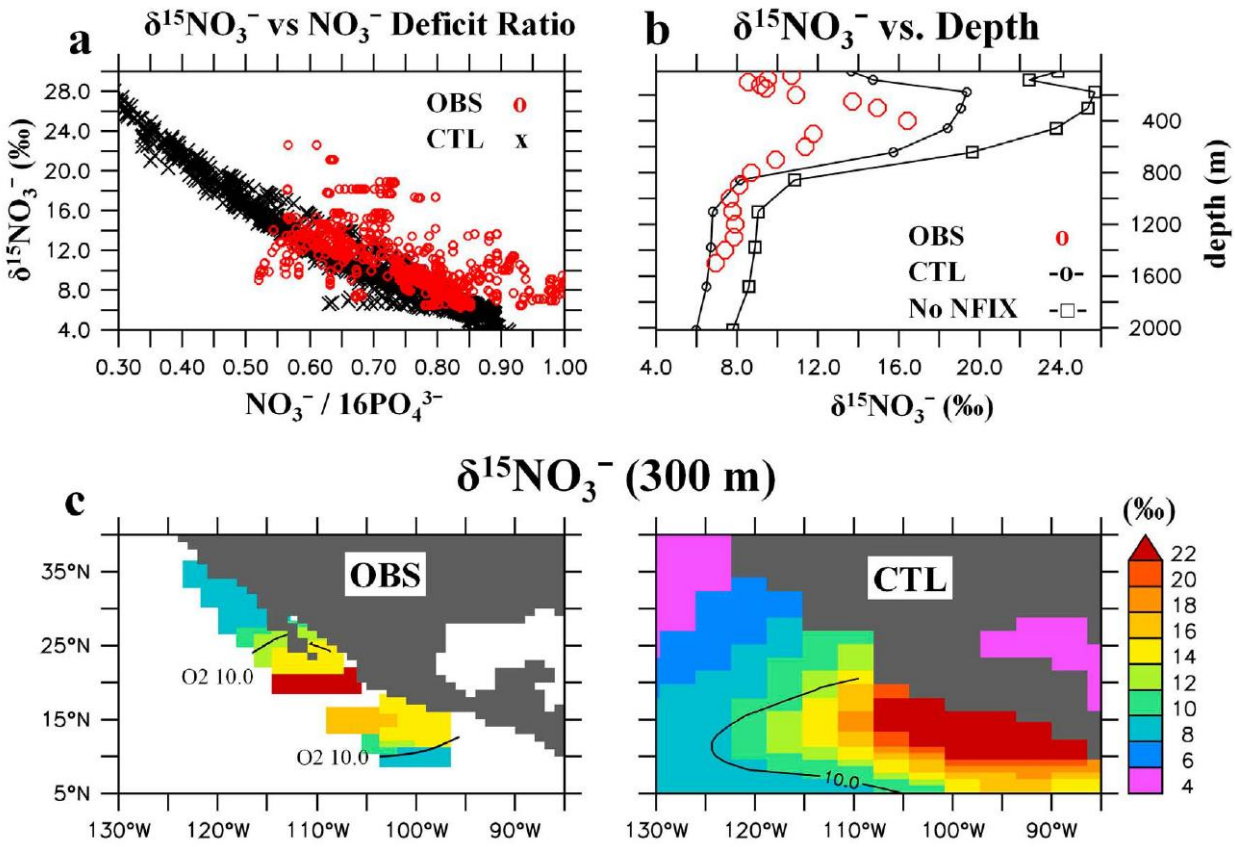

Figure 2.6. Comparison of the ETNP with the $\delta^{15}NO_3^-$ database and CTL. (a) $\delta^{15}NO_3^-$ vs. N' = $NO_3^- - 16PO_4^{3-}$; (b) horizontally averaged (within 10 μM O_2 contour) depth $\delta^{15}NO_3^-$ profiles including the experiment where the isotope effect of N_2 Fixation is neglected (No NFIX); (c) subsurface $\delta^{15}NO_3^-$ with a 10 μM O_2 contour line.

Since the locally high $\delta^{15}NO_3^-$ values exist in too small NO_3^- concentrations, when they transport out of the denitrification zone and mix with water with much higher NO_3^-, the high $\delta^{15}NO_3^-$ value is largely diluted away because the resulting $\delta^{15}NO_3^-$ value is weighted towards the water parcel with more NO_3^-. This "dilution effect" (Deutsch et al., 2004) reduces the impact that water column denitrification has on $\delta^{15}NO_3^-$ outside of denitrification zones, and thus decreases its actual isotope effect on setting the global mean $\delta^{15}NO_3^-$. This is the main reason why the model requires a relatively low sedimentary to water column denitrification ratio of ~1:2 to set the global mean $\delta^{15}NO_3^-$ to 5‰ compared to estimates from one-box models (Brandes and Devol, 2002; Altabet, 2007), which cannot account for any important effects that occur locally within the denitrification zone. We note that our model significantly overestimates NO_3^- consumption by water column denitrification in the

ETNP compared to observations (Figure 2.6a). Therefore, it is likely that our sedimentary to water column denitrification ratio of ~1:2 is too low, but it does highlight the importance that the NO_3^- consumption/dilution effect can have on determining global mean $\delta^{15}NO_3^-$.

Figure 2.6 shows model $\delta^{15}NO_3^-$ compared to observational $\delta^{15}NO_3^-$ data collected during November 1999 (Sigman et al., 2005) and October 2000 [*Altabet*, previously unpublished]. The model captures the general observed trend of increasing $\delta^{15}NO_3^-$ as NO_3^- is consumed during water column denitrification (Figure 2.6a). The model's too low N:P ratio for diazotrophs may partly explain its incapacity to simulate some of the relatively high N' values of observations. The range of simulated values is also likely to be more limited compared to the observations due to the missing interannual and synoptic climate variability in the model. Figure 2.6b compares the horizontally averaged $\delta^{15}NO_3^-$ depth profiles only within the hypoxic zone ($O_2 < 10$ μM) at 300 m (contoured on Figure 2.6c) to account for the displaced OMZ. Within this region, the model is able to capture the general vertical distribution of $\delta^{15}NO_3^-$ seen in the measured data, such as the surface minimum and subsurface maximum.

$\delta^{15}NO_3^-$ in the ETNP decreases towards the surface (Cline and Kaplan, 1975; Brandes et al., 1998; Voss et al., 2001a; Sigman et al., 2005) suggesting a source of isotopically light N at the surface. (Brandes et al., 1998) proposed that in the Arabian Sea as much as 30% of primary production must be supported by N_2 fixation in order to account for the low surface $\delta^{15}NO_3^-$. Other observations also suggest that the decrease in $\delta^{15}NO_3^-$ towards the surface is likely due to the fixation of atmospheric N_2 and the subsequent, closely coupled remineralization-nitrification cycle (Sigman et al., 2005). We test this hypothesis by comparing the observations with the model experiment in which the isotope effect of N_2 fixation is neglected ("No NFIX"). In this case, the model overestimates surface $\delta^{15}NO_3^-$ by ~12‰ (Figure 2.6b) and the surface minimum is not simulated. This experiment demonstrates that the input of isotopically light fixed-N from N_2 fixation in the model best explains the decreasing trend of $\delta^{15}NO_3^-$ observations towards the surface. In the model, 20% of the fixed-N loss via denitrification is re-introduced into the surface by N_2 fixation occurring directly above the denitrification zone in the ETNP. The fact that the difference

between the subsurface maximum and the near surface minimum is underestimated in the model (6‰ versus 8‰ in the observations) suggests that in the real world the locally re-introduced fraction could be larger than 20%.

2.4.3 North Atlantic

Uncertainties regarding processes that can affect the nitrogen isotope signal make it challenging to interpret and simulate nitrogen isotopes in the North Atlantic. Estimates of atmospheric N deposition (Duce et al., 2008b) and the assimilation-remineralization-nitrification cycle are not well constrained. Although atmospheric N deposition may be significant in this region (Michaels et al., 1996; Lipshultz et al., 2002; Knapp et al., 2005; Knapp et al., 2008), its isotopic composition is not well known and therefore is not included in the model at this time. Figure 2.7 shows the comparison of annual model $\delta^{15}NO_3^-$ with available observations from cruises in May 2001 and 2004 (*Altabet and Montoya*, previously unpublished), October 2002 (Knapp et al., 2008), and May 2005 (Bourbonnais et al., 2009). The model overestimates the $\delta^{15}NO_3^-$ values everywhere, by 0.9‰ on average and by 2‰ at 200 m depth, presumably mostly due to the underestimation of N_2 fixation, but possibly also because atmospheric N deposition and/or fractionation during the remineralization of organic matter are not included. Both of these processes would act to decrease subsurface values of $\delta^{15}NO_3^-$. Underestimated N' in the North Atlantic (Figure 2.C1) also indicates too little N_2 fixation, but we again note the too low N:P ratio for diazotrophs also contributes to this N' underestimation to some degree.

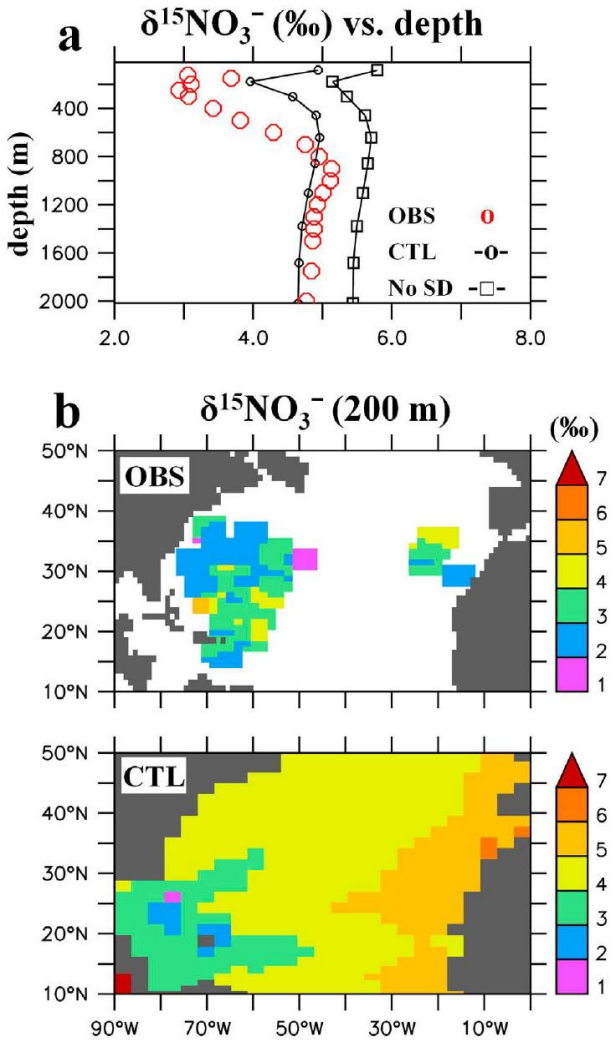

Figure 2.7. Comparison of the North Atlantic with the $\delta^{15}NO_3^-$ database and CTL. (a) horizontally averaged (over available data) depth $\delta^{15}NO_3^-$ profiles including the experiment where sedimentary denitrification is neglected (No SD); (b) subsurface $\delta^{15}NO_3^-$.

N_2 fixation is most likely underestimated in the model because it does not consider dynamic elemental cycling of the microbial loop. It has been suggested that DOP is more labile relative to DON and recycles through the microbial loop more efficiently, which can help relieve diazotrophs of P limitation in this region (Wu et al., 2000) and enhance N_2 fixation. The model is able to reproduce the pattern of low $\delta^{15}NO_3^-$ in the thermocline qualitatively, just not quantitatively to the extent present in the observations. Sedimentary denitrification in the North Atlantic stimulates just enough N_2 fixation in the model to generate a subsurface $\delta^{15}NO_3^-$ minimum. When sedimentary denitrification is switched off ("No SD"), the

thermocline minimum is not present. This suggests that sedimentary denitrification is an important factor influencing N_2 fixation in the Subtropical North Atlantic, but not the only factor.

2.5 Discussion and Conclusions

A new model of nitrogen isotopes has been implemented into the three-dimensional ocean component of a global Earth System Climate Model capable of millennial timescale simulations. Despite some model deficiencies, we have shown that this model can successfully reproduce the general spatial patterns of $\delta^{15}NO_3^-$ measured in the ocean. Sensitivity experiments allowed us to isolate the individual N isotope effects of various N-transformational processes on the global distribution of $\delta^{15}N$. Algal NO_3^- assimilation, water column denitrification, and N_2 fixation all have strong influences in setting the global patterns of $\delta^{15}NO_3^-$ in the ocean, whereas the effect of zooplankton excretion is weaker.

These simulations show that the isotope effect of algal NO_3^- assimilation can drive very large spatial gradients in both $\delta^{15}NO_3^-$ and δ^{15}N-POM depending on the ocean environment (Figure 3). In HNLC areas where surface NO_3^- utilization is low and algae are able to fractionate NO_3^- at their designated enrichment factor, the δ^{15}N-POM signature decreases. However, when NO_3^- utilization is high, the δ^{15}N-POM signature is more similar to the $\delta^{15}NO_3^-$ value it consumes because the effective degree of fractionation becomes much lower (see Section 2.3.1). Surface NO_3^- utilization gradients can transition rapidly, for example due to changes in ocean circulation or atmospheric Fe deposition, and can possibly drive large and rapid changes in $\delta^{15}NO_3^-$ and δ^{15}N-POM. The important influence of surface NO_3^- utilization on the global distribution of N isotopes in the model suggests that changes in surface NO_3^- utilization patterns throughout Earth's history could contribute to large fluctuations in $\delta^{15}N$ observed in sediment records, especially near fronts where large surface NO_3^- gradients exist (See also (Altabet and Francois, 1994; Farrell et al., 1995; Sigman et al., 1999; Brunelle et al., 2007; Galbraith et al., 2008; Robinson and Sigman, 2008)).

The model simulates a strong direct and indirect isotope effect of denitrification. High $\delta^{15}NO_3^-$ produced by water column denitrification has clear regional impacts and is also

responsible for overall elevated $\delta^{15}NO_3^-$ of the ocean relative to the N_2 fixation source (see below). The indirect effect of both water column and sediment denitrification is mediated by the production of N-deficient water, which creates an ecological niche for diazotrophs. This stimulates additional N_2 fixation when other suitable conditions for N_2 fixation also exist (e.g., warm (> 20°C), N-depleted water with sufficient P and Fe). This indirect effect also attenuates the horizontal circulation of high $\delta^{15}NO_3^-$ waters, originating from regions of water column denitrification, which causes its direct isotope effect to be regionalized to suboxic zones in the model.

Key features of the model have been identified that are in need of further development. The coarse resolution physical circulation model does not fully resolve the dynamics of coastal upwelling regimes, which in part drive the flux of organic matter towards the sea floor sediments and its remineralization in the water column, as well as indirectly influences ventilation of suboxic zones. This is critical in the simulation of water column denitrification and sedimentary denitrification, which are important processes with respect to the global N isotope balance. Future model versions will include additional vertical levels to better resolve continental shelves as well as higher horizontal resolution. The model neglects dynamic elemental stoichiometry such as high N:P ratios of diazotrophs and the more efficient recycling of DOP relative to DON in microbial loops, which can help relieve diazotrophs of their P limitation and allow them to fix additional N_2 into the oceanic fixed-N pool in oligotrophic waters. The ecosystem model also suffers from the exclusion of Fe as a prognostic tracer preventing it from being able to simulate differences in ecosystems limited by macronutrients (NO_3^-, PO_3^{3-}) versus micronutrients (Fe).

Future applications of this model will include simulations of past climates, and direct comparison with $\delta^{15}N$ sediment records will be used to test the model results. This approach may be a useful to quantify past interactions between the marine N cycle and its isotopes, as well as their impact on climate and may provide new insights into important physical and biogeochemical changes throughout Earth's history.

2.6 Appendix: Nitrogen Isotope Model

The open system fractionation equation is used for fractionation during algal NO_3^- assimilation (Altabet and Francois, 2001):

$$\delta^{15}P_O = \delta^{15}NO_3^- - \varepsilon_{ASSIM}(1 - u_{NO3}), \quad (2.3)$$

where $\delta^{15}P_0$ is the δ^{15}N of phytoplankton biomass assimilated during one time step, Δt, and u_{NO3} is the fraction of NO_3^- available that is converted into biomass ($u_{ASSIM} = J_O P_O \times \Delta t / NO_3^-$). When algae assimilate all available NO_3^- into their biomass (i.e. $u_{ASSIM} = 1$) they will incorporate the same δ^{15}N value as that of the source material. Many studies have estimated the fractionation factor in both laboratory and ocean environments. A wide variety of values have been reported in culture settings ranging from 0.7‰ to 23‰ (Wada and Hattori, 1978; Montoya and McCarthy, 1995; Waser et al., 1998; Needoba et al., 2003; Granger et al., 2004). A more confined range has been observed in field estimates from 4‰ to 15‰ (Wada, 1980; Altabet et al., 1991; Altabet et al., 1999b; Sigman et al., 1999; Altabet and Francois, 2001; Karsh et al., 2003; DiFiore et al., 2006). In our model we choose a constant value of 5‰ which is near the majority of estimates, although it is important to bear in mind the uncertainty in the parameter choice and the possibility that it varies in space and time.

Nitrate in suboxic waters have been observed to have much higher δ^{15}N values due to fractionation during denitrification. Observations from present day suboxic zones in the Eastern Tropical North Pacific (ETNP) and the Arabian Sea (AS) have reported fractionation factors ranging from 22-30‰ (Cline and Kaplan, 1975; Liu and Kaplan, 1989; Brandes et al., 1998; Altabet et al., 1999b; Voss et al., 2001a); we adopt a value of 25‰ in the model. Note that because these estimates were derived from field studies in which the isotope effect was estimated from the total nitrogen loss, they implicitly include the effect of anammox (Galbraith et al., 2008). Fractionation during denitrification is also simulated using the open system fractionation equation

$$\delta^{15}NO_3^{OX} = \delta^{15}NO_3^- - \varepsilon_{WCD}(1 - u_{NO3}), \quad (2.4)$$

where NO_3^{OX} is the oxygen-equivalent reduction of nitrate converted into N_2 gas during denitrification. The term u_{DENI} is the fraction of available NO_3 which is reduced into N_2 gas ($u_{NO3} = \mu_D D$ x 0.8 x $R_{O:N}$ x r^{NO3}_{sox} x L_{NO3} x Δt / NO_3).

Excretion is the process responsible for the step-wise enrichment of $\delta^{15}N$ along the trophic chain in our model and is simulated using the instantaneous fractionation equation:

$$\delta^{15}NO_3^- = \delta^{15}Z - \varepsilon_{EXCR}. \quad (2.5)$$

The instantaneous fractionation equation is used because excretion will always be a small fraction of the total zooplankton biomass and has been measured to be depleted by ~6‰ relative to its body (Montoya, 2008), which is the source of the excreted nitrogen. This leads to the average enrichment of ~3.4 per trophic level (Minagawa and Wada, 1984).

Implementing these fractionation equations into the marine ecosystem model requires us to consider the exchanges of ^{14}N and ^{15}N between the various N pools separately. Total nitrogen abundance now has the form

$$N = {}^{14}N + {}^{15}N \quad (2.6)$$

for each variable in the isotope model. A fractionation coefficient is calculated for each process so the same equations for total N can be applied to ^{15}N (Giraud et al., 2000). For example, consider fractionation during algal NO_3^- assimilation. The isotopic ratio of new nitrogen biomass (P_O) is found using equations (1) and (2):

$${}^{15}P_O = \beta_{ASSIM}\, {}^{14}P_O \quad (2.7)$$

where

$$\beta_{ASSIM} = \frac{{}^{15}NO_3}{{}^{14}NO_3} - \frac{\varepsilon_{ASSIM}(1-u_{NO3})R_{std}}{1000}. \quad (2.8)$$

Applying equations (A4) and (A5) gives the amount of new $^{15}P_O$ relative to the amount of total new nitrogen biomass, which is given by the primary production ($J_O P_O$), calculated by the marine ecosystem model.

$$^{15}P_O = \frac{\beta_{ASSIM}}{1+\beta_{ASSIM}} J_O P_O \tag{2.9}$$

Analogous derivations can be done for all fractionation coefficients. The time-dependent set of equations for ^{15}N which are embedded into the marine ecosystem model are as follows:

$$\frac{\partial^{15} NO_3}{\partial t} = \left(R_D \mu_D D + \frac{\beta_{EXCR}}{1+\beta_{EXCR}} \gamma_2 Z + R_P \mu_P P_O - \frac{\beta_{ASSIM}}{1+\beta_{ASSIM}} J_O P_O - \frac{\beta_{ASSIM}}{1+\beta_{ASSIM}} u_N J_D P_D \right) \times \left[1 - \frac{\beta_{WCD}}{1+\beta_{WCD}} 0.8 R_{O:N} r_{sox}^{NO3} L_{NO3} \right] \tag{2.10}$$

$$\frac{\partial^{15} P_O}{\partial t} = \frac{\beta_{ASSIM}}{1+\beta_{ASSIM}} J_O P_O - R_P \mu_P P_O - R_{P_O} G(P_O) Z - R_{PO} \mu_{P2} P_O^2 \tag{2.11}$$

$$\frac{\partial^{15} P_D}{\partial t} = \left(\frac{\beta_{ASSIM}}{1+\beta_{ASSIM}} u_N + \frac{\beta_{NFIX}}{1+\beta_{NFIX}} (1-u_N) \right) J_D P_D + -R_{P_D} G(P_D) Z - R_{P_D} \mu_P P_D \tag{2.12}$$

$$\frac{\partial^{15} Z}{\partial t} = \gamma_1 \left[R_{P_O} G(P_O) + R_{P_D} G(P_D) \right] Z - \frac{\beta_{EXCR}}{1+\beta_{EXCR}} \gamma_2 Z - R_Z \mu_Z Z^2 \tag{2.13}$$

$$\frac{\partial^{15}D}{\partial t} = (1-\gamma_1)\left[R_{P_O} GP_O + R_{P_D} GP_D \right] Z + R_{P_D}\mu_P P_D + R_{P_O}\mu_{P2} P_O^2 + R_Z \mu_Z Z^2 - R_D \mu_D D - R_D w_D \frac{\partial D}{\partial z}$$

(2.14)

where $R_{N=PO,\ PD,\ Z,\ D} = {}^{15}N / ({}^{14}N + {}^{15}N)$ is the ratio of heavy over total nitrogen. The complete parameter description is provided in Auxiliary Material: Appendix 2C. Here it suffices to note that the equations for total nitrogen (${}^{14}N + {}^{15}N$) are identical to the ones of ${}^{15}N$ except that $R_X = \beta_X/(1+\beta_X) = 1$ in the total nitrogen equations.

The model was carefully tested with zero fractionation in order to quantify and minimize numerical errors, which can occur for example due to slightly negative values of biological tracers caused by inaccuracies of the advection scheme. The biological code was adjusted to avoid negative concentrations as much as possible. Initially numerical errors in $\delta^{15}N$ ranged from ± 1‰ in grid points at the sea floor to ± 0.1‰ in the upper ocean. Setting $R_{std} = 1$ instead of $R_{std} = 0.0036765$, the actual atmospheric N_2 isotope ratio, reduces the numerical errors by over an order of magnitude. R_{std} is set to the value 1 so both isotope variables will be on the same order of magnitude. This prevents ${}^{15}N$ from becoming very close to zero as often, where inaccuracies of the advection scheme can cause it to be negative. This modification amounts to a scaling of ${}^{15}N$ and ${}^{14}N$ by a constant factor which does not affect the $\delta^{15}N$ dynamics. The remaining numerical errors of ±0.1‰ in the deep ocean and ±0.01‰ in the upper ocean are two orders of magnitude smaller than the observed variability. The model is integrated for over 5,000 years as it approaches equilibrium.

2.7 Appendix: Anisotropic Viscosity Scheme

Horizontal viscosity is required in ocean circulation models to resolve the western boundary currents and to smooth out numerical noise (Munk, 1950; Bryan et al., 1975; Large et al., 2001). Isotropic viscosity schemes apply one large viscosity value needed for these purposes everywhere in the model which is not physically realistic outside of these specific areas. A major deficiency when using isotropic viscosities is the underestimation of the Pacific Equatorial Undercurrent which in models is typically about 10% compared to what is

observed (Large et al., 2001). The Pacific Equatorial Undercurrent is a source of relatively warm, fresh, nutrient-poor and oxygen-rich water from the Western Pacific that flows into the Eastern Pacific which has important physical and biogeochemical effects. We implement an anisotropic viscosity scheme similar to (Large et al., 2001) in the tropics to better resolve equatorial dynamics. Figure 2-B1 shows zonal and meridional surface viscosities used and Figure 2-B2 shows a comparison at 125°W of the simulated currents with observations in the Eastern Tropical Pacific (Kessler, 2006), the region most significantly affected by the anisotropic viscosity scheme.

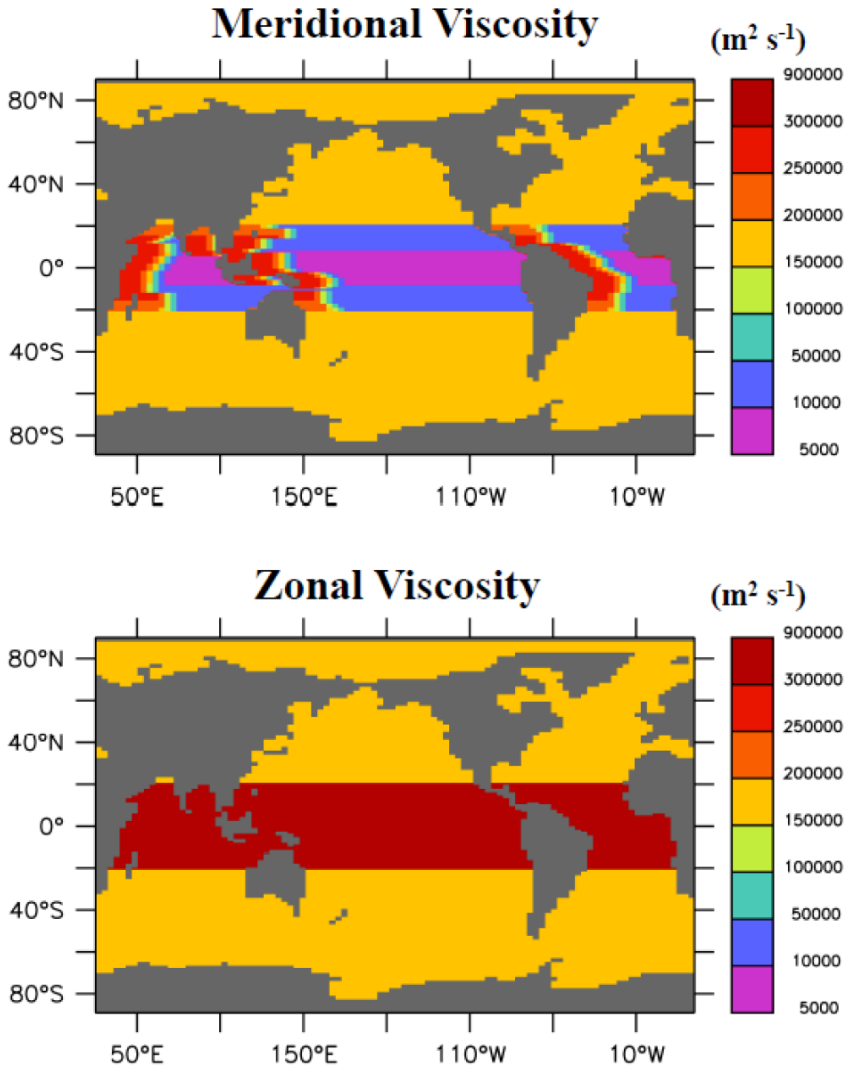

Figure 2.8 Surface viscosity in the meridional and zonal directions.

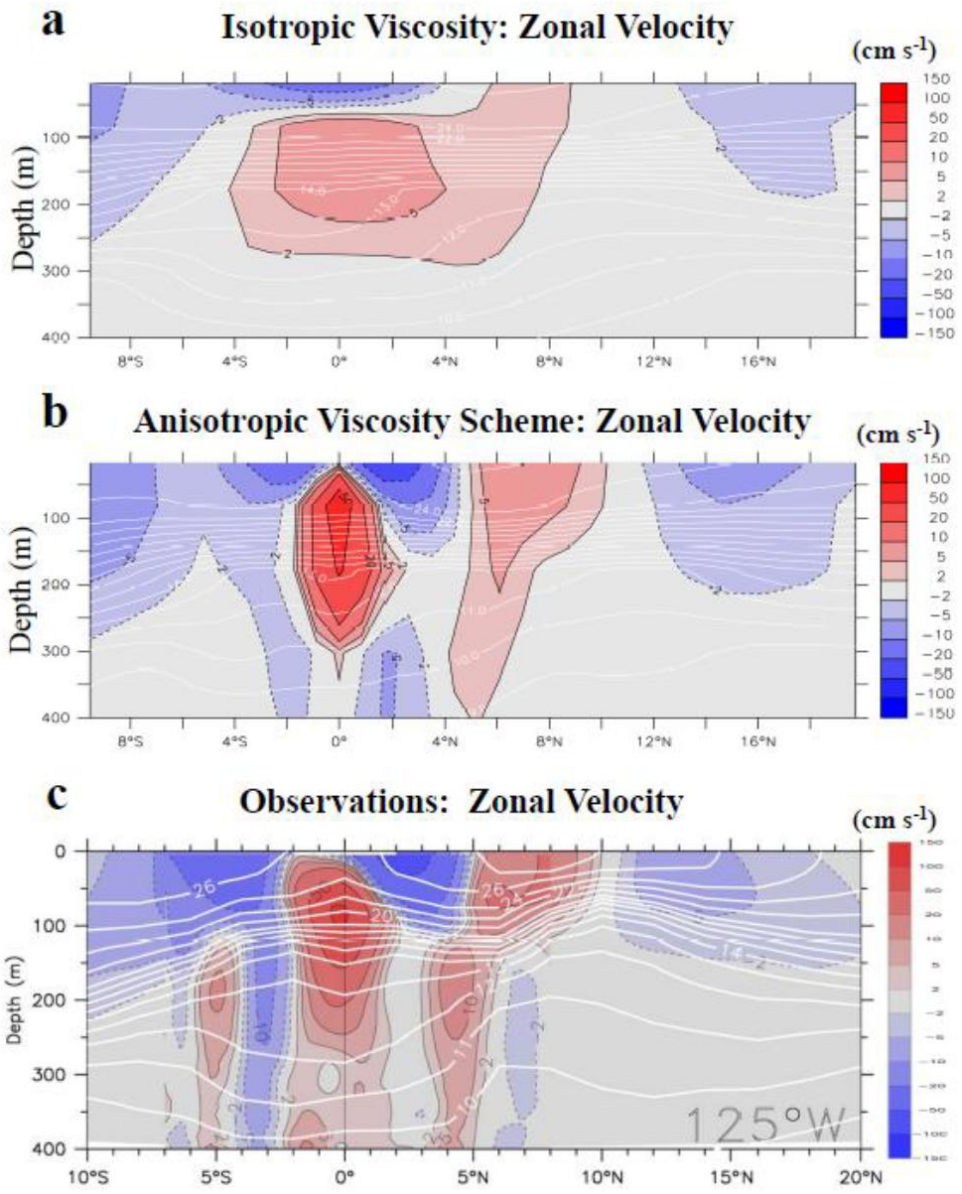

Figure 2.9 Annual zonal velocity along 125°W using (a) an isotropic viscosity, (b) the anisotropic viscosity scheme and (c) observations from (Kessler, 2006).

2.8 Appendix: Marine Ecosystem Model

This appendix provides a description of the parameters used in the full set of time-dependent equations in the marine ecosystem model (Table 2.3). It suffices to note that the equations for total nitrogen ($^{14}N + {}^{15}N$) ecosystem variables are identical to the ones of ^{15}N if $R_X = \beta_X/(1+\beta_X) = 1$, which are located in Appendix 2A.

Table 2.3 Marine Ecosystem Parameters.

Parameter	*Symbol*	*Value*	*Units*
Phytoplankton (P_O, P_D) Coefficients			
Initial slope of P-I curve	α	0.1	$(W\ m^{-2})^{-1}\ d^{-1}$
Photosynthetically active radiation	*PAR*	0.43	
Light attenuation in water	k_w	0.04	m^{-1}
Light attenuation through phytoplankton	k_c	0.03	$m^{-1}(mmol\ m^{-3})^{-1}$
Light attenuation through sea ice	k_i	5	m^{-1}
Maximum growth rate	a	0.14	d^{-1}
Half-saturation constant for N uptake	k_N	0.7	$mmol\ m^{-3}$
Specific mortality rate	μ_P	0.05	d^{-1}
Fast recycling term (microbial loop)	μ^*_{P0}	0.012	d^{-1}
Diazotrophs' handicap	c_D	0.4	
Zooplankton (Z) Coefficients			
Assimilation efficiency	γ_1	0.925	
Maximum grazing rate	g	1.575	d^{-1}
Prey capture rate	ε	1.6	$(mmol\ m^{-3})^{-2}d^{-1}$
Mortality	μ_Z	0.34	$(mmol\ m^{-3})^{-2}d^{-1}$
Excretion	γ_2	0.05	d^{-1}
Detritus (D) Coefficients			
Remineralization rate	μ_{D0}	0.048	d^{-1}
Sinking speed at surface	w_{D0}	7	$m\ d^{-1}$
Increase of sinking speed with depth	m_w	0.04	d^{-1}
E-folding temperature of biological rates	T_b	15.65	°C
Other Coefficients			
Molar elemental ratios	$R_{O:N}$	10.6	
	$R_{N:P}$	16	

The function J_O provides the growth rate of non-diazotrophic phytoplankton, determined from irradiance (I), NO_3^- and PO_4^{3-},

$$J_O(I, NO_3^-, PO_4^{3-}) = min(J_{OI}, J_{Omax}u_N, J_{Omax}u_P) \quad (2.15)$$

The maximum growth rate is dependent only on temperature (T):

$$J_{Omax} = a \bullet \exp(T/T_b) \quad (2.16)$$

such that growth rates increase by a factor of ten over the temperature range of -2 to 34 °C. We use a=0.14 d^{-1} for the maximum growth rate at 0 °C which was determined to optimize surface nutrient concentrations. Under nutrient-replete conditions, the light-limited growth rate J_{OI} is calculated according to:

$$J_{OI} = \frac{J_{Omax}\alpha I}{\left[J_{O\max}^2 + (\alpha I)^2\right]^{1/2}} \quad (2.17)$$

where α is the initial slope of the photosynthesis vs. irradiance (P-I) curve. The calculation of the photosynthetically active shortwave radiation I and the method of averaging equation (C-3) over one day is outlined in (Schmittner et al., 2005). This version also includes in the correction for the error in the calculation of light limitation in previous versions (Schmittner et al., 2008). Nutrient limitation is represented by the product of J_{Omax} and the nutrient uptake rates, $u_N = NO_3^-/(k_N + NO_3^-)$ and $u_P = PO_4^{3-}/(k_P + PO_4^{3-})$, with $k_P = k_N r_{P:N}$ providing the respective nutrient uptake rates.

Diazotrophs grow according to the same principles as the general phytoplankton class, but are disadvantaged in nitrate-bearing waters by a lower maximum growth rate, J_{Dmax}, which is set to zero below 15°C:

$$J_{Dmax} = c_D \bullet FeLim \bullet \max[0, a(\exp(T/T_b) - 2.61] \quad (2.18)$$

The coefficient c_D handicaps diazotrophs by dampening the increase of their maximal growth rate versus that of the general phytoplankton class with rising temperature. We use c_D = 0.4,

such that the increase per °C warming of diazotrophs is 40% that of other phytoplankton. This handicap is further decreased by the *Fe limitation* parameter (Figure 2.2a), which is scaled between 0 – 1 by multiplying a monthly climatology of aeolian dust deposition (Mahowald et al., 2005b) by a constant factor and setting the maximum value to 1. However, diazotrophs have an advantage in that their growth rate is not limited by NO_3^- concentrations:

$$J_D(I, PO_4) = min(J_{DI}, J_{Dmax}u_P) \quad (2.19)$$

although they do take up NO_3^- if it is available (see term 5 in the right hand side of eq. 2.12). The N:P of model diazotrophs is equal to the general phytoplankton class (16:1). Although there is evidence that the best-studied diazotrophs of the genus *Trichodesmium* have much higher N:P (e.g. (Letelier and Karl, 1996)), the mole abundant unicellular diazotrophs are largely uncharacterized (Zehr et al., 2001; Karl et al., 2002) and for simplicity of interpretation we opted to keep the N:P of both phytoplankton groups identical.

The first order mortality rate of phytoplankton is linearly dependent on their concentration, P_O. DOM and the microbial loop are folded into a single fast-remineralization process, which is the product of P_O and the temperature dependent term

$$\mu_P = \mu_{PO}\, exp(T / T_b). \quad (2.20)$$

Diazotrophs die at a linear rate where half of the resulting detritus is included into the fast-remineralization process.

Grazing of phytoplankton by zooplankton is unchanged from (Schmittner et al., 2005). Detritus is generated from sloppy zooplankton feeding and mortality among the three classes of plankton, and is the only component of the ecosystem model to sink. It does so at a speed of

$$w_D = \begin{Bmatrix} w_{D0} + m_w z, z \le 1000m \\ w_{D0} + m_w 1000m, z > 1000m \end{Bmatrix}, \quad (2.21)$$

increasing linearly with depth z from w_{D0}=7 md^{-1} at the surface to 40 md^{-1} at 1 km depth and constant below that, consistent with observations (Berelson, 2001). The remineralization rate of detritus is temperature dependent and decreases by a factor of 5 in suboxic waters, as O_2 decreases from 5 μM to 0 μM:

$$\mu_D = \mu_{DO}\, exp(T / T_b)[0.65+0.35tanh(O_2 - 6)] \quad (2.22)$$

Remineralization transforms the N and P content of detritus to NO_3^- and PO_4^{3-}. Photosynthesis produces oxygen, while respiration consumes oxygen, at rates equal to the consumption and remineralization rates of PO_4, respectively, multiplied by the constant ratio $R_{O:P}$. Dissolved oxygen exchanges with the atmosphere in the surface layer (F_{sfc}) according to the OCMIP protocol.

Oxygen consumption in suboxic waters ($O_2 < \sim 5$ μM) is inhibited, according to

$$r_{sox}^{O2} = 0.5\left[\tanh\left(O_2 - 5\right) + 1\right] \quad (2.23)$$

but is replaced by the oxygen-equivalent oxidation of nitrate,

$$r_{sox}^{NO3} = 0.5\left[1 - \tanh\left(O_2 - 5\right)\right]. \quad (2.24)$$

Denitrification consumes nitrate at a rate of 80% of the oxygen equivalent rate, as NO_3 is a more efficient oxidant on a mol per mol basis (i.e. one mol of NO_3 can accept $5e^-$ while 1 mol of O_2 can accept only 4 e^-).

We include the sedimentary denitrification metamodel equation of (Middleburg et al., 1996) which parameterizes sedimentary denitrification based on the labile carbon flux (F_c) into the sediments:

$$SedDeni = \alpha_{SD} \times 10 \wedge \left[-0.9543 + 0.7662 \times \log(F_c) - 0.2350 \times \log(F_c)^2 \right] \quad (2.25)$$

SedDeni is the amount of NO_3^- that is removed from the bottom water. We assume that the flux of labile carbon (F_c) occurs at a ratio of $R_{C:N}$ = 6.625 of the sinking nitrogen in the organic detritus. Because the continental shelves are not well resolved in the model, we use an additional sub-grid scale parameterization for them. The portion of each ocean grid box that is covered by a shallower continental shelf is recorded as the SHELF coefficient. The labile organic carbon (F_c) that is included in the sedimentary denitrification model in the shelf parameterization is the amount of organic carbon that sinks into the portion of the grid box covered by a shallower continental shelf (i.e., SHELF x F_c). In the model, ~80% of the sedimentary denitrification occurs within this shelf parameterization. The remaining organic matter (i.e., F_c x [1 - SHELF]) continues to sink to greater depths. The physical circulation model's inability to fully resolve coastal upwelling systems also underestimates primary production and sinking carbon fluxes on the continental shelves and hence sedimentary denitrification. To account for this, we arbitrarily multiply the sedimentary denitrification rate by a coefficient α_{SD} tuned to 4.5 to set the global deep oceanic $\delta^{15}NO_3$ average in the model to ~5‰. Without this parameterization, the deep oceanic $\delta^{15}NO_3$ average slowly drifts well above 10‰. Figure 2.2 shows the spatial distribution of sedimentary denitrification.

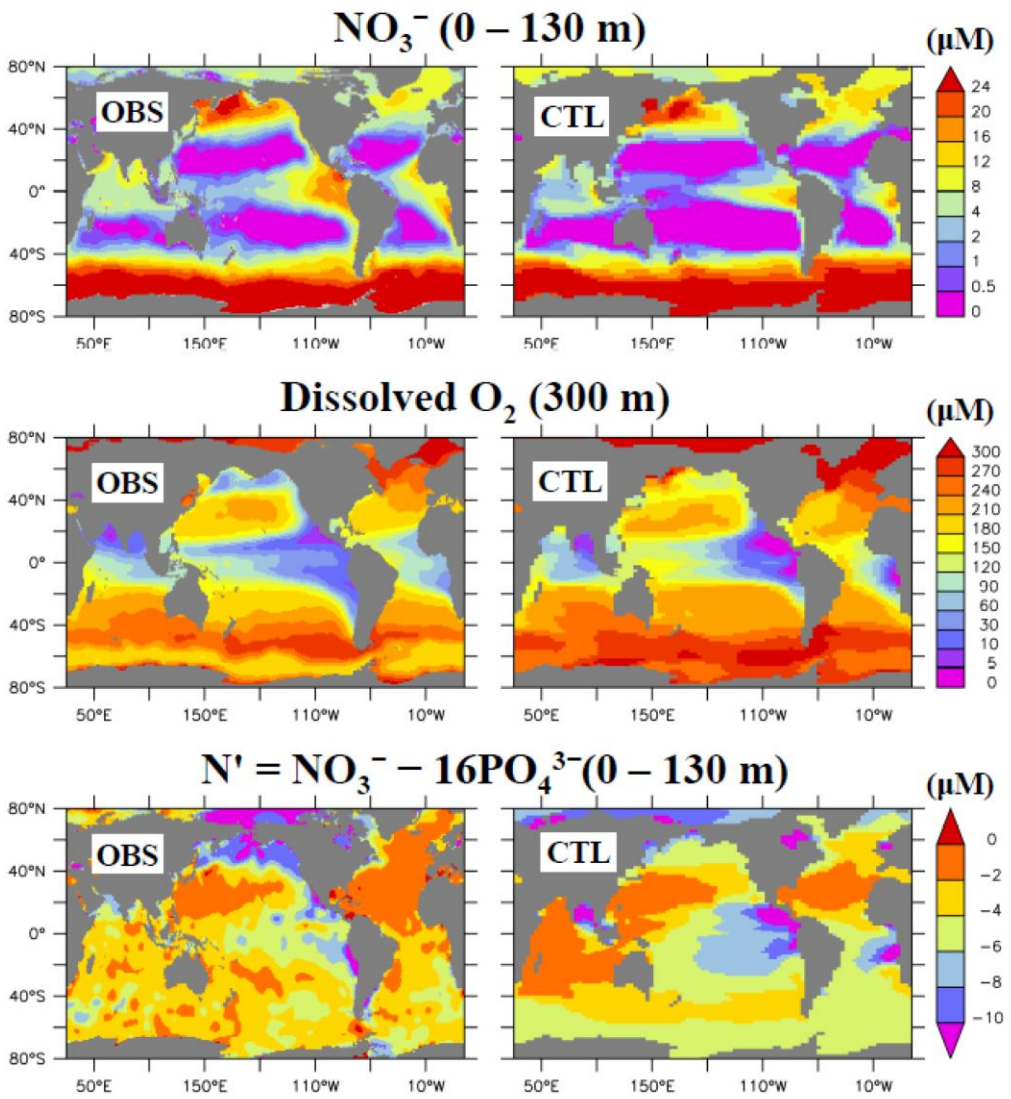

Figure 2.10 Comparison between annual WOA05 observations (Garcia et al., 2010a; Garcia et al., 2010b) with CTL of (top) surface NO_3^-, (center) subsurface O_2, and (bottom) surface N'.

Acknowledgements. We would like to thank Daniel Sigman, Angela Knapp, and Peter DiFiore for contributing data to this study. The research for this study was conducted at the College of Oceanic and Atmospheric Sciences at Oregon State University. This work was funded by the National Science Foundation and the SFB754 project from the German Science Foundation (DFG).

3 Nitrogen Isotope Simulations Show the Importance of Atmospheric Iron Deposition for Nitrogen Fixation Across the Pacific Ocean

This chapter is based on the manuscript from Christopher J. Somes, Andreas Schmittner, and Mark A. Altabet

Abstract

Nitrogen (N) fixation by specialized microorganisms (diazotrophs) influences global plankton productivity because it provides the ocean with most of its bio-available N. However, its global rate and large-scale spatial distribution is still regarded with considerable uncertainty. Here we use a global ocean nitrogen isotope model, in comparison with $\delta^{15}NO_3^-$ observations, to constrain the pattern of N_2 fixation across the Pacific Ocean. N_2 fixation introduces isotopically light atmospheric N_2 from to the ocean ($\delta^{15}N = 0‰$) relative to the oceanic average near 5‰, which makes nitrogen isotopes suitable to infer patterns of N_2 fixation. Including atmospheric iron limitation of diazotrophy in the model shifts the pattern of simulated N_2 fixation from the South Pacific to the North Pacific and from the East Pacific westward. These changes considerably improve the agreement with meridional transects of available $\delta^{15}NO_3^-$ observations, as well as excess P ($PO_4^{3-} - NO_3^-/16$), confirming that atmospheric iron deposition is indeed important for N fixation in the Pacific Ocean. This study highlights the potential for using $\delta^{15}N$ observations and model simulations to constrain patterns and rates of N fixation in the ocean.

3.1 Introduction

Nitrogen (N) fixation is the dominant source of biologically available nitrogen (fixed-N) into the ocean (Codispoti, 2007), which is performed by specialized prokaryotes (diazotrophs)

that can reduce N_2 gas instead of oceanic fixed-N (NO_3^-, NO_2^-, NH_4^+) during photosynthesis. Since diazotrophs are not limited by fixed-N, they can grow in N-depleted surface water provided other required nutrients (e.g., phosphorus (P) and iron (Fe)) are available. Diazotrophs can have an important influence on climate because fixed-N limits primary production and biological sequestration of atmospheric CO_2. The efficiency, with which diazotrophs can balance the N-loss from denitrification and anammox, the major sinks for fixed-N, determines if the oceanic fixed-N inventory could fluctuate significantly enough to affect atmospheric CO_2.

Throughout much of the contemporary ocean, biological productivity is limited by fixed-N suggesting other factors, such as light, temperature, P and Fe availability, and/or NO_3^- inhibition, are preventing diazotrophs from fixing atmospheric N. It has been observed that blooms of *Trichodesmium*, one of the most important and best studied diazotrophs, occur more frequently and are more extensive in warm (>25°C) surface water where fixed-N is depleted and rates of atmospheric Fe deposition are high such as the North Atlantic, Indian, and North Pacific compared to areas of low Fe deposition such as the South Pacific where the abundance of *Trichodesmium* appears to be much lower (Carpenter, 1983; Karl et al., 2002; Carpenter and Capone, 2008). This pattern of less N_2 fixation in Fe-depleted waters is also consistent in the South Atlantic (Mark Moore et al., 2009). This suggests that temperature and Fe availability may be the most important factors that determine where N_2 fixation is able to occur. However, other more uncharacterized unicellular diazotrophs have been observed to grow in cooler water near 20°C (Needoba et al., 2007), and it has been suggested that they also may significantly contribute to the global N_2 fixation rate (Zehr et al., 2001; Montoya et al., 2004).

The large spatial and temporal variability of diazotrophs makes it difficult to constrain the global rate of N_2 fixation. Recent estimates range widely between ~100 – 200 Tg N yr^{-1} and predict significantly different spatial patterns (Gruber and Sarmiento, 1997; Karl et al., 2002; Moore and Doney, 2007a). For example, a model using xsP ($PO_4^{3-} - NO_3^-/16$) observations within an ocean circulation model estimates that N_2 fixation is tightly coupled with denitrification in the Pacific Ocean (Deutsch et al., 2007), but does not explicitly account for

Fe. In contrast, the Biogeochemcial Elemental Cycling model (Moore and Doney, 2007b), which explicitly includes the effects of Fe availability, predicts that N_2 fixation should be more abundant in the Western North Pacific, where atmospheric Fe deposition is greater, and suggests that the Pacific represents a fixed-N sink because the absence of sufficient Fe prevents N_2 fixation from balancing denitrification throughout much of the South Pacific.

N_2 fixation introduces relatively isotopically light N ($\delta^{15}N = 0‰$) into the ocean compared to the global mean $\delta^{15}NO_3^-$ near 5‰. Therefore, the ratio of the two stable nitrogen isotopes, represented in the $\delta^{15}N$ notation where $\delta^{15}N = [(^{15}N/^{14}N)_{sample}/(^{15}N/^{14}N)_{atmosphere} - 1]\bullet1000$, may be a powerful tool to trace patterns of N_2 fixation. Here we compare a model of nitrogen isotopes, embedded within the ocean component of a global Earth System Climate Model, with $\delta^{15}NO_3^-$ measurements across the Pacific Ocean to constrain N_2 fixation focusing on the effect of atmospheric Fe limitation of diazotrophy.

3.2 Model Description

The marine ecosystem/biogeochemical model including N isotopes is the 2N2PZD (2 Nutrients, 2 Phytoplankton, Zooplankton, Detritus) model of (Somes et al., 2010b) that includes N_2 fixation, water column denitrification, and benthic denitrification. It has run for over 1500 years as it approaches equilibrium. Diazotrophs grow according to the same principles as the "general" phytoplankton class in the model, but we also account for some of their different characteristics. Since fixing dissolved N_2 is energetically more costly than assimilating fixed-N, the growth rate of diazotrophs is lower than that of general phytoplankton in the model. It is zero in waters cooler than 15°C and increases 50% slower with temperature than the growth rate of general phytoplankton (note this value is increased from 40% in (Somes et al., 2010b), which results in an additional ~20 Tg N yr^{-1} of N_2 fixation). Diazotrophs are not limited by NO_3^- and can out-compete general phytoplankton in surface waters that are depleted in fixed-N, but still contain sufficient P (i.e., high xsP water due to denitrification). However, diazotrophs will consume NO_3^- if it is available, consistent with culture experiments (Mulholland et al., 2001; Holl and Montoya, 2005), which is another factor that inhibits N_2 fixation in the model. Denitrification, and the propagation of N-deficient waters into the shallow thermocline by physical transport processes, creates an

ecological niche for diazotrophs stimulating N_2 fixation (Tyrrell, 1999a). Fe is currently not included as a prognostic tracer in the model. However, we include a simple parameterization of atmospheric Fe limitation of diazotrophy as described in Section 3.3.

The nitrogen isotope model simulates the distribution of the two stable nitrogen isotopes, ^{14}N and ^{15}N, in all N species included in the marine ecosystem model. The processes in the model that fractionate nitrogen isotopes are algal NO_3^- assimilation (ε_{ASSIM} = 5‰), zooplankton excretion (ε_{EXCR} = 6‰), water column denitrification (ε_{WCD} = 25‰), and N_2 fixation (ε_{NFIX} = 1.5‰). Fractionation results in the isotopic enrichment of the more reactive, thermodynamically preferred, light ^{14}N into the product of each reaction by a process-specific fractionation factor (Mariotti et al.). Although little fractionation occurs during N_2 fixation in the model, it has an important effect on $\delta^{15}N$ by introducing isotopically light atmospheric N_2 ($\delta^{15}N$ = 0‰) into the oceanic fixed-N pool. Benthic denitrification has been observed to have little effect on the oceanic isotopic N pool because denitrifiers consume nearly all NO_3^- diffusing into the reactive zones within the sediments, leaving the oceanic N pool mostly unaltered (Brandes and Devol, 2002) (Lehmann et al., 2007). Therefore, in the model, there is no fractionation during benthic denitrification (ε_{BD} = 0‰), although this is a simplification of observations .

3.3 Atmospheric Fe Limitation of Diazotrophy

The nitrogenase enzyme, which fixes N_2 in diazotrophs, has a large structural iron (Fe) requirement (Raven, 1988; Sanudo-Wilhelmy et al., 2001). Diazotrophs may depend on Fe from atmospheric deposition in oligotrophic waters, where a deep pycnocline inhibits upward mixing of subsurface Fe-replete waters into the euphotic zone. Therefore, we include an atmospheric Fe limitation of diazotrophy experiment (Figure 3.1, FeLim), where diazotrophs' growth rate is further reduced by the Fe limitation parameter (FeL), which scales an estimate of monthly climatological atmospheric dust deposition (Mahowald et al., 2005a) between 0 and 1 (Figure 3.1) by multiplying atmospheric dust deposition rate by a constant factor, and setting the maximum value to 1 (i.e., maximum growth rate = $\mu_D \bullet FeL$). This parameterization does not account for any Fe that reaches the surface through vertical mixing or upwelling. Since this source of Fe will be accompanied by large concentrations of

subsurface NO_3^- and PO_4^{3-}, we assume that the faster-growing general phytoplankton class will consume all of this Fe along with the macronutrients. The model does not include Fe input from rivers or shelf sediments.

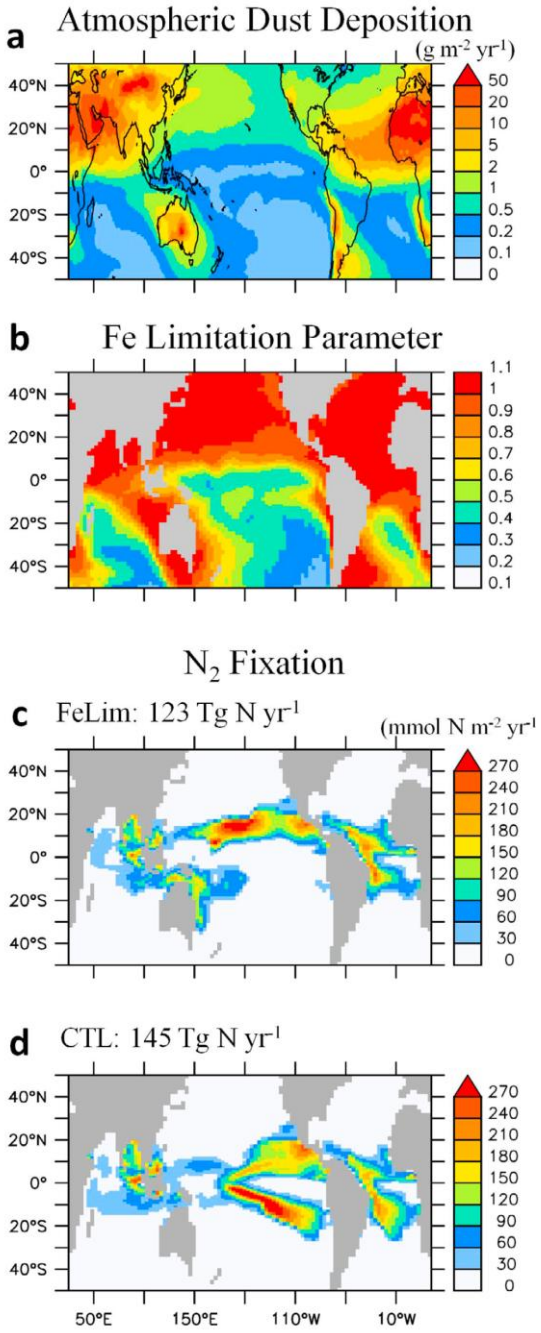

Figure 3.1. Top Panel: Annual rates of dust deposition (Mahowald et al., 2005b) and *FeLim* parameter used to decrease the growth rate of diazotrophs. Bottom Panel: Vertically integrated N_2 fixation in FeLim and CTL.

3.4 Results

The control (CTL) simulation does not include Fe limitation of diazotrophs (i.e., maximum growth rate = μ_D) and results in large N_2 fixation rates in the Central and Eastern Tropical South Pacific (Figure 3.1). The only factor that prevents N_2 fixation from occurring in the Eastern Tropical Pacific of CTL is the presence of high surface NO_3^- in the core of the HNLC region, where diazotrophs consume NO_3^- instead of fixing dissolved N_2 to meet their N requirement for growth. This tight coupling of N_2 fixation and denitrification in the Eastern Tropical South Pacific is consistent with the model of (Deutsch et al., 2007), which does not explicitly include Fe limitation or NO_3^- inhibition. However, we note that the general pattern of N_2 fixation in (Deutsch et al., 2007) throughout the rest of the tropical/subtropical Pacific is actually more consistent with the simulation including Fe limitation of diazotrophs (FeLim) than CTL, perhaps because atmospheric Fe deposition is greater there.

Global patterns of N_2 fixation in FeLim—such as high values in the tropical/subtropical North Pacific, the western tropical/subtropical South Pacific, the western tropical/subtropical South Atlantic, the tropical/subtropical North Atlantic and the Indian Ocean—are more consistent with direct observations (e.g., (Karl et al., 2002; Carpenter and Capone, 2008)), and with results from a more complex ecosystem/biogeochemical model (Moore and Doney, 2007b). Nevertheless, N_2 fixation in our model does not extend northward of ~30°N in the North Pacific, whereas some observations show N_2 fixation as far north as 35–40°N (Needoba et al., 2007; Kitajima et al., 2009). We hypothesize this discrepancy occurs due to the oversimplified fast-recycling microbial loop parameterization, which recycles organic matter to inorganic nutrients at N:P=16. It has been suggested that dissolved organic P recycles more efficiently relative to dissolved organic N and may also be directly consumed (Wu et al., 2000), which is a mechanism that could help relieve diazotrophs of their P limitation throughout the tropical/subtropical oligotrophic ocean and stimulate additional N_2 fixation.

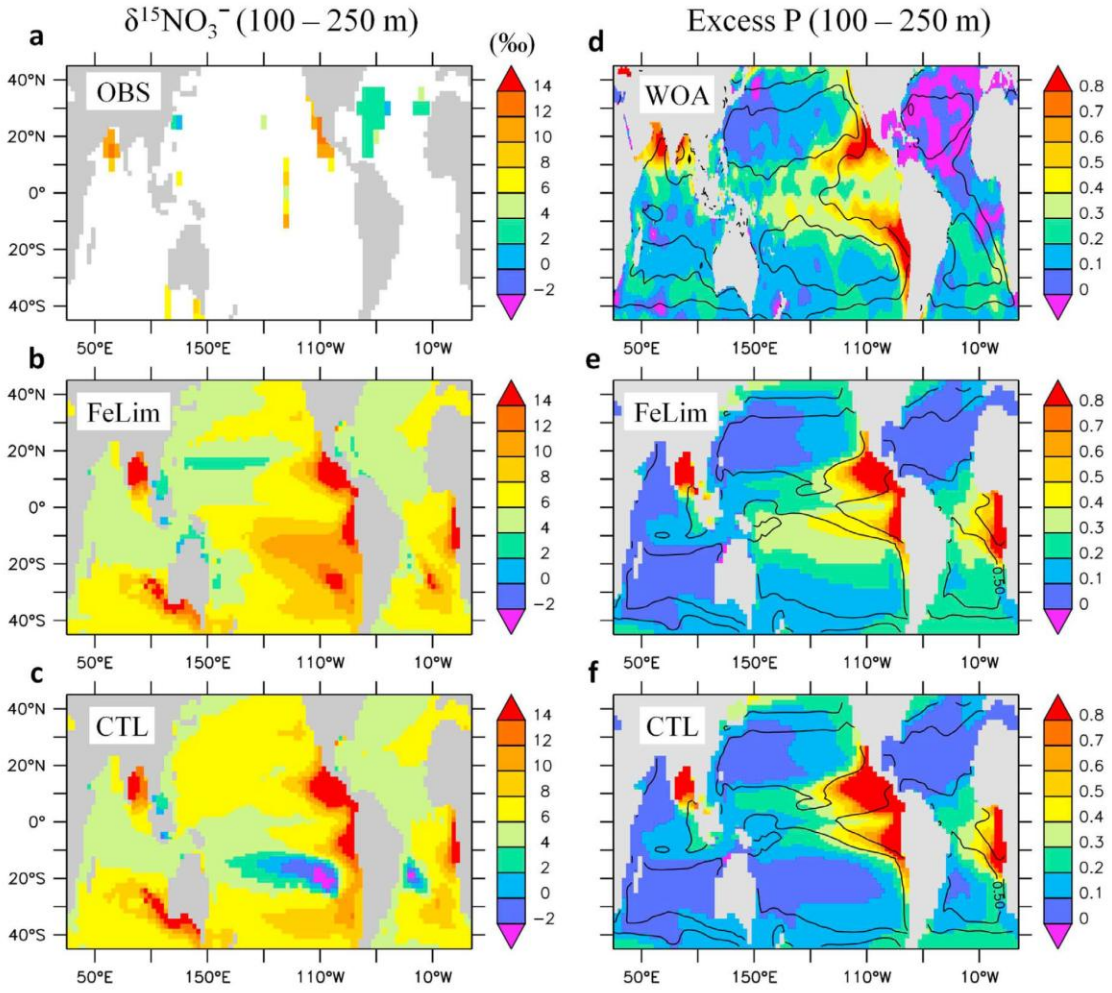

Figure 3.2. Comparison of FeLim and CTL with $\delta^{15}NO_3^-$ observations (Somes et al., 2010b) (a – c) and World Ocean Atlas 2005: xsP = $PO_4^{3-} - NO_3^-/16$ and near-surface (0 – 100m) NO_3^- contours of 5.0 and 0.5 μM (d – f). Note that due to the too low N:P for diazotrophs in the model (N:P = 16:1) compared to observations (N:P = ~50:1) (Letelier and Karl, 1996, 1998a; Krauk et al., 2006; White et al., 2006), a slight overestimation of xsP is to be expected where N_2 fixation occurs.

Global measures of $\delta^{15}NO_3^-$ and xsP improve in FeLim compared to CTL (Table 3.1). Generally lower $\delta^{15}NO_3^-$ and xsP in the Northern Hemisphere relative to the Southern Hemisphere in FeLim, due to more N_2 fixation occurring in the Northern Hemisphere where more atmospheric Fe deposition exists, result in a better match with observations than in CTL (Figure 3.2). The Central and Western Tropical Pacific represent regions where N_2 fixation may occur as xsP flows westward "downstream" from the suboxic zones. Measured $\delta^{15}NO_3^-$ shows a decreasing trend northwards in the two transects across the Pacific (Figure 3.3), with a minimum near the equator in the Central Pacific. This equatorial minimum is

reproduced in the model due to the low degree of surface NO_3^- utilization as a result of extensive NO_3^- supply to the surface from equatorial upwelling. The northward decreasing $\delta^{15}NO_3^-$ trend in FeLim in both transects is due to more N_2 fixation occurring north of the equator, where sufficient atmospheric Fe deposition exists (Figure 3.1). When atmospheric Fe limitation of diazotrophy is not included in the model (CTL), the opposite $\delta^{15}NO_3^-$ trend is simulated because more N_2 fixation occurs south of the equator, in contrast to the observations.

Table 3.1 Global measures of $\delta^{15}NO_3^-$ and xsP model performance: correlation coefficient (r), standard deviation (STD), and root mean squared (RMS) error. STD and RMS have been normalized by the standard deviation from the observations.

	$\delta^{15}NO_3^-$			***Excess P***		
Model	***r***	***STD***	***RMS***	***r***	***STD***	***RMS***
CTL	0.668	1.76	1.33	0.520	1.30	1.27
FeLim	0.680	1.33	0.982	0.530	0.898	1.01

Global rates of N_2 fixation, water column denitrification, and benthic denitrification are smaller in FeLim (123, 89.4, 35.3 Tg N yr^{-1}, respectively) compared to CTL (145, 119, 34.6 Tg N yr^{-1}, respectively) because a tighter coupling of N_2 fixation and denitrification exists in CTL in the Eastern Pacific. More N_2 fixation occurring in and around denitrification zones leads to increased export production and remineralization of organic matter at depth, lower oxygen concentrations, and more denitrification. Since denitrification creates an ecological niche for diazotrophs, its increase will stimulate additional N_2 fixation, creating a positive feedback effect. This results in a bigger suboxic zone and more denitrification in the Eastern Tropical South Pacific in CTL compared to FeLim. The amount of xsP water that communicates with the Southern Ocean through the subsurface and then escapes the Pacific Ocean though the Antarctic Circumpolar Current makes the Pacific Ocean a fixed-N sink of 10 Tg N yr^{-1} in CTL. Since there is less xsP water south of the equator in FeLim (Figure 3.2), the Pacific Ocean is a nitrogen sink of only 4 Tg N yr^{-1}, even though Fe limits N_2 fixation

throughout much of the South Pacific. Note that both model versions underestimate xsP off of Peru and Chile because the coarse-resolution model cannot capture suboxia there. In the real ocean, a part of this water may sustain high xsP until it reaches a region with sufficient Fe (e.g., North Atlantic or North Indian Ocean), which could take hundreds of years, and result in a significant decoupling of N_2 fixation from denitrification that occurs in the Fe-depleted Southern Hemisphere (see also Falkowski (1997)).

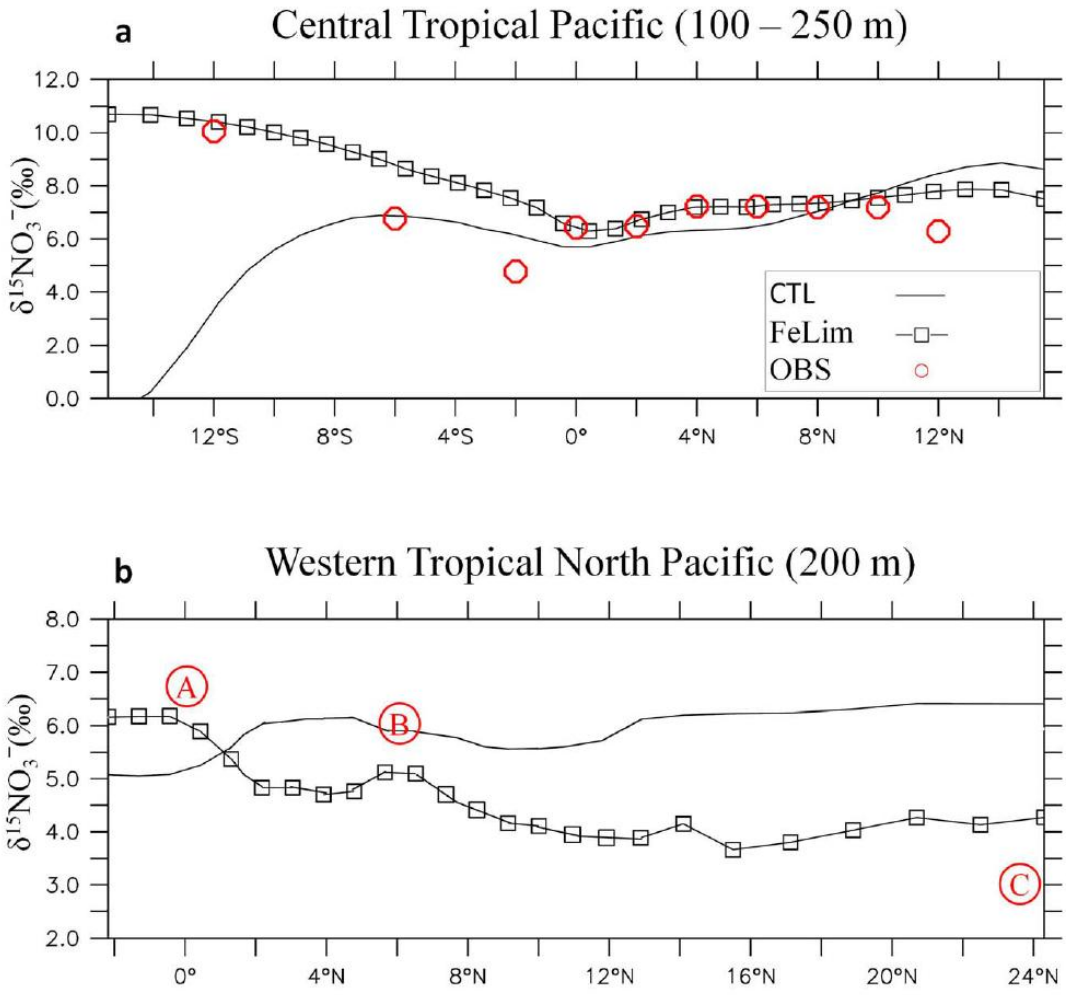

Figure 3.3. Comparison of FeLim and CTL $\delta^{15}NO_3^-$ with observations in the (a) Central Equatorial Pacific (140°W) (100 – 250 m) (Altabet, 2001) (reanalysis), and (b) Western North Pacific (100 – 250 m) (model transect connects through latitude/longitude of each data point): (A) ~6.75‰ at 0°N/S, 140°E (Yoshikawa et al., 2006); (B) ~6.0‰ at 6°N, 125°E (Kienast et al., 2008); (C) ~3.0‰ at 25°N, 123°E (Liu et al., 1996).

3.5 Conclusion

Model simulations that include Fe limitation of diazotrophy show a much better agreement with $\delta^{15}NO_3^-$ and xsP observations compared to a model that neglects this effect (Table 3.1, Figures 3.2, 3.3). Nitrate isotope observations show a decreasing northward trend across two transects in the Central and Western Pacific (Figure 3). Comparisons with model results reveal that these trends can be best explained by the input of isotopically light N by N_2 fixation, where higher rates of atmospheric Fe deposition exist. This highlights the potential of $\delta^{15}NO_3^-$ as a tool to infer the spatial pattern of N_2 fixation. If no N_2 fixation was occurring, the $\delta^{15}NO_3^-$ value would be expected to be very high ($\delta^{15}NO_3^- > 10‰$) due to the nearly complete utilization of surface NO_3^- in the oligotrophic ocean (Altabet and Francois, 1994; Somes et al., 2010b), which is a drastically different $\delta^{15}N$ signature than what would be expected if N_2 fixation was significantly contributing to the local N pool ($\delta^{15}N_2 = 0‰$). Our results suggest that $\delta^{15}N$ observations, in combination with models, can be used to constrain N_2 fixation patterns in present and past oceans.

Acknowledgements. We thank Eric Galbraith, Moritz Lehman, Joseph Montoya, Ricardo Letelier, and Alan Mix for helpful comments. This research was conducted at the College of Oceanic and Atmospheric Sciences at Oregon State University and IFM-GEOMAR. This work was funded by the National Science Foundation and the SFB754 project from the German Research Foundation (DFG).

4. Coherent climate-driven changes in the global marine nitrogen cycle during the past 80,000 years

This chapter is based on a manuscript from Eric Galbraith, Markus Kienast and the NICOPP working group including Jan-Erik Tesdal, Christopher Somes, and others

Abstract

The intimate relationship between the marine nitrogen cycle and the physical ocean environment suggests that anthropogenic climate change will impact the marine ecosystem. However, the strength and nature of this coupling are poorly quantified. Here, we investigate how natural climate changes affected the marine nitrogen cycle during the last 80,000 years, using a new database of sedimentary nitrogen isotope measurements that provides, for the first time, a synoptic global view. Our N isotope measurements ($\delta^{15}N$) from the modern seafloor reveal large-scale spatial patterns spanning a global $\delta^{15}N$ range of ~12 ‰. These patterns can be explained by the interplay between N_2 fixation, denitrification, and the cycling of nitrate, as confirmed by good agreement with the predictions of an ocean-biogeochemistry-isotope model integrated under pre-industrial forcing. A compilation of 78 sediment cores reveals that the climate changes of the last ice age and deglaciation wrought global-scale changes in nitrogen cycling. During warmer periods, high-latitude nitrate utilization by phytoplankton was reduced, while both denitrification and N_2 fixation operated at higher rates. But rather than simply following a unidirectional trajectory, the global warming of the deglacial transition was marked by widespread, millennial-timescale changes in the nitrogen cycle that paralleled known changes in ocean circulation and climate. Our results confirm that the marine nitrogen cycle is highly sensitive to climate, and demonstrate the power of a global array of sedimentary nitrogen isotope records in documenting its response.

4.1 Introduction

Nitrogen is a critical element for life. But despite the ubiquity of dissolved N_2 gas in the atmosphere and ocean, its bio-available forms (N_{bio}) are scarce in the sunlit surface layer, and its limited supply places the primary nutritional constraint on photosynthesis. Within the oceans, N_2 is fixed to N_{bio} almost entirely by micro-organisms near the ocean surface, and returned to N_2 by denitrification in anoxic zones of the water column and sediment, turning over the N_{bio} inventory on a timescale of 1-5 ky (Codispoti et al., 2001). The nitrogen cycle can alter the radiative properties of the atmosphere, through the generation of N_2O (Ravishankara et al., 2009) and by supporting the biological sequestration of CO2 in the ocean (Ganeshram et al., 1995).

Humans are transforming the nitrogen cycle by approximately doubling the rate of terrestrial N_2 fixation and by supplying N_{bio} to the ocean surface through rivers and aerosols (Gruber and Galloway, 2008). In addition, anthropogenic warming is expected to increase the rate of denitrification, by expanding water column oxygen minimum zones (Gruber and Galloway; Schmittner et al.), and to modify the supply routes of nitrate through changes in ocean circulation (Sarmiento et al., 1998). However, the observational record of nitrate concentrations is much shorter than the residence time of N_{bio} and is barely able to resolve decadal fluctuations in nitrate availability (Deutsch et al., 2011), preventing the identification of climatic trends.

In contrast, the geological record spans millennia and includes large climate shifts, such as the ice age cycles. The nitrogen stable isotope ratio ($\delta^{15}N$) of sinking organic matter is preserved in marine sediments, providing a window into past changes in both the utilization of N_{bio} at the ocean surface by phytoplankton, and the inventory-altering processes of N_2 fixation and denitrification. Over recent decades, an understanding of nitrogen isotope systematics has developed from field and laboratory studies, and nitrogen isotope records have been generated from seafloor sediments extending back thousands (or in some cases millions) of years. The sedimentary record of the last ice age cycle is particularly

well sampled, providing the opportunity to construct synoptic global views that can help bridge modern oceanographic knowledge with $\delta^{15}N$ records of the more ancient Earth (Godfrey and Falkowski, 2009). However these efforts have, to date, proceeded piecemeal. Here we present the first global analysis of available $\delta^{15}N$ observations, extending from the present day to 80 thousand years ago (80 ka), early in the last ice age.

4.2 A synoptic view of N isotopes in the modern ocean

Figure 4.1a shows our compilation of more than 1500 measurements of the $\delta^{15}N$ of total combustible (bulk) nitrogen at the modern seafloor. In general, the distribution is consistent with expectations from the processes that influence nitrogen isotopes (see Appendix 4.4), both inventory-altering (water column denitrification and N_2 fixation), and internal-cycling (due to nitrate utilization by phytoplankton). Attribution of the large-scale patterns to these fractionating processes is further bolstered by the general agreement between the seafloor $\delta^{15}N$ (Fig. 4.1a) and the $\delta^{15}N$ of sinking organic matter predicted by a global ocean-biogeochemistry model simulation (Fig. 4.1b) (Somes et al., 2010b).

Both the sediment data and the model show north-south gradients, with low $\delta^{15}N$ where nitrate-rich waters are transported upwards across the pycnocline (i.e. at high latitudes and along equatorial upwellings), and high $\delta^{15}N$ in between. In addition, east-west gradients place higher values on the eastern sides of the Pacific and Atlantic oceans. The model produces these broad isotopic gradients through either inventory-altering or internal-cycling processes, with intervening zones of overlap, as expected from local studies (Altabet et al.; Farrell et al.; Ganeshram et al.) and illustrated in Figure 4.1, panels c and d. In general, inventory-altering fractionation is more important in the tropics, where high values are generated by water column denitrification (solid contours, Figure 4.1d) and low values by nitrogen fixation (dashed contours, Figure 4.1d). Meanwhile, the effect of internal-cycling is strong at all latitudes, with the greatest impact in the most most nitrate-rich and nitrate poor regions (contours, figure 4.1c). We note that the high $\delta^{15}N$ predicted in the northeast (instead of northwest) Indian Ocean results from a common physical circulation bias of ocean models that places the Indian Ocean oxygen minimum zone on the wrong side of the basin, rather than a misunderstanding of the isotopic effects. Similarly, the eastern South Atlantic oxygen

minimum zone is too strong in the model, leading to abundant water column denitrification and ^{15}N enrichment in a region where denitrification has only been observed on the shelf (Kuypers et al., 2005).

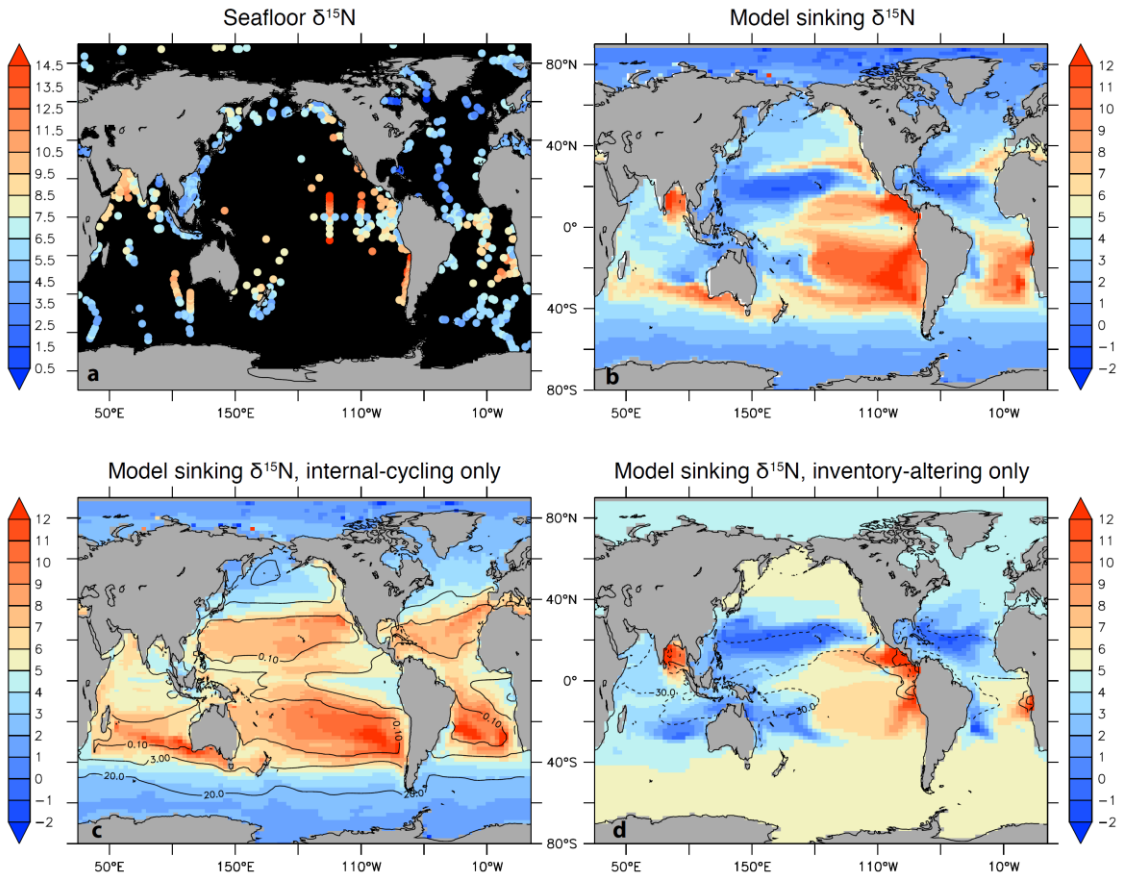

Figure 4.1 The nitrogen isotopic composition of sedimentary organic matter, observed and simulated. a) The $\delta^{15}N$ of seafloor sediments as measured by combustion of whole sediment, averaged on the model grid. b) Simulated $\delta^{15}N$ of sinking particulate organic nitrogen at 100 m, at steady state, using the UVic ocean-biogeochemistry model (Somes et al., 2010b). c) Simulated $\delta^{15}N$ of sinking particulate organic nitrogen at 100 m including only "internal-cycling" fractionation (shading), compared to modeled surface nitrate concentrations (contours, in μM). d) Simulated $\delta^{15}N$ of sinking particulate organic nitrogen at 100 m including only "inventory-altering" fractionation (shading), compared to integrated water column denitrification rates (solid contours, 30 and 800 mmol N m^{-2} y^{-1}) and integrated water column N_2 fixation rates (dashed contours, 30 mmol N m^{-2} y^{-1}). Note that the mean ocean $\delta^{15}N$-NO_3 of 5 ‰ is determined by the global balance of water column and sedimentary denitrification (see 4.4), and is the same for b, c, and d.

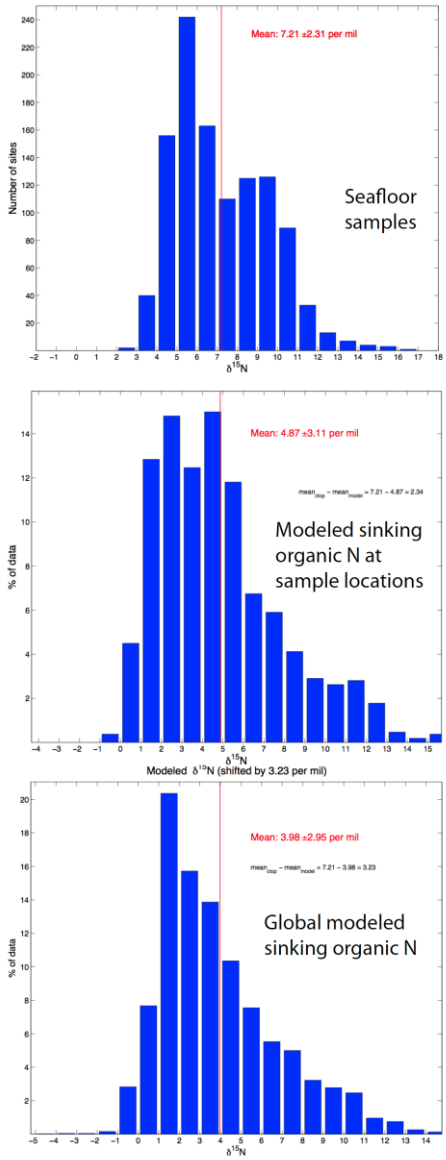

Figure 4.2 Frequency distribution of sedimentary $\delta^{15}N$ values at the seafloor and in the model. Note the panels are aligned relative to their means (red lines). The overall higher seafloor values are likely due to isotopic alteration during the sinking and sedimentation of organic matter. Other discrepancies could be due to any combination of errors in the physical, biogeochemical, or isotopic components of the model.

Other than these errors, the primary model-data discrepancy is a low model bias of 2.3 ± 2.5 ‰ (Fig. 4.2). This agrees, both in magnitude and distribution, with the widely-documented enrichment of $\delta^{15}N$ in oxygenated, slowly-accumulating sediments (Altabet and Francois, 1994). Importantly, the alteration appears to be consistent across broad spatial scales, rather than suffering from local variability. Presumably, the ^{15}N-enrichment is caused by the preferential loss of ^{15}N-depleted nitrogen during the remineralization of sinking and freshly-sedimented organic matter. Techniques to measure the $\delta^{15}N$ of selected compounds and of fossil-bound organic matter (Robinson et al., 2005; McCarthy et al., 2007; Ren et al., 2009; Higgins et al., 2010; Bridoux et al., 2011; Möbius et al., 2011; Sherwood et al., 2011) are currently helping to quantify this small but significant offset, while simultaneously providing new insight on ^{15}N variability among groups of organisms in the same community (Brunelle et al., 2007; Ren et al., 2009). Nonetheless, the robust global patterns support the interpretation of bulk $\delta^{15}N$ as a record of integrated, whole community N export, an interpretation which will be improved with increasing understanding of nitrogen diagenesis.

4.3 Past changes in the nitrogen cycle

Our database includes 78 records of bulk sediment $\delta^{15}N$ covering the period 30 – 5 ka (Tesdal et al., 2012) These records show variability on timescales ranging from centuries to millennia, with large regional contrasts, as previously discussed at depth in the literature. In order to extract unifying patterns of variability from the dataset, we performed a Principal Component (PC) analysis of these records (see 4.4.2), the results of which are summarized in Figure 4.3. The two leading PCs explain 63% and 15% of the variance in the global dataset (Figure 4.3a). The first PC shows a glacial-interglacial pattern that is very similar to the mean of all records. Furthermore, it parallels the deglacial increase of global average surface temperature, as estimated by Shakun et al. (2012) (Figure 4.3a). The second $\delta^{15}N$ PC is dominated by a deglacial excursion between 18 and 10 ka, reflecting regionally-specific modulation of the deglacial transition and, remarkably, bearing some similarity to the second surface temperature PC of (Shakun and Carlson, 2010).

The regressions of the $\delta^{15}N$ PCs against the original data show how they are manifested at different sediment locations (Figure 4.3b, 4.3c). We interpret the deglacial PCs as a

combination of inventory-altering and internal cycling changes. It is not yet possible to separate the two types of changes quantitatively, given their spatial overlap (e.g. Figure 4.1c, 4.1d) and incomplete data coverage, but the sign of change can be inferred for each type.

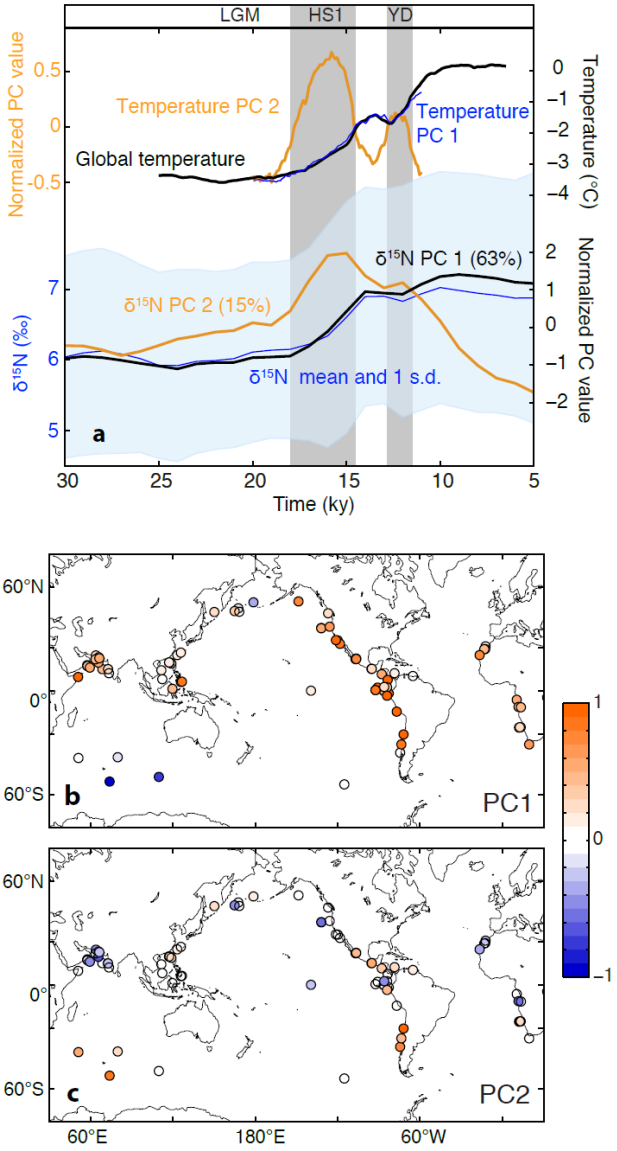

Figure 4.3 Global climate and the marine nitrogen cycle at the end of the last ice age. a) Timeseries of marine and terrestrial temperature records, presented as a global stack (Shakun et al.) (black) and the first two Principal Components (Shakun and Carlson, 2010) (PC1 blue, scaled by 50%, and PC 2 orange), compared to the two leading PC timeseries of 78 $\delta^{15}N$ records (black and orange) as well as the mean (blue) and 1 standard deviation envelope of all $\delta^{15}N$ records (blue shading). The vertical green bars indicate the Heinrich Stadial 1 (HS1) and Younger-Dryas (YD) intervals. b, c) Regression coefficients of the first and second PCs against the data. Only significant ($p < 0.1$) regressions are shaded.

The spatial pattern of PC1 (Figure 4.3b) is broadly similar to the pattern of fractionation caused by internal-cycling (Figure 4.1c). The fact that this pattern shows a positive regression over the deglaciation is therefore consistent with an enhancement of isotopic dipole due to internal-cycling (see 4.4.1): a deglacial increase in the nitrate concentrations of the North Pacific (Galbraith et al., 2008) and Southern Ocean (Robinson et al., 2005) led to more residual nitrate, enriched in ^{15}N, being fed downstream into the thermocline. This agrees with prior suggestions that the excess nitrate in these regions increased at the end of the last glacial maximum (Franois et al., 1997), perhaps due to weakening polar ocean stratification (Franois et al., 1997) or to decreasing dust-born iron supply (Martin, 1990).

At the same time, the tropical pattern of deglacial change is consistent with an intensification of inventory-altering fractionation, with positive values near all zones of water-column denitrification (the eastern tropical Pacific (Ganeshram et al., 1995) and the Arabian Sea (Altabet et al., 1995)). This increase in denitrification could have been related to large-scale deoxygenation of the upper ocean (Jaccard and Galbraith, 2012) and/or to local oxygen minimum zone dynamics such as enhanced wind-driven upwelling (Altabet et al., 1995) or shoaling of the thermocline (Schmittner et al.; Deutsch et al.). The fact that sites in the tropical western Atlantic and Pacific show little deglacial $\delta^{15}N$ increase is consistent with a deglacial increase in N_2 fixation, accumulating ^{15}N-depleted, newly-fixed nitrogen in those regions. This is in conflict with the suggestion that the dwindling of dust deposition on the ocean decreased N_2 fixation due to enhanced iron-limitation (Falkowski, 1997). Instead, the increase of N_2 fixation, even in the face of intensifying iron-limitation, requires that increasing N-limitation caused by accelerated denitrification allowed N_2 fixers an advantage against their non-diazotrophic rivals (Tyrrell, 1999b; Deutsch et al., 2004; Ren et al., 2009).

Notably, sites on the west coast of Africa show changes that are similar to those near the Indo-Pacific oxygen minimum zones, despite the lack of water column denitrification in the Atlantic. This could reflect two things: either the intensified internal-cycling fractionation raised $\delta^{15}N$ throughout much of the global thermocline, by supplying more residual ^{15}N-enriched nitrogen from high latitudes, or the mean ocean $\delta^{15}N$ increased. The latter would

require that the proportion of denitrification taking place in the water column vs. sediments increased significantly (Deutsch et al., 2004) (see 4.4.3), despite the expansion of sedimentary denitrification on shelves flooded by deglacial sea level rise. This question could be resolved with better global data coverage, and would greatly benefit from a record of deep ocean nitrate $\delta^{15}N$.

Both types of deglacial changes in the nitrogen cycle would have decreased the oceanic storage of CO_2 via the biological pump. The inventory-altering processes would have been expected to reduce the size of the nitrate inventory, exacerbating the nitrogen limitation of export production and possibly driving the whole ocean N:P to lower values (Deutsch et al., 2004), while the increase of nitrate concentrations in the North Pacific and Southern Oceans would have increased the ocean's preformed nutrient fraction, reducing the efficiency of the biological pump for a given nutrient inventory (Ito and Follows, 2005). These changes could have played a significant role in the deglacial rise of *p*CO2.

Turning to PC2, we find that regressions are significant at fewer sites, but maintain reasonable coherency between neighbours, and largely reflect temporal contrasts in the local impact of deglaciation (Figure 4.3c). For example, sites where PC1 and PC2 regressions are both positive, found on the Chilean and Central American coasts, record a deglacial $\delta^{15}N$ peak and/or a strong early rise of $\delta^{15}N$. Meanwhile, a positive PC1 and negative PC2 regression indicate a relatively late (after ~15 ka) rise of $\delta^{15}N$, most notable in the Arabian Sea and tropical African coasts. The similarity between the PC2 timeseries of $\delta^{15}N$ and global surface temperature (Figure 4.3a) is not matched by spatial similarities in the regressions (Shakun and Carlson, 2010), showing that the $\delta^{15}N$ is not responding to local temperature changes. Rather, both PCs reflect deglacial changes in the large-scale overturning of the ocean (Shakun and Carlson, 2010) that would have altered both the supply of nitrate to the surface and the intensity of denitrifying oxygen minimum zones (Schmittner et al., 2007).

We extended our analysis beyond the last glacial maximum, to 80 ka. The resulting dataset contains 48 records, with diminished global coverage and a notable data absence in the

Southern Ocean. Nonetheless, the first PC that emerges from the data analysis reveals a rhythm of change related to global climate over this time interval (Fig. 4.4a), closely matching the average value of the records, and agreeing very well with the first PC of the 5–30 ka interval. The regression of the new PC1 on the data is spatially similar to that of PC1 from the analysis above (Fig. 4.4b), suggesting that the same inventory-altering and internal-cycling mechanisms were at play throughout. However, the nitrogen cycle does not appear to have responded in a linear way to global climate (as reflected by deep ocean temperature/ice volume). In particular, the $\delta^{15}N$ records trend toward higher values from 80 to 20 ka, while the $\delta^{15}N$ increase at the relatively subdued Marine Isotope Stage (MIS) 4-3 transition is of similar magnitude to the deglacial transition. We suggest that both these features can be largely explained by changes in the global rate of sedimentary denitrification. The gradual decline of sedimentary denitrification, which we estimate based on changes in sea level (see 4.4.4, Fig. 3a), would have contributed to the long-term trend by gradually increasing the mean ocean $\delta^{15}N$. Subsequently, the rapid increase of sedimentary denitrification during the latter half of the deglaciation would have favoured a lower mean ocean $\delta^{15}N$, opposing the effect of increasing water column denitrification and thereby muting the $\delta^{15}N$ response relative to the MIS 4-3 transition.

This work confirms, from a global perspective, that the marine nitrogen cycle is intimately linked to climate. Improving the accuracy of $\delta^{15}N$ records requires a better understanding of isotopic alteration during the sinking and sedimentation of organic matter, as well as pursuing compound-specific and protected nitrogen isotope measurements. In addition, this global analysis reveals the degree to which the isotopic effects of inventory-altering processes overlap with those of internal cycling, making it difficult to separate the two. This problem cannot be resolved simply by measuring specific N fractions in sediment, which will be equally affected by both processes. Instead, it will require ancillary environmental information, sufficient high-resolution $\delta^{15}N$ records that spatial patterns can be mapped in detail, and improved global models with better simulations of suboxic zones and N_2 fixation.

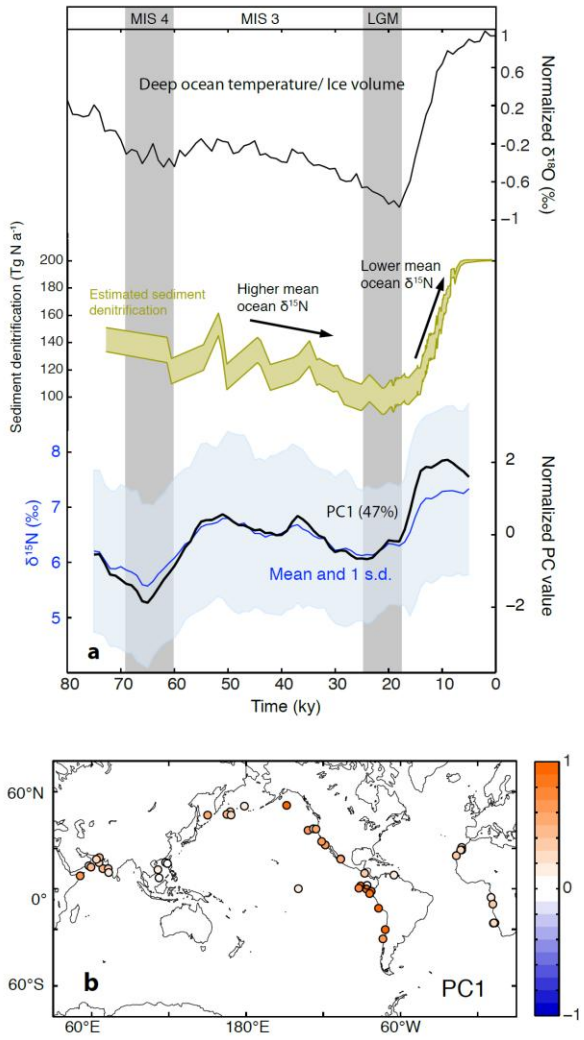

Figure 4.4. Principal Component analysis of 48 $\delta^{15}N$ records over the last 80,000 years, compared to global climate. a) A global stack of benthic foraminiferal $\delta^{18}O$ {Lisieki and Raymo, 2004}, reflecting a combination of deep ocean temperature and global land ice volume, with the long-term mean removed, compared to the first PC timeseries of the detrended $\delta^{15}N$ records (black), as well as the mean (blue) and 1 standard deviation envelope (blue shading). b) Regression coefficients of the first PC against the data. Only significant ($p<0.1$) regressions are shaded.

4.4 Supplementary Information

4.4.1 Nitrogen isotopic fractionation in the ocean

Field observations and laboratory experiments have shown that the $\delta^{15}N$ of sinking organic matter differs from the $\delta^{15}N$ of mean ocean nitrate (5 ‰) due to two classes of fractionating processes (Gruber and Galloway, 2008). When included in the global ocean circulation model, each of the fractionating processes produces zones of high $\delta^{15}N$ and zones of low $\delta^{15}N$, which we refer to as "dipoles".

The first dipole arises from the internal cycling of nitrogen within the ocean, due to fractionation during the growth of phytoplankton and redistribution of dissolved nitrogen by the large-scale ocean circulation. The light isotope is preferentially incorporated in phytoplankton biomass, leading to a ^{15}N enrichment in the residual nitrate (with a typical fractionation factor, ε, of ~ 6 ‰ (Tyrrell; Schmittner et al.)). This residual nitrate is then advected and mixed into neighbouring regions, according to the ocean circulation. Thus, plankton growing on nitrate directly upwelled from the deep ocean will tend to have low $\delta^{15}N$, while plankton growing downstream on residual nitrate have high $\delta^{15}N$.

The second dipole arises from inventory-altering processes, including the addition of N_{bio} to the ocean by N_2 fixation and the removal of N_{bio} by denitrification. N_2 fixation adds new nitrogen with a low isotopic signature (-1 ‰), while water column denitrification strongly fractionates during the production of N_2, leaving residual nitrate that is greatly enriched in ^{15}N (ε ~ 15 ‰, (Franois et al., 1997)). Water column denitrification occurs in only three regions of the modern ocean: the Eastern Tropical North Pacific, Eastern Tropical South Pacific, and the Arabian Sea, whereas N_2 fixation appears to occur throughout a broad swath of the tropics (Ganeshram et al., 1995).

The mean ocean $\delta^{15}N$ of nitrate appears to be determined by how much denitrification happens in the sediments (where little fractionation is expressed, due to near-complete nitrate consumption) vs. the water column (Altabet et al., 1995). As such, higher proportions of water column denitrification will cause the whole-ocean $\delta^{15}N$ to increase. The effective fractionation from water column denitrification may also depend on how much occurs

through the anammox pathway, as well as the degree of consumption within oxygen minimum zones.

4.4.2 Principal Component Analysis

Sediment records containing gaps of more than 4 ky over the period 5-25 ka were removed from the dataset, leaving 78 records. The 5-25 ka mean was removed from each record, and missing values were replaced with zeros. The eigenproblem was solved for the covariance matrix, and the Principal Components (PCs) obtained by projection of the eigenvectors onto the data, normalized to their standard deviations. The maps (Figure 4.3) show the regression coefficients of the data on the first and second PCs, wherever the regression was highly significant ($p<0.1$). The longer timeseries, 5-80 ka , was treated similarly.

4.4.3 Model simulations

The standard simulation was integrated under pre-industrial conditions to a steady-state. The mean oceanic $\delta^{15}N$ in the model depends on the balance of water column vs. sedimentary denitrification, as discussed above, and was tuned to produce a value of 5 ‰ by adjusting the amount of sediment denitrification (Ren et al., 2009). The internal-cycling impact on $\delta^{15}N$ (Figure 4.1c) was estimated by setting N_2 fixation and denitrification to zero, and integrating the model to steady state with the same inventory of nitrogen. The inventory-altering impact on $\delta^{15}N$ (Figure 4.1d) was estimated by setting the fractionation factors for N assimilation and excretion to zero, so that only N_2 fixation and denitrification altered the N isotopes.

4.4.4 Sediment denitrification

The rate of sedimentary denitrification was estimated using a satellite-colour based algorithm for export production, realistic seafloor bathymetry, and a standard algorithm for sedimentary denitrification, as described by (Bianchi et al.). This was then modified using a timeseries of sea level change, according to the compilation of (Codispoti et al., 2001). The low and high estimates shown in Figure 4.4 were derived by removing export production from emerged ocean regions, and redistributing the emerged export production globally, respectively. Note that this estimate considers eustatic sea level change only.

5 Isotopic constraints on the pre-industrial oceanic fixed nitrogen budget

This chapter is based on the manuscript in preparation from Christopher J. Somes, Andreas Oschlies, and Andreas Schmittner

Abstract

The size of the bio-available "fixed" nitrogen inventory in the ocean influences global marine productivity because fixed nitrogen limits biological growth throughout much of the sunlit surface waters. Despite its importance, the rates for the major source and sink terms of the oceanic fixed nitrogen budget, N_2 fixation and denitrification/anammox (N-loss), respectively, are regarded with considerable uncertainty. These processes leave distinguishable imprints on the ratio of stable nitrogen isotopes, $\delta^{15}N$, which can therefore help to infer their patterns and rates. Here we use $\delta^{15}N$ observations in the water column and in a new seafloor database to constrain rates of N_2 fixation and N-loss in a global coupled three-dimensional circulation-biogeochemistry-isotope model. Sensitivity experiments were performed to quantify uncertainties associated with the isotope effect of N-loss in the water column and sediments. They show that the level of nitrate utilization in suboxic zones, that is the balance between nitrate consumption by N-loss processes and nitrate replenishment by mixing (dilution effect), significantly affects the isotope effect of water column N-loss on global mean $\delta^{15}NO_3^-$. Experiments with lower levels of nitrate utilization within the suboxic zone (i.e., higher nitrate concentrations) require more N_2 fixation relative to water column N-loss, and thus higher ratios of benthic to water column N-loss to satisfy the global mean NO_3^- and $\delta^{15}NO_3^-$ constraints in the modern ocean. This suggests that nitrate utilization and dilution effects in the suboxic zone plays an important role in global nitrogen isotope cycling. Increasing the net fractionation factor for benthic N-loss ($\varepsilon_{BN\text{-}l}$=0–4‰) requires higher ratios of benthic to water column N-loss rates (1.4:1–3.2:1). The model experiment that best reproduces observed seafloor $\delta^{15}N$, most notably in the North Pacific, one of the largest basins of benthic N-loss in the global ocean, supports the high-end estimates for the net

fractionation factor benthic N-loss ($\varepsilon_{BN\text{-}l} \geq 4$ ‰). If this is indeed true on a global scale, our model estimates that rates of N_2 fixation, water column N-loss, and benthic N-loss were in the range 220–370, 70–90, and 150–280 Tg N yr^{-1}, respectively, assuming a balanced fixed nitrogen budget in the pre-industrial ocean. Although uncertainties still exist, this model result suggests that previous estimates of N_2 fixation have been severely underestimated and the oceanic residence time for fixed nitrogen is between 1,500 and 3,000 years.

5.1 Introduction

Biotically available "fixed" nitrogen (fixed-N) is one of the major limiting nutrients throughout the sunlit surface ocean. Its generally low abundance in sunlit surface waters limits the growth of primary producers that form the base of ocean ecosystems, which provide energy for more complex higher-level organisms (e.g., marine animals). Thereby, fixed-N also limits the biological sequestration of atmospheric carbon dioxide (CO_2) into phytoplankton biomass, part of which subsequently sinks towards the deep ocean. Whenever respiration of organic matter back into CO_2 occurs at depth not in immediate contact with the atmosphere, the so-called "biological carbon pump" affects the partitioning of CO_2 among the oceanic and atmospheric pools. It has been suggested that large changes in the oceanic fixed-N inventory can modulate the strength of the biological carbon pump and thereby influence atmospheric CO_2 over glacial/interglacial timescales (McElroy, 1983; Falkowski, 1997). Since processes that control the size of the fixed-N inventory are sensitive to climate (Gruber, 2004; Galbraith et al., 2012, in review), they may have an important feedback on atmospheric CO_2 concentrations in past and future climates.

N_2 fixation, the conversion of N_2 gas into fixed-N by specialized microorganisms (diazotrophs), provides the ocean with most of its fixed-N. Other contributions to the fixed-N pool are from river input and atmospheric N deposition, which are estimated be approximately an order of magnitude lower than N_2 fixation in pre-industrial times (Galloway et al., 2004; Codispoti, 2007; Duce et al., 2008a; Gruber, 2008). However, industrial N emissions and fertilizer production through the Haber-Bosch process that eventually cycles fixed-N into the atmosphere and rivers, have been steadily increasing in

recent decades and are estimated to become comparable to "natural" N_2 fixation in following decades (Galloway et al., 2004).

Denitrification and anammox are the most important fixed-N removal processes in the ocean. They convert fixed-N into N_2 gas under suboxic conditions (O_2 < ~10 uM) in the water column and seafloor sediments. "Canonical" denitrification occurs when heterotrophic bacteria replace O_2 consumption with the reduction of nitrate (NO_3^-) to dinitrogen gas (N_2) as the electron acceptor during respiration once O_2 is no longer available in sufficient quantity. Anammox, on the other hand, is a chemoautotrophic process that converts nitrite (NO_2^-) and ammonium (NH_4^+) into N_2 gas, which provides energy for growth (Thamdrup and Dalsgaard, 2002; Kuypers et al., 2003). Since both denitrification and anammox processes occur in oxygen minimum zones (OMZs), the relative importance of each process is uncertain. Recent studies have found that water column denitrification dominates N-loss in the Arabian Sea (Ward et al., 2009; Bulow et al., 2010), while anammox is more important in the ETSP (Lam et al., 2009). Given that both canonical denitrification and anammox lead to a net conversion of fixed-N to gaseous N, and occur within close proximity, here we refer to the term "N-loss" as the combined net fixed-N removal from these two processes.

While the major source and sink processes of the fixed-N budget, N_2 fixation and denitrification/anammox (N-loss), respectively, are relatively well known, estimating their global rates remains a challenge. Recent estimates for N_2 fixation range widely between ~100 – 300 Tg N yr^{-1} as well as predicting different spatial patterns (Brandes and Devol, 2002) (Gruber and Sarmiento, 1997; Karl et al., 2002; Moore and Doney, 2007b; Somes et al., 2010a; Monteiro et al., 2011). Methods historically used to measure N_2 fixation have been found to be underestimating N_2 fixation by at least a factor of 2 (Mohr et al., 2010; Großkopf et al., 2012, in review). New important N_2-fixing species are also still being discovered (Montoya et al., 2004; Foster et al., 2011; Zehr, 2011), suggesting additional N_2 fixation could be taking place in the ocean than previously thought.

Estimates of N-loss vary considerably as well. In the water column, studies suggest global rates between 50–150 Tg N yr^{-1} and in the sediments generally between 100–300 Tg N yr^{-1}

(Middelburg et al., 1996)(Bohlen et al., 2012, submitted), (Galloway et al., 2004; Gruber, 2004; Codispoti, 2007). The high-end estimates for N-loss are substantially larger than the high-end estimates for N_2 fixation, which has led to the debate whether the ocean could be rapidly losing as much as 400 Tg N yr^{-1} (Codispoti et al., 2001; Brandes and Devol, 2002; Codispoti, 2007), about 0.07% of the total fixed-N inventory per year, or whether the nitrogen budget is balanced (Gruber and Sarmiento, 1997; Gruber, 2004; Altabet, 2007; Bianchi et al., 2012).

Stable nitrogen isotopes can provide constraints on N_2 fixation and N-loss because they leave distinguishable imprints on the ratio of oceanic $\delta^{15}N$, defined as $\delta^{15}N=[(^{15}N/^{14}N)_{sample} / (^{15}N/^{14}N)_{atmospheric} - 1]\cdot 1000$. Diazotrophs fix ^{15}N-depleted atmospheric N_2 into their biomass ($\delta^{15}N_{DIAZ}= -2–0$ ‰) relative to the global ocean mean ($\delta^{15}NO_3^- = \sim 5.5$ ‰). Denitrifying bacteria preferentially consume ^{15}N-depleted nitrate, the lighter and hence more reactive isotope, during water column N-loss ($\varepsilon_{WCN\text{-}l}$=20–30 ‰), leaving the oceanic nitrate pool enriched in ^{15}N (Cline and Kaplan, 1975; Voss et al., 2001a). Benthic N-loss is observed to have a much lower net fractionation factor ($\varepsilon_{BN\text{-}l}$=1–3 ‰), which is attributed to near complete NO_3^- utilization in pore-water sediments (Brandes and Devol, 2002; Lehmann et al., 2004). However, recent studies (Lehmann et al., 2007; Granger et al., 2011; Alkhatib et al., 2012) investigating fractionation involved with the nitrification-denitrification loop in the sediments suggest a larger net fractionation factor for benthic N-loss ($\varepsilon_{BN\text{-}l}$ =4–8 ‰). The global ocean mean $\delta^{15}NO_3^-$ provides an additional constraint on the fixed-N budget because the combination of the different isotope effects of N_2 fixation and total N-loss, along with their respective rates, determines global mean $\delta^{15}NO_3^-$.

Global nitrogen isotope models can estimate the relative rates of N_2 fixation, water column and benthic denitrification required to match the global ocean mean $\delta^{15}NO_3^-$. The input of ^{15}N-depleted nitrogen from N_2 fixation must compensate for the preferential removal of ^{15}N-depleted nitrate by N-loss processes to set the global ocean mean $\delta^{15}NO_3^-$ to ~5.5 ‰. Assuming constant isotope effects for water column and benthic N-loss, one can calculate the relative rates needed to match the observational constraint. For example, when using a fractionation factor of 0 ‰ for benthic N-loss, its only isotope effect will be an indirect one

by stimulating additional N_2 fixation in a balanced fixed-N budget. Then it can be calculated how much "extra" N_2 fixation needs to be stimulated by benthic N-loss to balance the remaining ^{15}N-enriched nitrate produced by water column N-loss.

Modeling studies that take into account these different isotope effects to constrain rates of N_2 fixation and N-loss have produced differing results. For example, Brandes and Devol (Brandes and Devol, 2002) used a one-box model to calculate the rates of N_2 fixation and N-loss needed to obtain the observed global mean $\delta^{15}NO_3^-$, using fractionation factors of 1.5 ‰, and 25 ‰ for benthic N-loss and water column N-loss, respectively. They estimated that a ratio of benthic to water column N-loss (BN-l:WCN-l) of 3.7:1 is required to achieve the observed oceanic mean $\delta^{15}NO_3^-$, supporting the high-end estimates for benthic N-loss.

Another study used a more complex 6-box model to investigate global nitrogen isotope cycling (Deutsch et al., 2004). They found that it is important to account for the locally reduced nitrate concentrations in suboxic zones that mix into surrounding oxic waters with higher nitrate. Since the mixed $\delta^{15}NO_3^-$ value will be weighted towards the higher nitrate concentration, the local utilization of nitrate reduces the influence of the ^{15}N-enriched nitrate from water column N-loss on the global mean $\delta^{15}NO_3^-$, a mechanism referred to as the "dilution effect". For example, if the nitrate concentration in the suboxic zone contains only half the nitrate in surrounding oxic waters, the $\delta^{15}NO_3^-$ signature of the oxic water will have twice the influence on total $\delta^{15}NO_3^-$ of these water masses if they mix together. This conservation of mass is implicit within the physical transport terms (i.e., mixing, advection) of ocean circulation models. Deutsch et al. (Deutsch et al., 2004) used fractionation factors of 0 ‰, and 25 ‰ for benthic N-loss and water column N-loss, respectively, in their model. They estimated that a lower BN-l:WCN-l ratio compared to the Brandes and Devol (Brandes and Devol, 2002) of 2.7:1 would be required to satisfy the global ocean $\delta^{15}NO_3^-$ result due to the dilution effect.

Later, Altabet (Altabet, 2007) used a one-box model approach, but parameterized the isotope effects of local nitrate utilization during water column N-loss. He argues that these effects would reduce the isotope effect of water column N-loss by ~13 ‰ compared to the inherent

microbial process ($\varepsilon_{WCN\text{-}l}$ = 25 ‰). Applying this reduced isotope effect for water column N-loss (~12 ‰), and 0 ‰ for benthic N-loss, respectively, he estimated that the BN-l:WCN-l ratio should be ~1:1. These box model studies highlight how sensitive the global ocean mean $\delta^{15}NO_3^-$ can be to different assumptions made for the isotope effects of N-loss, and their associated rates needed to achieve the observed global mean $\delta^{15}NO_3^-$.

In this study, we go beyond earlier box-model approaches and employ a global coupled circulation-biogeochemistry-isotope model to investigate to what extent rates of N_2 fixation and N-loss can be constrained by $\delta^{15}N$ observations in the water column and seafloor sediments. In particular, we will investigate the uncertainties associated with (i) the effects of nitrate utilization and dilution on the isotope effect of water column N-loss and (ii) the net fractionation factor associated with benthic N-loss. In addition to water column $\delta^{15}NO_3^-$ observations, a new global seafloor sediment $\delta^{15}N$ database (Tesdal et al., 2012) is used to evaluate the model experiments. The rates of N_2 fixation and N-loss implicit in the model simulations that perform best with respect to observed $\delta^{15}NO_3^-$ and seafloor $\delta^{15}N$ then provide our best estimate of N_2 fixation and N-loss in the real ocean.

5.2 Model Description

The global coupled circulation-biogeochemistry-isotope model used is based on the version of *Somes et al.*, (Somes et al., 2010b). A technical description of the model is located in Sections 5.7 and 5.8 and a brief overview is provided below.

5.2.1 Physical Model

The physical model is based on the University of Victoria Earth System Climate Model (Weaver et al., 2001), version 2.9 (Eby et al., 2009),. It includes a global, three-dimensional general circulation model of the ocean (Modular Ocean Model 2) with physical parameterizations such as diffusive mixing along and across isopycnals, eddy induced tracer advection (Gent and Mcwilliams, 1990), the computation of tidally induced diapycnal mixing over rough topography (Simmons et al., 2004), and an anisotropic viscosity scheme (Large et al., 2001) in the tropics. Nineteen vertical levels are used with a horizontal resolution of 1.8ºx3.6º. A two dimensional, single level energy-moisture balance model of the atmosphere

and a dynamic-thermodynamic sea ice model are used, forced with prescribed NCEP/NCAR monthly climatological winds (Kalnay et al., 1996).

5.2.2 Biogeochemical-Ecosystem Model

The marine ecosystem-biogeochemical model is an improved version of the model used in Somes et al., (Somes et al., 2010b) (see Figure 5.1). The organic compartments include two classes of phytoplankton, N_2-fixing diazotrophs (P_D) and an "ordinary" nitrate assimilating phytoplankton class (P_O), as well as zooplankton (Z), and sinking detritus (D). The inorganic variables include dissolved oxygen (O_2) and two nutrients, nitrate (NO_3^-) and phosphate (PO_4^{3-}), both of which are consumed by phytoplankton.

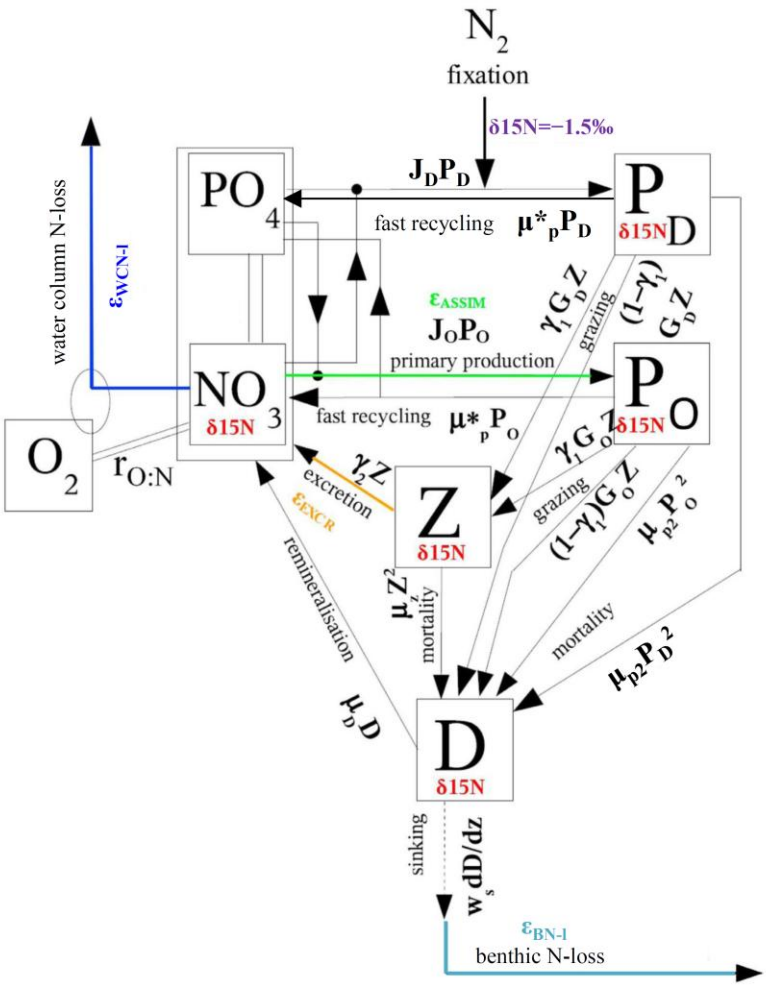

Figure 5.1: Schematic of the marine ecosystem/biogeochemical model compartments including the nitrogen isotope parameters (colors).

This model version deviates from that of (Somes et al., 2010b) by including varying elemental stoichiometry. While general phytoplankton N:P remains at the canonical Redfield ratio (N:P=16), diazotroph N:P is set to 40, which is in better agreement with most observations (N:P=20–50+) (Letelier and Karl, 1998b; Sanudo-Wilhelmy et al., 2004), as well as an optimality-based growth model (Klausmeier et al., 2004). Since zooplankton are capable of maintaining their own stoichiometry (Sterner and Elser, 2002), we set zooplankton N:P to 16:1 and assume that they excrete excess N when grazing diazotrophs. Detrital N and P are explicitly calculated as separate prognostic variables. The C:N ratio for all compartments is held constant at C:N=6.625.

Diazotrophs grow according to the same principles as the general phytoplankton class in the model, but we account for their different characteristics. N_2 fixation is energetically more costly than assimilating fixed-N. Diazotrophs must break down the strong triple-N bond and undergo extra respiration to keep the N_2-fixing compartment anoxic since O_2 inhibits the expression of the N_2-fixing gene (nifH). Thus, the growth rate of diazotrophs is reduced compared to ordinary phytoplankton by a handicap factor (c_{Diaz}=0.13). Diazotroph growth is not explicitly set to 0 at 15°C as in previous model versions (Schmittner et al., 2008; Somes et al., 2010b), but are now allowed to grow at low rates in cooler waters according to Equation ?, consistent with observations (Pandey et al., 2004; Le Quéré et al., 2005).

Diazotrophs are not limited by nitrate and can out-compete general phytoplankton in surface waters that are depleted in fixed-N, but still contain sufficient P and Fe (i.e., water with low nitrate from N-loss and high atmospheric Fe deposition). They will consume nitrate if available, consistent with culture experiments (Mulholland et al., 2001; Holl and Montoya, 2005), which is another factor that inhibits N_2 fixation in high-nutrient low-chlorophyll (HNLC) regions in the model. Diazotroph prey-capture rate is also reduced relative to the general phytoplankton class to account for lower grazing on diazotrophs versus other phytoplankton (Table 5.5) (Mulholland, 2007), which was at an equal level in Somes et al. (2010b).

Due to uncertainties in modeling the iron cycle (Aumont et al., 2003; Moore et al., 2004; Galbraith et al., 2010), iron is currently not included as a prognostic tracer. Instead, a monthly Fe limitation mask is calculated based on aeolian Fe deposition estimates (Mahowald et al., 2005b; Mahowald et al., 2006; Mahowald et al., 2009). This Fe mask is multiplied to diazotroph's maximum growth rate to account for Fe limitation (Somes et al., 2010a).

Water column N-loss occurs when organic matter is respired under suboxic conditions. It is parameterized in the model according to equation ? that determines the relative amount of nitrate consumption that takes place during respiration at low ambient oxygen concentrations. We use a threshold of 5 μM O_2 that sets the level where respiration by denitrification overtakes aerobic respiration. This parameterization was designed to best capture the decreasing NO_3^-:PO_4^{3-} ratios in suboxic zones. Anammox is also removing fixed-N in these areas of low oxygen and high organic matter recycling. Since the model does not differentiate between different species of dissolved inorganic nitrogen, this water column "N-loss" parameterization implicitly captures total fixed-N loss from both water column denitrification and anammox.

Benthic N-loss is included using a new empirical function deduced from benthic flux measurements (Bohlen et al., 2012, in review). This function estimates N-loss in the sediments based on organic carbon rain rate into the sediments, and bottom water O_2 and NO_3^- concentrations (Equation ?). It provides an efficient alternative to coupling a full sediment model that would significantly reduce simulation speed. Note that all organic matter instantaneously remineralizes in the bottom water when it hits the seafloor sediment interface. Nitrate is then removed from the bottom water according to this benthic N-loss function. While the organic carbon rain rate predicts benthic N-loss rates to first-order, Bohlen et al. (2012, in review) found a strong non-linear relationship to the empirical parameter $O_2^* = O_2 - NO_3^-$parameter of oxygen and nitrate concentrations in the bottom water overlying the sediments. Benthic N-loss rates are significantly higher as O_2^* decreases (i.e., when O_2 is low and NO_3^- is high) for similar organic carbon rain rates. We also include a sub-grid scale continental shelf within this benthic N-loss scheme to account for shallow

continental shelves that are not fully resolved in the model's coarse-resolution grid (see Appendix B).

5.2.3 Nitrogen Isotope Model

The nitrogen isotope model simulates the two stable nitrogen isotopes, ^{14}N and ^{15}N, in all N species included in the marine ecosystem model. Fractionation results in the preferential incorporation of the more reactive, thermodynamically preferred ^{14}N isotope into the product of each reaction by a process-specific fractionation factor, α (Mariotti et al., 1981). We report these values in the more commonly used "δ" notation, where the fractionation factor takes the form $\varepsilon = (1 - \alpha) \times 1000$. The processes in the model that fractionate nitrogen isotopes are phytoplankton nitrate assimilation (ε_{ASSIM} = 5‰), N_2 fixation (ε_{NFIX} = 1.5‰), zooplankton excretion (ε_{EXCR} = 6‰), water column N-loss ($\varepsilon_{WCN\text{-}l}$ = 25‰), and benthic N-loss ($\varepsilon_{BCN\text{-}l}$ = 0, 2, 4‰). For example, diazotroph biomass becomes 1.5‰ depleted in $\delta^{15}N$ relative to the source (atmospheric $\delta^{15}N_2$=0‰) giving diazotroph biomass a $\delta^{15}N$ signature of −1.5‰ when they fix atmospheric N_2 for growth.

We refer to the fractionation factor as the ε value chosen for the fractionation equation and the "isotope effect" as the overall effect the process has on the $\delta^{15}N$ distribution in the ocean. The total isotope effect also includes effects from source values and processes that alter the impact of the net fractionation, such as nitrate utilization and dilution. N_2 fixation, for example, has a low fractionation factor, but a strong isotope effect by introducing very ^{15}N-depleted nitrogen ($\delta^{15}N_{NFIX}$ = −1.5 ‰) into the oceanic fixed-N pool relative to mean ocean $\delta^{15}NO_3^-$ near 5.5 ‰. In the model, fractionation factors are constant in space and time, and chosen to best represent estimates from field observations (Somes et al., 2010b).

5.3 Nitrogen Isotope Sensitivity Experiments

The model experiments were initialized with World Ocean Atlas 2009 (WOA09) observations (temperature, salinity, oxygen, nitrate, and phosphate) (Antonov et al., 2010; Garcia et al., 2010a; Garcia et al., 2010b; Locarnini et al., 2010). They integrated for over 10,000 years with pre-industrial boundary conditions as the nitrogen cycle approached equilibrium. While the scarcity of water column observations makes it difficult to estimate

global mean $\delta^{15}NO_3^-$, vertical $\delta^{15}NO_3^-$ profiles throughout the global ocean converge to ~5‰ at depths below 2000 m (Somes et al., 2010b). Therefore during these multi-millenia simulations, total benthic N-loss rate (through $\alpha_{BN\text{-}l}$) and N_2 fixation (through prey-capture rate, ω_{Diaz}, and mortality, ν_{Diaz}) were manually adjusted to maintain deep ocean (2,000–6,000 m) $\delta^{15}NO_3^-$ at ~5‰ and global NO_3^- at ~31 μM for each isotope sensitivity experiment (Table 5.1, 5.2). All model experiments were integrated over 3,000 years in their final parameter setting as they reach steady-state. The results shown here are annual averages from the final 500 years of integration.

Table 5.1 Model parameters changed for the sensitivity experiments: limitation of water column denitrification (limWCD), benthic denitrification fractionation factor ($\varepsilon_{BN\text{-}l}$), benthic denitrification multiplication factor ($\alpha_{BN\text{-}l}$), diazotroph prey-capture rate (ω_{Diaz}), and diazotroph mortality rate (ν_{Diaz}) to set global mean NO_3^- to ~31μM and global deep ocean (2000–6000 m) mean $\delta^{15}NO_3^-$ to ~5‰.

Experiment	**limWCD** ($\mu M\ NO_3^-$)	$\varepsilon_{BN\text{-}l}$ (‰)	$\alpha_{BN\text{-}l}$	ω_{Diaz} $(mmol\ m^{-3})^{-2}d^{-1}$	ν_{Diaz} d^{-1}
1	20	0	1.35	0.11	0.25
2	26	0	1.6	0.09	0.25
3	32	0	1.5	0.128	0.25
4	32	2	1.9	0.078	0.25
5	32	4	3.2	0.001	0.16

5.3.1 Water column N-loss Experiments

This set of experiments was designed to test the importance of the isotope effect of water column N-loss on the global ocean mean $\delta^{15}NO_3^-$. We follow a method introduced by Moore and Doney (2007b) that limits the rate of water column N-loss (limWCN-l) at a given nitrate thresholds of 20, 26, and 32 μM (Table 2, Figure 2). These values were chosen to produce water column N-loss rates that lie within the range of modern estimates between 70–150 Tg N yr^{-1}. Note only the highest threshold applied (limWCN-l=32) captures the average nitrate concentration in the suboxic zones suggested by WOA09, while the other experiments underestimate nitrate there. Models with higher thresholds have lower levels of nitrate utilization in the suboxic zones that affect the strength of the dilution effect. In order to

exclude impacts on the distribution of other biogeochemical tracers (oxygen, phosphate), the remineralization of organic matter was left unchanged in these sensitivity experiments. Only nitrate consumption during water column N-loss was turned off below the respective nitrate threshold.

5.3.2 Benthic N-loss Fractionation Experiments

Field studies estimate the fractionation factor of benthic N-loss to be much smaller than that of water column N-loss, but to what extent still remains uncertain. The small increase in bottom water $\delta^{15}NO_3^-$ overlying benthic denitrification zones suggests the fractionation factor should be in the range 1–3 ‰ (Brandes and Devol, 2002; Lehmann et al., 2004). However, more recent studies have suggested a much higher net fractionation for benthic N-loss (Lehmann et al., 2007; Granger et al., 2011; Alkhatib et al., 2012). They suggests the ^{15}N-enriched ammonium measured in the overlying bottom water, presumably released from the sediments, was due to fractionation during nitrification-denitrification loop in the sediments. These studies suggest a net fractionation factor for benthic N-loss in the range 4–8 ‰. We performed experiments with benthic N-loss fractionation at 0, 2, and 4 ‰ to test its effect on the global nitrogen isotope budget.

5.4 Results

5.4.1 Patterns of N_2 fixation and N-loss

(i) N_2 fixation

Diazotrophs perform N_2 fixation primarily in the tropics/subtropics where sufficient atmospheric Fe deposition occurs (e.g., North Atlantic, Western Pacific, and North Indian Ocean). Besides temperature and Fe availability, another important factor that determines where diazotrophs are most abundant include competition for resources with other phytoplankton (i.e., N vs. P limitation). N-loss processes consume nitrate and increase N-limitation "downstream" of N-loss zones. In the model, this creates an ecological niche for diazotrophs because they are not limited by nitrate. Nitrate depletion at the surface with respect to phosphate thus stimulates N_2 fixation as long as temperatures are high enough and sufficient Fe is available (Figure 5.2).

Table 5.2: Model results for the different sensitivity experiments with the observational estimate given in parenthesis.

Experiment			**Global Results**						**Suboxic Zone (O_2 < 10 µM) Results**		
Number	**limWCN-l** ($\mu M\ NO_3^-$)	$\varepsilon_{BN\text{-}l}$ (‰)	**N_2 fixation** ($Tg\ N\ yr^{-1}$)	**W.C. N-loss** ($Tg\ N\ yr^{-1}$)	**Benthic N-loss** ($Tg\ N\ yr^{-1}$)	**NO_3^-** (31.1µM)	**Deep ocean $\delta^{15}NO_3^-$** (5.0‰)	**Global ocean $\delta^{15}NO_3^-$** (~5.5 ‰)	**NO_3^-** (33.5 µM)	**$\delta^{15}NO_3^-$** (~12 ‰)	**NO_3:16 PO_4** (0.700)
1	20	0	253	144	109	31.2	5.01	5.57	24.9	17.6	0.512
2	26	0	238	112	126	31.3	5.04	5.62	29.0	15.9	0.593
3	32	0	207	86.9	121	31.2	4.98	5.56	33.5	14.0	0.678
4	32	2	229	78.3	151	30.8	5.04	5.57	33.2	13.7	0.682
5	32	4	349	77.2	272	30.9	5.04	5.43	33.1	12.0	0.737

Table 5.3 $\delta^{15}N$ Box Model Parameter List

	ε_{NFIX} (‰)	WCN-l rate (Tg N yr^{-1})	$\varepsilon_{WCN\text{-}l}$ (‰)	WCN-l zone $\delta^{15}NO_3^-$ (‰)	$\varepsilon_{BN\text{-}l}$ (‰)	BN-l zone $\delta^{15}NO_3^-$ (‰)	BN-l / WCN-l (one-box model)	BN-l / WCN-l (reported)
B&D02 [1]	1	75	25	5	1.5	5	4.31	3.73
DEU04	0	70	25	12	0	5	2.69	2.71
ALT07 [2]	1	90	25	18	0	5	1.01	~1.00
limWCD=20 $\varepsilon_{BN\text{-}l}$=0	1.5	144	25	18.2	0	5.86	0.787	0.757
limWCD=26 $\varepsilon_{BN\text{-}l}$=0	1.5	112	25	15.7	0	5.79	1.13	1.13
limWCD=32 $\varepsilon_{BN\text{-}l}$=0	1.5	87.6	25	13.8	0	5.74	1.40	1.39
limWCD=32 $\varepsilon_{BN\text{-}l}$=2	1.5	78.3	25	13.4	2	5.88	1.96	1.93
limWCD=32 $\varepsilon_{BN\text{-}l}$=4	1.5	77.0	25	11.6	4	5.96	3.58	3.53

[1]Brandes and Devol (2002) reported ratio also included isotope effects from atmospheric N deposition, river input, and sediment burial, which are excluded in the one-box model calculation to maintain consistency with the other model results. This slightly reduces the BN-l:WCN-l ratio in their model and suggests the other model estimates may be slightly overestimating BN-l:WCN-l as well.

[2] Altabet (2007) used a combination of reducing the fractionation factor of water column N-loss (to account for circulation effects not included in the one-box model) and increasing initial $\delta^{15}NO_3^-$ so the $\delta^{15}N$ signature of nitrogen removed was −7 ‰. To maintain consistency with the other models, we leave $\varepsilon_{WCN\text{-}l}$ at 25 ‰ and increase water column N-loss zone $\delta^{15}NO_3^-$ to 18 ‰ achieve his suggested $\delta^{15}N$ value for nitrogen removal of −7 ‰.

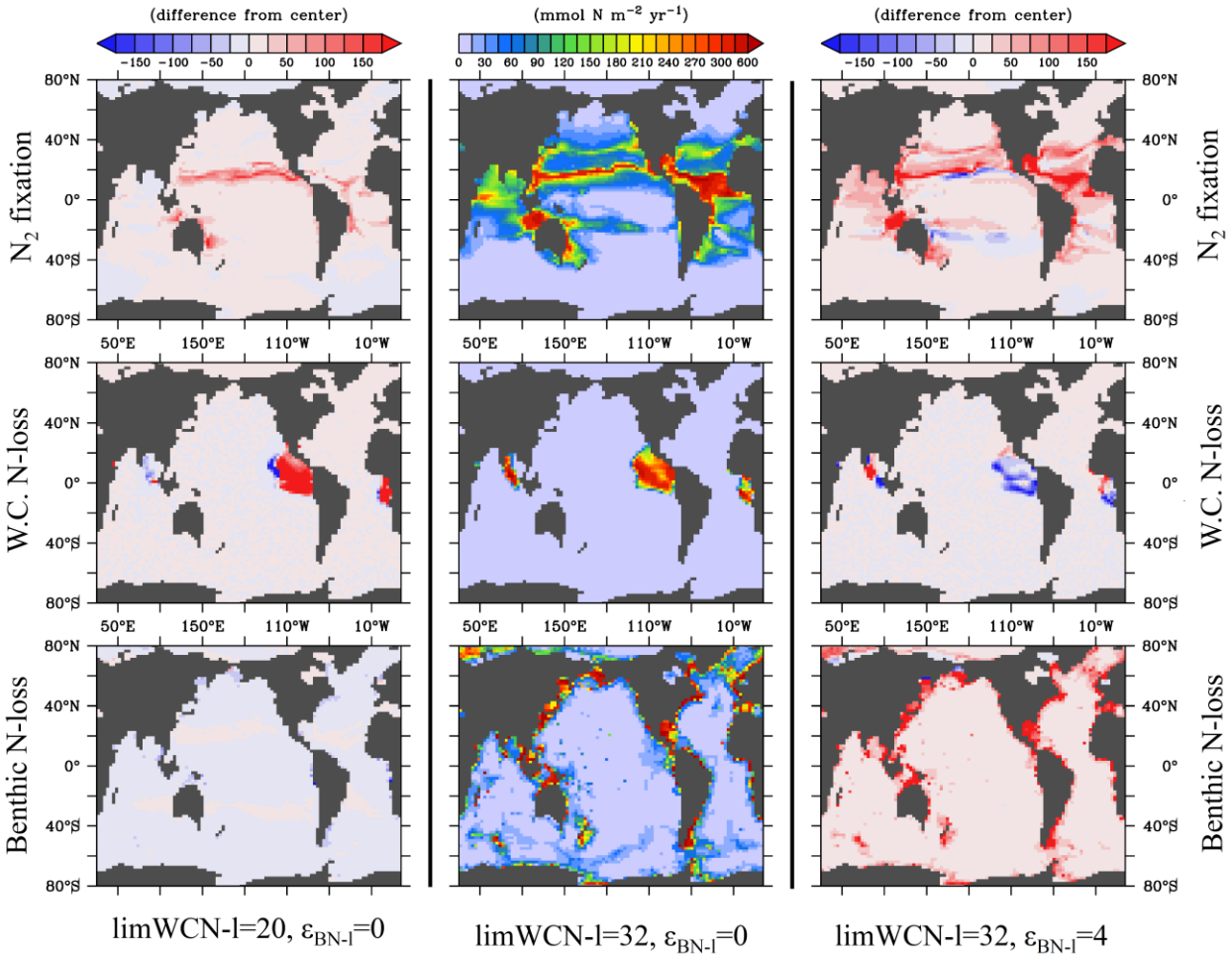

Figure 5.2: Global distribution of annual vertically integrated N_2 fixation (top row), water column N-loss (middle row) and benthic N-loss (bottom row) for the experiments limWCD=20,ε_{BD}=0 (left), limWCD=32,ε_{BD}=0 (center), and limWCD=32,ε_{BD}=4 (right). See text for model experiment details.

(ii) Water Column N-loss

Water column N-loss occurs when organic matter is respired within suboxic zones. This occurs in the Eastern Tropical North/South Pacific, the Bay of Bengal, and the Eastern Tropical Atlantic in the model (Figure 5.2). Note that in the real ocean, large rates of water column N-loss also occur in the Arabian Sea, which is not reproduced in the model. Instead, the model displaces the suboxic zone to the Bay of Bengal, which is very close to the suboxic threshold in nature. Similar discrepancies between simulated and observed regions of water column N-loss in the Indian Ocean have also been found in other models (Moore and Doney, 2007b; Gnanadesikan et al., 2012). Its causes are not fully understood and may include a misrepresentation of local currents in the Indian Ocean. Although denitrification is not

regularly observed in the Atlantic Ocean, anammox bacteria have been found in the Eastern Tropical South Atlantic suggesting that N-loss events can occur there (Kuypers et al., 2005). Nevertheless, the model seems to significantly overestimate N-loss in the Atlantic Ocean. While the simulated suboxic zones are generally located in the right oceanographic regions, deficiencies in the coarse-resolution circulation-biogeochemistry model generally result in the suboxic regions being too large and displaced towards the equator in the Pacific (Somes et al., 2010b). For example, poleward undercurrents and eddies that ventilate the eastern Pacific suboxic zones with relatively oxygen-rich water are not fully resolved in the coarse-resolution model used, a fact that might contribute to the overestimated volume of suboxic waters in the model.

(iii) Benthic N-loss

Benthic N-loss occurs where there are large rain rates of particulate organic carbon (POC) into the seafloor sediments, primarily along on the continental shelves and shelf-slopes (Middelburg et al., 1996; Bianchi et al., 2012; Bohlen et al., 2012, in review). Since these exist in all ocean basins, benthic N-loss has a more global distribution compared to water column N-loss that is predominant in three distinct tropical suboxic regions (Figure 5.2). The percentage of total benthic denitrification simulated on the continental shelves (0–150m), shelf-slopes (150–2000m), and deep seafloor (2000–6000m) is 35%, 45%, and 20%, respectively, which do not vary by more than ±5 % for the different model experiments.

5.4.2 Seafloor $\delta^{15}N$ Constraint

We compare sinking $\delta^{15}N$ in the model with a new global database of seafloor $\delta^{15}N$ (Tesdal et al., 2012) (Figure 5.3). It is composed of 1653 bulk $\delta^{15}N$ measurements covering all ocean basins. This seafloor $\delta^{15}N$ database provides a more complete view of the global nitrogen isotope distribution compared to available water column $\delta^{15}NO_3^-$ observations, which are sparse in spatial and temporal scales (Somes et al., 2010b). Since seafloor $\delta^{15}N$ measurements represent the accumulation of material spanning the last hundreds to thousands of years, they remove seasonal, interannual, or anthropogenic variability that can impact any single water column observation, making seafloor $\delta^{15}N$ an ideal dataset to constrain the annual average of the pre-industrial ocean.

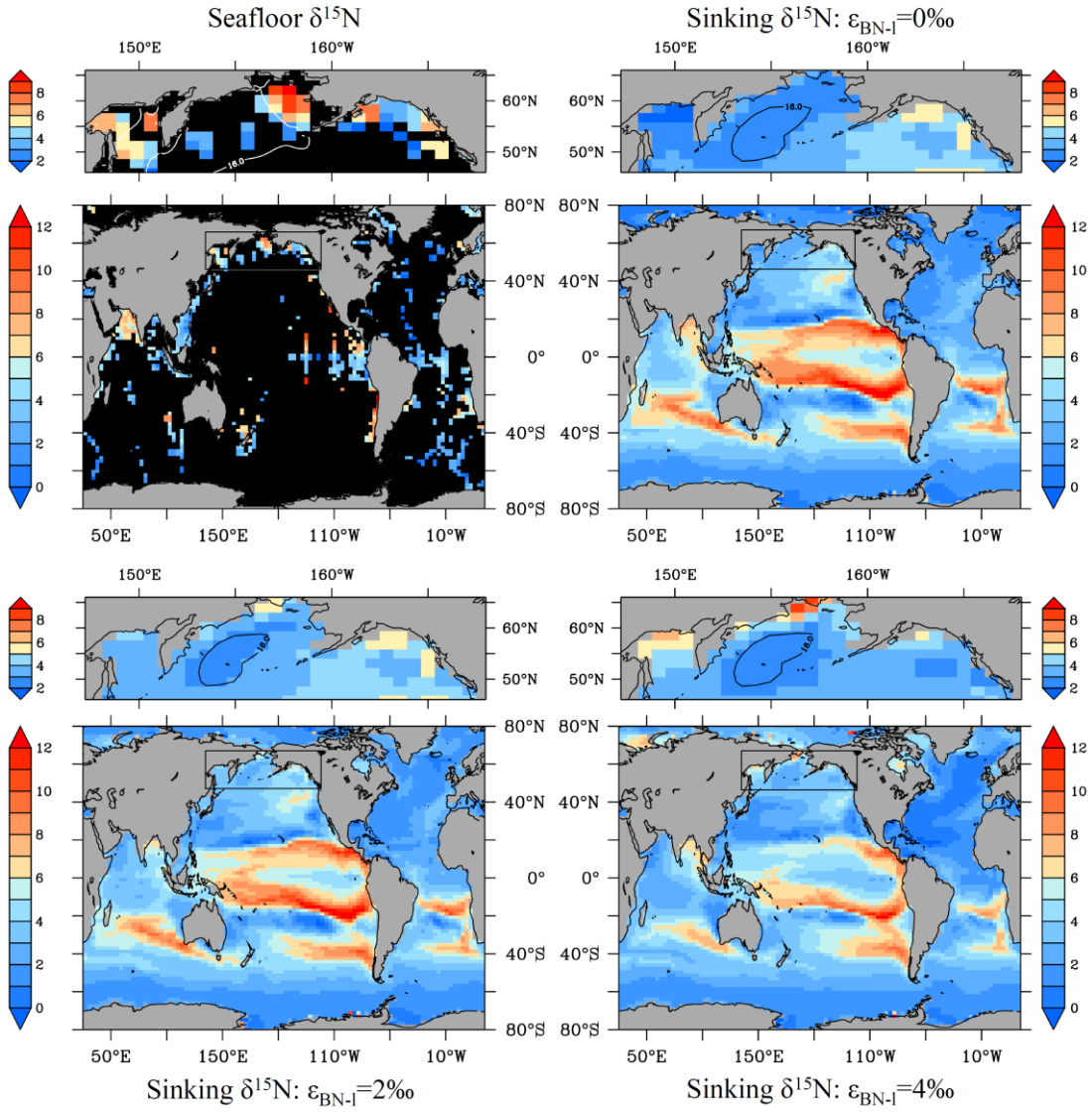

Figure 5.3 Seafloor $\delta^{15}N$ (Tesdal et al., 2012) comparison with model sinking $\delta^{15}N$ with $\varepsilon_{BN\text{-}l}$=0, 2, and 4‰, where limWCN-l=32 for all experiments shown here. Note a simple diagenetic model was applied to model sinking $\delta^{15}N$ to account for diagenetic alteration during burial into the seafloor sediments based on seafloor depth (Robinson et al., 2012, submitted). See text for additional details.

Diagenetic alternation of $\delta^{15}N$ occurs as sinking $\delta^{15}N$ becomes incorporated into the seafloor sediments, which can potentially bias the interpretation of bulk sediment $\delta^{15}N$. However, an analysis investigating diagenetic $\delta^{15}N$ alteration shows a clear relationship with water depth (Robinson et al., 2012, submitted). Data at > 50 sites where sinking $\delta^{15}N$ from traps were compared to seafloor $\delta^{15}N$ show a ~1 ‰ $\delta^{15}N$ diagenetic increase per kilometer of water

depth. We accordingly adjust the model sinking $\delta^{15}N$ by increasing its values by 1.0 ‰ km^{-1} when comparing to the seafloor $\delta^{15}N$ database to account for diagenetic $\delta^{15}N$ alteration that is not incorporated into the model. After this simple diagenetic adjustment is applied, the globally averaged model sinking $\delta^{15}N$ then becomes < ±0.7 ‰ different than averaged seafloor $\delta^{15}N$ data for all experiments, whereas originally there was a ~2.8 ‰ offset.

The model reproduces the major trends of the observational seafloor $\delta^{15}N$ dataset (Figure 5.3). The isotope effects of phytoplankton NO_3^- assimilation, water column N-loss , and N_2 fixation drive these major patterns of $\delta^{15}N$ in the model (Somes et al., 2010b). Relatively ^{15}N-depleted sinking nitrogen ($\delta^{15}N$ =0–4‰) occur in HNLC regions of the Southern Ocean and Eastern Equatorial Pacific where NO_3^- utilization by phytoplankton is low. Here phytoplankton are able to preferentially incorporate ^{15}N-deleted nitrate into their biomass due to the high availability of nitrate (ε_{ASSIM} = 5 ‰), which eventually sinks towards the ocean seafloor. This results in more ^{15}N-enriched nitrate as nitrate is further utilized in surface waters. In the southern hemisphere subtropical gyres where nitrate is nearly fully utilized, phytoplankton must consume the ^{15}N-enriched nitrate remaining in the surface water, causing much higher sinking $\delta^{15}N$ values there (> 6 ‰).

Very high seafloor $\delta^{15}N$ values (> 10 ‰) are observed near suboxic zones where water column N-loss occurs due to its strong preferential to consume ^{15}N-depleted nitrate. (ε_{WCN-l}=25 ‰). Modeling the correct extent of the suboxic zones remains a challenge in global coarse-resolution models due to the small spatial scale of suboxic zones. While the suboxic zones are generally simulated in the correct ocean basins (e.g., Eastern Tropical Pacific, Northern Indian), they are all too large and displaced in the model. Since water column N-loss has a strong local effect on $\delta^{15}N$, this displacement causes rather poor model fits when comparing to the seafloor $\delta^{15}N$ database (e.g., r < 0.45, Table 5.4). If all displaced OMZ regions with less than 30 μM are not included when calculating the global metrics, the correlation coefficient increases from 0.42 to 0.60, showing that the bias from the displaced suboxic zones is one of the main deficiencies of the model. The model experiments that contain the lowest amount of water column N-loss (limWCN-l=32) represent the seafloor $\delta^{15}N$ database the best (Table 5.4).

Table 5.4: Statistical Measures of Seafloor $\delta^{15}N$ Model Performance [a]

Experiment			Statistical Measures					
Number	limWCN-l	$\varepsilon_{BN\text{-}l}$	Global Seafloor $\delta^{15}N$			North Pacifc Seafloor $\delta^{15}N$		
			R	STD	RMS	R	STD	RMS
1	20	0	0.292	1.89	1.93	−0.291	0.535	1.52
2	26	0	0.339	1.50	1.54	−0.300	0.531	1.45
3	32	0	0.391	0.984	1.10	−0.295	0.561	1.45
4	32	2	0.395	0.902	1.05	−0.133	0.420	1.24
5	32	4	0.423	0.812	1.00	0.387	0.440	1.07

[a]Correlation coefficient (R), standard deviation (STD), and root mean squared (RMS) error normalized by the standard deviation of the observations in the global ocean and North Pacific (45°N–65°N).

N_2 fixation introduces ^{15}N-deleted nitrogen ($\delta^{15}N$ =−1.5 ‰) into the ocean. It occurs primarily in tropical/subtropical water "downstream" of N-loss zones where nitrate has been depleted and aeolian Fe deposition is high. Aeolian Fe deposition is generally higher in the western portion of the tropics/subtropics and also with greater magnitude in the North Hemisphere relative to the south. In the model, this causes a trend of lower sinking $\delta^{15}N$ values in the northern gyres, which is supported by the observational seafloor $\delta^{15}N$ (Figure 4), as well as water column observations (Somes et al., 2010a). The basin of lowest values of seafloor $\delta^{15}N$ in fact occur in the North Atlantic, which is known to support high rates of N_2 fixation (Karl et al., 2002). Note that atmospheric nitrogen deposition is not included in this model version. Since pre-industrial deposition rates are estimated to be approximately an order magnitude lower than N_2 fixation, it likely has a small effect. However, atmospheric N deposition can introduce even more ^{15}N-depleted nitrogen in the North Atlantic ($\delta^{15}N \leq -4$ ‰) (Ryabenko et al., 2012), which could bias the model-data comparison.

The subpolar North Pacific contains large continental shelves and is one of the largest benthic N-loss zones in the ocean. Seafloor $\delta^{15}N$ show high values (6–10‰) in the Bering Sea Shelf and Sea of Okhotsk where high rates of benthic N-loss occur in the model (Figure 4, top sub-panels). Only the model experiment with the largest net fractionation factor of benthic denitrification ($\varepsilon_{BN\text{-}l} = 4$ ‰) reproduce the observational trends of high seafloor $\delta^{15}N$ in the Bering Sea and Sea of Okhotsk (Table 5.3). This supports the view of a large net fractionation factor for benthic N-loss of at least 4‰ in this region (Lehmann et al., 2007; Granger et al., 2011).

Nitrate utilization phytoplankton must also be considered in this region where strong surface nitrate gradients occur. Since the coarse-resolution model does not fully resolve the shallow continental shelves, nor the small-scale processes that take place on them, we focus on $\delta^{15}N$ in the core of the HNLC region ($NO_3^- > 16$ μM, contoured in Figure 4, top sub-panels). The model underestimates surface nitrate throughout the North Pacific HNLC region. One reason this likely occurs is due to no iron limitation for the ordinary phytoplankton class, which would allow the overconsumption of nitrate. This would be expected to result in too much nitrate utilization at the surface, which would produce too high $\delta^{15}N$ in this region. In contrast, all model experiments still underestimate $\delta^{15}N$ in the core of the HNLC region. Only the model experiment that contains the highest net fractionation factor for benthic N-loss ($\varepsilon_{BN\text{-}l} = 4$ ‰) shows a positive correlation with the seafloor $\delta^{15}N$ database there (Table 4). This model-data comparison supports the view of net fractionation factors for benthic N-loss to be ≥ 4 ‰, at least in the North Pacific. A higher net fractionation factor of benthic N-loss then requires much higher benthic to water column N-loss (BN-l:WCN-l) ratios to match observed global mean $\delta^{15}NO_3^-$, which is investigated below.

5.4.3 Water column $\delta^{15}NO_3^-$ Constraint

The global ocean mean $\delta^{15}NO_3^-$ is determined by the rates and isotope effects of the source and sink terms of the fixed-N budget: N_2 fixation, water column N-loss, and benthic N-loss. N_2 fixation provides the ocean with ^{15}N-depleted nitrogen ($\delta^{15}N_{NFIX} = -1.5$ ‰). N-loss processes, on the other hand, preferentially consumes this ^{15}N-depleted nitrogen, leaving the global mean nitrate pool enriched in ^{15}N (global mean $\delta^{15}NO_3^- = \sim 5.5$ ‰). The average net

fractionation that occurs during total N-loss determines how high the global mean $\delta^{15}NO_3^-$ will be relative to the ^{15}N-depleted nitrogen source from N_2 fixation. We focus on two isotope effects with high uncertainty in this study: (i) nitrate utilization and dilution impacts on the isotope effect of water column N-loss and (ii) the net fractionation factor associated with benthic N-loss.

(i) Nitrate utilization and dilution isotope effect

The elevated $\delta^{15}NO_3^-$ signature produced in suboxic zones depends on the degree of nitrate utilization there. That is, the balance between the isotope effects of nitrate consumption by N-loss processes and the replenishment by mixing (dilution effect (Deutsch et al., 2004)). This balance determines the average $\delta^{15}NO_3^-$ value that N-loss processes consume and convert to N_2 gas.

The dilution effect takes into account that $\delta^{15}NO_3^-$ will be weighted towards the water parcel with higher nitrate when mixing occurs. For example, if the nitrate concentration in the suboxic zone is only half of the nitrate concentration in surrounding oxic waters, the $\delta^{15}NO_3^-$ signature of the oxic water will have twice the influence on total $\delta^{15}NO_3^-$ of these water masses if they mix together. Note that the dilution effect is implicit within the physical circulation model.

High levels of nitrate utilization reduces the influence of the isotope effect of water column N-loss on global mean $\delta^{15}NO_3^-$. As average $\delta^{15}NO_3^-$ increases in suboxic zones as N-loss occurs, the nitrate removed then becomes more ^{15}N-enriched and has a $\delta^{15}NO_3^-$ signature that is closer to the ocean average. The influence of the isotope effect of water column N-loss is reduced when the $\delta^{15}NO_3^-$ signature of the consumed nitrogen is closer to the global ocean mean. For example, if the average $\delta^{15}NO_3^-$ value in the suboxic zone was 30.5 ‰, then the nitrogen removed would have a isotopic signature 25 ‰ depleted and equal to the global mean ($\delta^{15}NO_3^-$=5.5 ‰). Since the nitrogen being removed has a $\delta^{15}N$ signature equal to the global mean, in this case there would be no affect on global mean $\delta^{15}NO_3^-$, even though the N-loss processes are still fractionating during nitrate consumption. This suggests that all of the local isotope effects influencing suboxic zone $\delta^{15}NO_3^-$ (e.g., N_2 fixation and NO_3^-

assimilation at the surface above the suboxic zone, as well as nitrate consumption and dilution effects in the suboxic zone) need to be simulated correctly to capture the real isotope effect of water column N-loss.

Experiments with high nitrate utilization in the suboxic zone required lower ratios of benthic to water column N-loss (BN-l:WCN-l) compared to the experiments with low nitrate utilization. This nitrate utilization effect alone varied BN-l:WCN-l ratios by nearly a factor of 2 in our sensitivity experiments (Table 5.2, 5.3). Benthic N-loss is needed in the model to stimulate additional N_2 fixation to balance global mean $\delta^{15}NO_3^-$ to the observed level. When nitrate utilization is high, the influence of the isotope effect of water column is reduced and therefore less benthic N-loss, and lower BN-l:WCN-l ratios, are required to balance global mean $\delta^{15}NO_3^-$.

The model experiment that best reproduces nitrate and $\delta^{15}NO_3^-$ observations in the suboxic zone is limWCN-l=32 (Table 5.2, Figure 5.4). It gives a good agreement with the amount of nitrate drawdown, as well as the slope of the increasing $\delta^{15}NO_3^-$ as nitrate is consumed according to off-shelf observations in suboxic zones. The experiments with higher levels of nitrate utilization (limWCN-l=20, 26) show too much nitrate consumption there. Due to deficiencies in the simulated suboxic zones, it still cannot be confirmed if the balance between nitrate consumption and replenishment is completely consistent with suboxic zones in the real ocean with the limWCN-l=32 experiment. However, the high sensitivity of estimated rates of N_2 fixation and N-loss caused by varying $\delta^{15}NO_3^-$ in the suboxic zones in our model experiments that test different levels of nitrate utilization suggests nitrate utilization plays an important role in global nitrogen isotope cycling. This highlights the need for higher resolution models that fully resolve all of the ventilation pathways (e.g., coastal undercurrents and eddies) of suboxic zones.

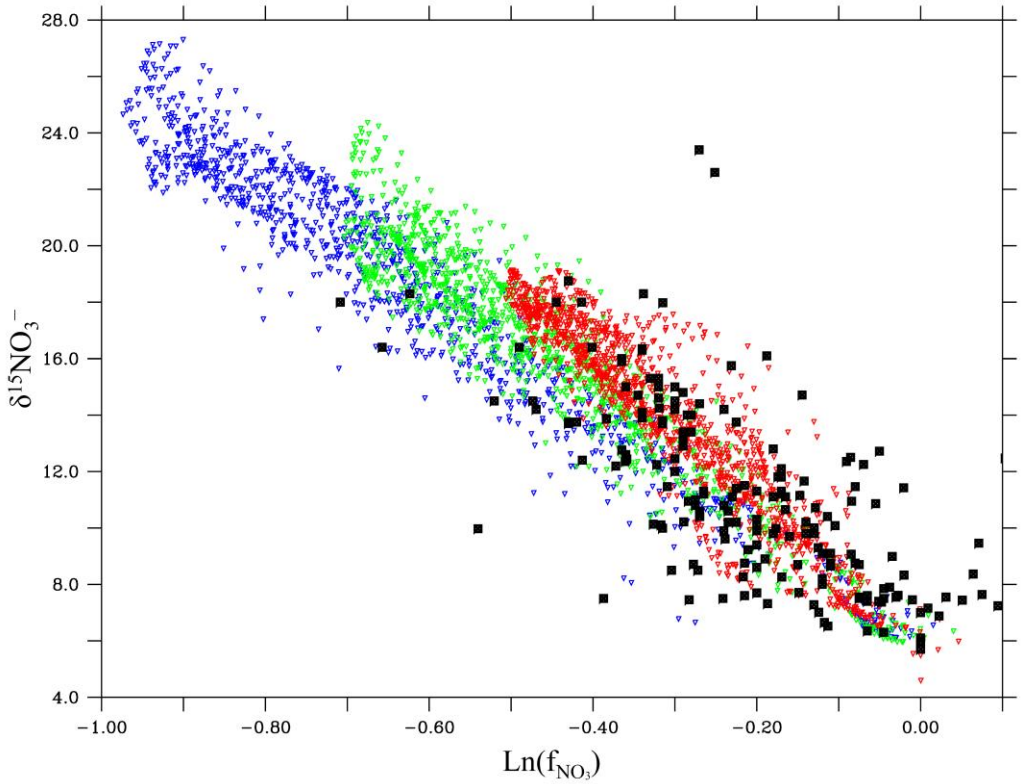

Figure 5.4 Annual mean $\delta^{15}NO_3^-$ versus expected nitrate (f_{NO_3}) shows the increase of $\delta^{15}NO_3^-$ as NO_3^- is consumed in suboxic zones ($O_2 < 10$ μM) from the isotope effect of water column N-loss in limWCD=20 (blue), limWCD=26 (green), limWCD=32 (red) and observations (black) from the Eastern Tropical North Pacific and Arabian Sea (Cline and Kaplan, 1975; Voss et al., 2001a; Somes et al., 2010b). Note $\varepsilon_{BN\text{-}l}$=0‰ for the model experiments shown here. Expected nitrate for the model is determined to be at the elemental ratio $15 \cdot PO_4^{3-}$ based on suboxic zone NO_3^-:PO_4^{3-} ratios in experiments where water column N-loss was switched off and all other parameters remained unchanged (not shown). Note that we exclude observations near the seafloor to avoid any impact from benthic N-loss.

(ii) Isotope effect of benthic N-loss

Recent studies (Lehmann et al., 2007; Granger et al., 2011; Alkhatib et al., 2012) have suggested a higher net fractionation factor should be associated with benthic N-loss ($\varepsilon_{BN\text{-}l}$=4–8‰) compared to previous estimates ($\varepsilon_{BN\text{-}l}$=1–3‰) (Brandes and Devol, 2002; Lehmann et al., 2004). They suggest benthic N-loss should have a much higher net fractionation factor due to the measured high $\delta^{15}NH_4^+$ that is presumably released from the sediments where benthic N-loss occurs. They propose this signal is due to fractionation during nitrification-denitrifcation loop in the sediments. If this high net fractionation factor is indeed correct, higher BN-l:WCN-l ratios would be required to balance the nitrogen isotope budget because

additional N_2 fixation would be needed to balance this "extra" ^{15}N-enriched nitrogen produced in the sediments where benthic N-loss occurs. We test the sensitivity of this effect by running experiments with $\varepsilon_{BN\text{-}l}$ set at 0, 2, and 4‰, while holding the limWCN-l parameter constant at 32, which best represented $\delta^{15}NO_3^-$ observations in the suboxic zone.

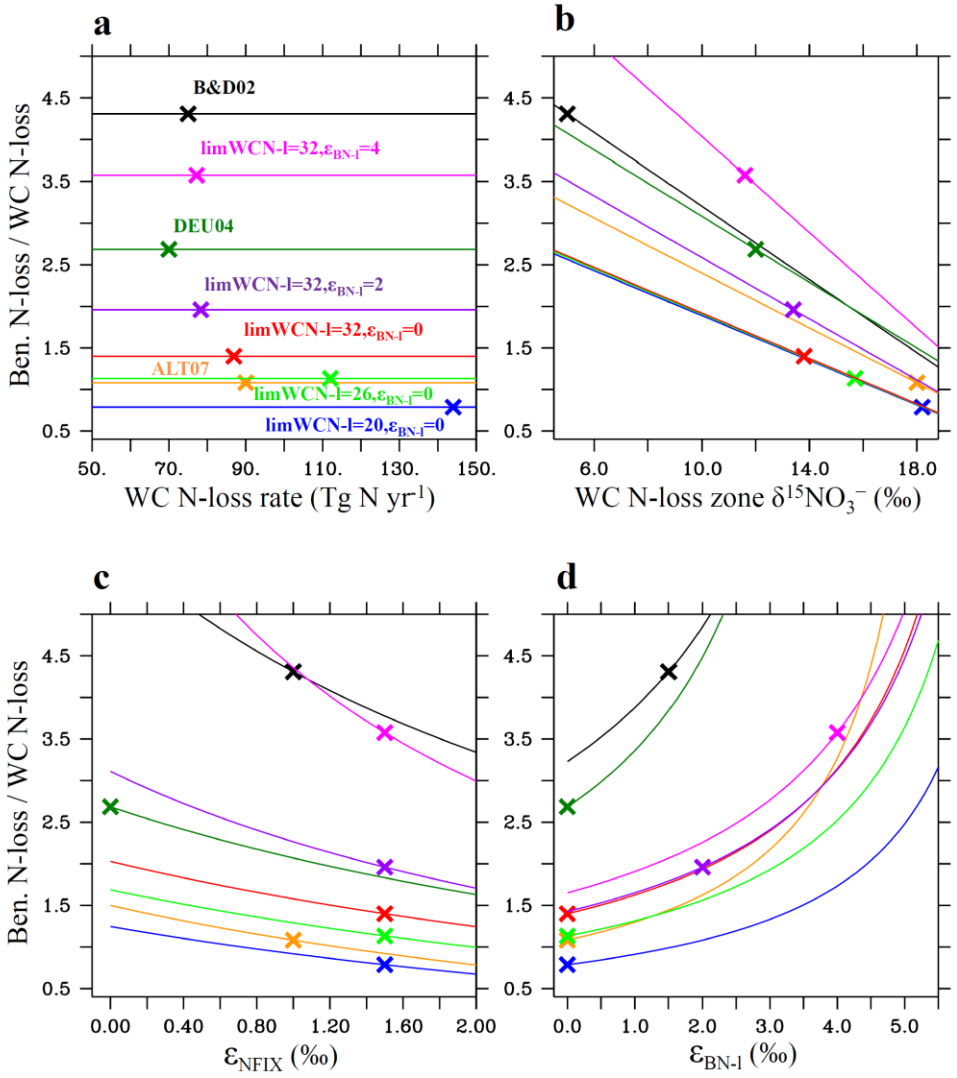

Figure 5.5 Results of the one-box $\delta^{15}NO_3^-$ model with different nitrogen isotope parameter settings according to previous configurations (Brandes and Devol, 2002; Deutsch et al., 2004; Altabet, 2007) and this study (Table 3). Each panel shows the sensitivity of one parameter on the ratio of benthic N-loss to water column N-loss needed to achieve observed mean $\delta^{15}NO_3^-$ in a steady-state scenario while all other parameters all held constant: (a) water column N-loss rate, (b) average initial $\delta^{15}NO_3^-$ value where water column N-loss occurs, (c) water column N-loss fractionation factor ($\varepsilon_{WCN\text{-}l}$), and (d) fractionation factor of N_2 fixation (ε_{NFIX}), which makes diazotroph biomass depleted in $\delta^{15}N$ by this value. Note the crosses (X) show the parameter chosen for each reported model configuration.

The range of relative rates of BN-l:WCN-l required to closely reproduce observed global mean $\delta^{15}NO_3^-$ for our sensitivity experiments ($\varepsilon_{BN\text{-}l}$ = 0–4 ‰) varied from 1.4:1–3.5:1. This represents a considerable range of benthic N-loss rates and suggests that a misrepresentation of this isotope effects can significantly bias the estimate for the BN-l:WCN-l ratio. The lack of water column $\delta^{15}NH_4^+$ measurements overlying sites of benthic denitrification make it difficult to constrain the global response at this time. We note our data-model analysis with the seafloor $\delta^{15}N$ database support these high estimates for the net fractionation factor of benthic N-loss ($\varepsilon_{BN\text{-}l}$ > 4‰) (Section 5.4.2 and Figure 5.4). If these high-end estimates are validated on the global scale, this could require even higher BN-l:WCN-l ratios than predicted by these sensitivity experiments (BN-l:WCN-l > 3.5).

5.5 Discussion

Our nitrogen isotope sensitivity experiments using a coupled global model and a one-box model of $\delta^{15}N$ produce a large range of potential N_2 fixation and N-loss rates that vary by over a factor of 2 (Table 5.2, Figure 5.5). We show that different nitrogen isotope parameters chosen for isotope effect of water column and benthic N-loss significantly affect the estimates of the BN-l:WCN-l ratio needed to satisfy the global mean $\delta^{15}NO_3^-$ constraint. This is in general agreement with previous box model studies that also estimate a large range from 1:1–3.6:1 (Brandes and Devol, 2002; Deutsch et al., 2004; Altabet, 2007), when different isotope effects for N-loss were used in their respective models. These results show the importance of correctly modeling each isotope effect to simulate the balance of N_2 fixation and denitrification that determines the observed global mean $\delta^{15}NO_3^-$.

We use a global one-box $\delta^{15}NO_3^-$ model that includes N_2 fixation, water column N-loss, and benthic N-loss to perform a more thorough sensitivity analysis of the key nitrogen isotope parameters. This model is designed to calculate the required ratio of benthic to water column N-loss to maintain the observed global mean $\delta^{15}NO_3^-$ in a steady-state pre-industrial ocean. Its assumes that both the fixed marine nitrogen inventory as well as the inventory of $\delta^{15}NO_3^-$ are both in steady-state in the pre-industrial ocean. The model then calculates the benthic to water column N-loss ratio required for different nitrogen isotope parameters chosen from

previous model studies and the sensitivity experiments from this study (Table 5.2) using equation ?.

The one-box model used here accurately reproduces the reported BN-l:WCN-l ratios of the various model configurations used in this study as well as previous studies despite the large range of model design and parameter selections (Table 5.3). This suggests our one-box model may be reliable to estimate the sensitivity of the different nitrogen isotope parameters in a steady-state scenario. The one-box model confirms that the BN-l:WCN-l ratio needed to match global mean $\delta^{15}NO_3^-$ is very sensitive to the level of nitrate utilization in the OMZ and net fractionation factor chosen for benthic N-loss (Figure 5.5b,d). The range of uncertainty for these two effects can alone account for large range of estimates for benthic N-loss (100–280 Tg N yr^{-1}) from previous nitrogen isotope models (Brandes and Devol, 2002; Deutsch et al., 2004; Altabet, 2007).

The large uncertainty associated with the net fractionation factor of benthic N-loss adds further difficulties to constrain the BN-l:WCN-l ratio using the global mean $\delta^{15}NO_3^-$ constraint. Our experiments show that increasing this factor from 0 to 4‰ requires almost triple the benthic N-loss rate needed to maintain the global mean $\delta^{15}NO_3^-$ at observed levels near 5.5‰. Recent estimates suggest that the net fractionation factor may be even higher (4–8‰) due to fractionation within the nitrification-denitrification loop in the sediments (Granger et al., 2011; Alkhatib et al., 2012). If these high-end estimates are validated on a global scale, this could require larger BN-l:WCN-l ratios than our largest value simulated here (> 3.5).

The level of nitrate utilization in OMZs has a strong influence on the isotope effect of water column N-loss, which impacts the BN-l:WCN-l ratio. It determines the $\delta^{15}NO_3^-$ signature in suboxic zones that is consumed by N-loss processes. The one-box model results shows that if this effect is not modeled accurately, it can lead to large biases into the estimates for BN-l:WCN-l ratios.

For example, Brandes and Devol (Brandes and Devol, 2002) did not account for the locally high $\delta^{15}NO_3^-$ of suboxic zones in their one-box model (Figure 5.5b). The $\delta^{15}NO_3^-$ they remove during water column N-loss is thus much more depleted in ^{15}N compared to the other models that take into account nitrate utilization in the suboxic zone. This increases the isotope effect of water column N-loss in the Brandes and Devel (Brandes and Devol, 2002) model configuration and it thus needs more N_2 fixation to maintain global mean $\delta^{15}NO_3^-$, which is achieved by imposing a higher BN-l:WCN-l ratio. If they would have accounted for a more realistic suboxic zone $\delta^{15}NO_3^-$ signature in the range of the other model configurations, our one-box model suggests their estimate for BN-l:WCN-l would have been at least a factor of 2 lower (Figure 5.5b).

The average level of nitrate utilization throughout the ocean's prominent suboxic zones remains difficult to determine. While studies in the ETNP and Arabian Sea OMZs do not typically show nitrate depleted below half of its expected value (Voss et al., 2001a), recent results from the ETSP suboxic zone show more than two-thirds of the expected nitrate was consumed (Ryabenko et al., 2012). However, they note large rates of benthic N-loss occuring within close proximity were likely contributing to this nitrate deficit. Furthermore, evidence from an eddy entraining suboxic water from the ETSP OMZ showed an even larger levels of nitrate utilization as it moved offshore (Ryabenko et al., 2012) These results suggests that average level of nitrate utilization in the global suboxic zones may be lower than off-shore observations from the Arabian Sea and ETNP included in Figure 5.5. This would support lower ratios of BN-l:WCN-l in the global ocean (Altabet, 2007).

The 6-box model of Deutsch et al. (2004) accounts for local nitrate utilization with a designated suboxic box, but still estimates a higher BN-l:WCN-l ratio (2.79) compared to the results from the coupled model experiment when the fractionation factor for benthic N-loss was also set to 0 (BN-l:WCN-l = 1.4). The most significant difference between the Deutsch et al. (2004) and the other model configurations is the isotope effect of N_2 fixation. Deutsch et al. (2004) chose to use a $\delta^{15}N_{NFIX}$ signature of 0 ‰ , while all other models selected between −1–−1.5 ‰. If the Deutsch et al. (2004) study would have chosen the same value as here ($\delta^{15}N_{NFIX} = -1.5$ ‰), our one-box model suggests this would decrease their estimated

BN-l:WCN-l ratio from 2.69 to 1.83, which would then be more consistent with the results from our coupled model. This shows that even small differences (< 2 ‰) for the isotope effect of N_2 fixation can alter ratio of BN-l:WCN-l by 30 % or even more depending on the model configuration used (Figure 5.5c).

The high sensitivity of the different nitrogen isotope effects for water column and benthic N-loss show how a slight misrepresentation can significantly bias the estimates for global rates of N_2 fixation, water column N-loss, and benthic N-loss. Our model experiments that best reproduce seafloor $\delta^{15}N$ observations, most notably in the Bering Sea where benthic N-loss is abundant, suggest the net fractionation factor for benthic N-loss should be at least 4 ‰ there. Although the average degree of nitrate utlilization in the suboxic zones is also uncertain, our experiment using limWCN-l = 32 best represented off-shore observations from the ETNP and Arabian Sea. Other observations from the ETSP show higher levels of nitrate utilization so we choose our experiment limWCN-l as the low-end of our range. Assuming this range for nitrogen isotope parameters, our model estimated a range for BN-l:WCN-l of 2.86–3.52. These model experiments estimate that rates of N_2 fixation, water column N-loss, and benthic N-loss are in the range 220–380, 70–90, and 150–280 Tg N yr^{-1}, respectively, assuming a balanced fixed nitrogen budget. This model result suggests that the residence time of oceanic fixed-N is between 1,500 and 3,000 years and the oceanic fixed nitrogen inventory may be susceptible to fluctuations on the timescale of the large-scale ocean circulation (1,000–1,500 years).

We note our best estimate is in general agreement with the final results of Brandes and Devol (2002), despite that our $\delta^{15}N$ model configuration for the isotope effects of water column and benthic N-loss in our best model experiments are much different (Table 5.3). This suggests that even though the simple one-box model of Brandes and Devol (2002) was able to reach a similar result, it was likely for the wrong reasons. Whereas with our coupled three-dimensional model, we were able to make direct comparisons to $\delta^{15}N$ observations where N-loss occurs in the water column and sediments to better validate the isotope effects in water column and benthic N-loss simulated in the model. This highlights the importance of direct

comparison of observations to models to confirm that models can capture the correct response of these important processes for global nitrogen isotope cycling.

5.6 Conclusions

Our study uses water column $\delta^{15}NO_3^-$ and seafloor $\delta^{15}N$ ratios to constrain the rates of N_2 fixation, water column N-loss, and benthic N-loss in the global ocean. The uncertainty associated with isotope effects of N-loss in the water column and sediments makes it difficult to constrain the rates N_2 fixation and total N-loss. Previous studies using $\delta^{15}N$ have estimated large ranges for the ratio of BN-l:WCN-l from 1:1–3.7 (Brandes and Devol, 2002; Deutsch et al., 2004; Altabet, 2007). Here we used a set of experiments using a coupled three-dimensional model and a one-box model to show that nitrate utilization in the suboxic zone and the net fractionation factor of benthic N-loss, both of which are not well constrained, can lead to ratios of BN-l:WCN-l that vary by over a factor of 2 within their level of uncertainty.

With our coupled three-dimensional model, we were able to compare $\delta^{15}N$ observations in the water column and seafloor in the regions where N-loss processes occur to constrain the nitrogen isotope parameters associated with water column and benthic N-loss. This highlights the importance of using models that can resolve all of the locally important nitrogen isotope effects that affect $\delta^{15}N$ in N-loss zones. The model experiments that best reproduce $\delta^{15}N$ observations in the water column and sediments estimate the rates of N_2 fixation, water column N-loss, and benthic N-loss in the range 220–370, 70–90, and 150–280 Tg N yr^{-1}, respectively, assuming a balanced fixed-N budget in the pre-industrial ocean.

5.7 Appendix: Nitrogen Isotope Model Description

5.7.1 Fractionation Equation

Fractionation is calculated using kinetic fractionation (Mariotti et al., 1981):

$$\frac{^{15}N_{pro}}{^{14}N_{pro}} = \alpha \frac{^{15}N_{sub}}{^{14}N_{sub}} \tag{5.1}$$

where α is the kinetic fractionation factor associated with the process and the N_{pro} and N_{sub} refer to the nitrogen of the product and substrate of the reaction, respectively. In the model, we include ^{15}N as the prognostic variable instead of the ratio $^{15}N/^{14}N$. The ^{15}N equations are embedded within the marine ecosystem model that calculates total N ($^{T}N=^{15}N+^{14}N$). Solving equation A1 for $^{15}N_{pro}$ with respect to $^{T}N_{pro}$ yields

$$^{15}N_{pro} = \frac{\alpha R_{sub}}{1+\alpha R_{sub}} {}^{T}N_{pro}. \quad (5.2)$$

where R_{sub} is the isotopic ratio $^{15}N/^{14}N$ of the substrate of the reaction.

This equation can be equivalently expressed in the commonly used delta ("δ") notation by applying the relation (Mariotti et al., 1981):

$$\alpha = 1 - \varepsilon/1000 \quad (5.3)$$

which gives positive values for ε with this definition. Equation 5.2 then becomes

$$^{15}N_{pro} = \frac{\beta}{1+\beta} {}^{T}N_{pro} \quad (5.4)$$

where $\beta = R_{sub} + \varepsilon \cdot R_{sub} /1000$ (Giraud et al., 2000), which is the nitrogen isotope equation coded into the marine ecosystem-biogeochemistry model. Converted into full delta notation, this isotope equation yields

$$\delta^{15}N_{pro} = \delta^{15}N_{sub} - \frac{R_{sub}}{R_{std}}\varepsilon. \quad (5.5)$$

where R_{std} is a chosen standard ratio that scales the delta notation, commonly chosen as the ratio of atmospheric N_2. Note we use a R_{std} value of 1 so that ^{14}N and ^{15}N have concentrations of the same order of magnitude. This reduces the impact of numerical noise

caused by the advection scheme on the $\delta^{15}N$ value. If the atmospheric N_2 ratio is used (R_{std}=0.0036765), the ^{15}N concentration would be over two orders of magnitude smaller and be more susceptible to become negative by numerical noise, which would produce erroneous $\delta^{15}N$ values.

5.7.2 Coupled Model Equations

The fractionation equation used for NO_3^- consumption during phytoplankton uptake and water column N-loss with a constant fractionation factor, ε, is as follows:

$$\delta^{15}N_{pro} = \delta^{15}N_{sub} - \frac{R_{sub}}{R_{std}}\varepsilon(1-u)/u \cdot \ln(1-u). \quad (5.6)$$

where u is the fraction of available total nitrate consumed during each time-step. This fractionation equation is used to ensure that if a significant portion of the nitrate is consumed in one time-step, mass balance of the different nitrogen isotope species is conserved. In the experiments here, we artificially limit water column N-loss at high enough nitrate concentration so this term has a negligible effect for water column N-loss in this study.

Since zooplankton excretion and benthic N-loss are parameterized in the model, the instantaneous fractionation equation is used with a given fractionation factor to mimic the net fractionation that occurs during the integrated reaction:

$$\delta^{15}N_{pro} = \delta^{15}N_{sub} - \frac{R_{sub}}{R_{std}}\varepsilon \quad (5.7)$$

The full set of time-dependent equations for ^{15}N that are embedded into the marine ecosystem biogeochemical model are as follows:

$$\frac{\partial {}^{15}NO_3^-}{\partial t} = {}^{T}R_D \mu_D D + \frac{\beta_{excr}}{1+\beta_{excr}} \mu_{Z0} Z + {}^{T}R_{P_G} \mu_{P_G 0} P_G - \frac{\beta_{assim}}{1+\beta_{assim}} J_G P_G - \frac{\beta_{assim}}{1+\beta_{assim}} u_{NO_3^-} J_D P_D$$
$$- \mu_D D \left(\frac{\beta_{WCN-l}}{1+\beta_{WCN-l}} 0.8 r_{O:N} \rho_{sox}^{NO_3^-} L_{WCN-l} \right) - \frac{\beta_{BN-l}}{1+\beta_{BN-l}} \alpha_{BN-l} BN - l \cdot L_{BN-l}$$

(5.8)

$$\frac{\partial {}^{15}N\text{-}P_O}{\partial t} = \frac{\beta_{assim}}{1+\beta_{assim}} J_G P_G - {}^{T}R_{P_G} \mu_{P_G} P_G - {}^{T}R_{P_G} G(P_G) Z - {}^{T}R_{P_G} \nu_{P_G} P_G^2 \quad (5.9)$$

$$\frac{\partial {}^{15}N\text{-}P_D}{\partial t} = \left(\frac{\beta_{assim}}{1+\beta_{assim}} u_{NO_3^-} + \frac{\beta_{nfix}}{1+\beta_{nfix}} (1 - u_{NO_3^-}) \right) J_G P_G - {}^{T}R_{P_D} \mu_{P_D} P_D - {}^{T}R_{P_D} G(P_D) Z$$
$$- {}^{T}R_{P_D} \nu_{P_D} P_D^2 \quad (5.10)$$

$$\frac{\partial {}^{15}N\text{-}Z}{\partial t} = \gamma \left[{}^{T}R_{P_G} G(P_G) + {}^{T}R_P G(P_D) \right] Z - \frac{\beta_{excr}}{1+\beta_{excr}} \mu_{Z0} Z - {}^{T}R_Z \nu_Z Z^2 \quad (5.11)$$

$$\frac{\partial {}^{15}N\text{-}D}{\partial t} = (1-\gamma) \left[{}^{T}R_{P_G} G(P_G) + {}^{T}R_P G(P_D) \right] Z - {}^{T}R_D \mu_D D + {}^{T}R_{P_G} \nu_{P_G} P_G^2 + {}^{T}R_{P_D} \nu_{P_D} P_D^2 + {}^{T}R_Z \nu_Z Z^2$$
$$- {}^{T}R_D w_D \frac{\partial D}{\partial z} \quad (5.12)$$

where ${}^{T}R_X = {}^{15}N_X / ({}^{15}N_X + {}^{14}N_X)$. Here it suffices to note that the equations for total nitrogen (${}^{14}N + {}^{15}N$) are identical to the ones of ${}^{15}N$, except that ${}^{T}R_X = \beta_X / (1 + \beta_X) = 1$ in the total nitrogen equations. The parameter list is given in Table A1.

5.7.3 One-box Model Equations

The one-box δ^{15}N model assumes the fixed nitrogen inventory and the nitrogen isotope inventory are both in steady-state. This yields the equations:

$$NFix = WCN\text{-}l + BN\text{-}l \tag{5.13}$$

$$NFix \cdot \left(\frac{\beta}{1+\beta}\right)_{NFix} = WCN-l \cdot \left(\frac{\beta}{1+\beta}\right)_{WCN-l} + BN-l \cdot \left(\frac{\beta}{1+\beta}\right)_{BN-l} \tag{5.14}$$

where β_i is the fractionation factor (α) multiplied by the $^{15}N/^{14}N$ ratio of the substrate being reacted upon (see equation A4). Solving for benthic to water column N-loss ratio gives

$$\frac{BN-l}{WCN-l} = \frac{\left(\frac{\beta}{1+\beta}\right)_{WCN-l} - \left(\frac{\beta}{1+\beta}\right)_{NFix}}{\left(\frac{\beta}{1+\beta}\right)_{NFix} - \left(\frac{\beta}{1+\beta}\right)_{BN-l}}. \tag{5.15}$$

These results are displayed in Table 3 and Figure 6.

5.8 Appendix: Marine Ecosystem-Biogeochemistry Description

This appendix provides a description of the parameters used in the full set of time-dependent equations in the marine ecosystem model. It suffices to note that the equations for total nitrogen ($^{14}N + {}^{15}N$) ecosystem variables are identical to the ones of ^{15}N if $R_X = \beta_X/(1+\beta_X) = 1$, which are located in Appendix 5.7.

The function J_O provides the growth rate of non-diazotrophic phytoplankton, determined from irradiance (I), NO_3^- and PO_4^{3-},

$$J_O(I, NO_3^-, PO_4^{3-}) = min(J_{OI}, J_{Omax}u_N, J_{Omax}u_P) \tag{5.16}$$

The maximum growth rate is dependent only on temperature (T):

$$J_{Omax} = a \bullet \exp(T/T_b) \tag{5.17}$$

such that growth rates increase by a factor of ten over the temperature range of -2 to 34 °C. We use a=0.35 d^{-1} for the maximum growth rate at 0 °C which was determined to best represent average phytoplankton assemblage growth rates (Eppley, 1972). Under nutrient-replete conditions, the light-limited growth rate J_{OI} is calculated according to:

$$J_{OI} = \frac{J_{Omax}\alpha I}{\left[J_{O\max}^2 + (\alpha I)^2\right]^{1/2}} \tag{5.18}$$

where α is the initial slope of the photosynthesis vs. irradiance (P-I) curve. The calculation of the photosynthetically active shortwave radiation I and the method of averaging equation (C-3) over one day is outlined in (Schmittner et al., 2005). This version also includes in the correction for the error in the calculation of light limitation in previous versions (Schmittner et al., 2008). Nutrient limitation is represented by the product of J_{Omax} and the nutrient uptake rates, $u_N = NO_3^-/ (k_N + NO_3^-)$ and $u_P = PO_4^{3-} / (k_P + PO_4^{3-})$, with $k_P = k_N r_{P:N}$ providing the respective nutrient uptake rates.

Diazotrophs grow according to the same principles as the general phytoplankton class, but are disadvantaged in nitrate-bearing waters by a lower maximum growth rate, J_{Dmax}, which is set to zero below 15°C:

$$J_{Dmax} = c_D \cdot FeLim \cdot a \cdot \exp(T / T_b) \tag{5.19}$$

The coefficient c_D handicaps diazotrophs by dampening the increase of their maximal growth rate versus that of the general phytoplankton class with rising temperature. We use c_D = 0.13, such that the growth rate of diazotrophs is 13% that of ordinary phytoplankton. This handicap is further decreased by the *Fe limitation* parameter, which is scaled between 0 – 1 by multiplying a monthly climatology of aeolian dust deposition (Mahowald et al., 2005b; Mahowald et al., 2006; Mahowald et al., 2009) by a constant factor and setting the maximum value to 1 (Somes et al., 2010a). However, diazotrophs have an advantage in that their growth rate is not limited by NO_3^- concentrations:

$$J_D(I, PO_4) = min(J_{DI}, J_{Dmax}u_P) \quad (5.20)$$

although they do take up NO_3^- if it is available (see term 5 in the right hand side of eq. A10). The N:P of model diazotrophs is set to 40:1.

The first order mortality rate of phytoplankton is linearly dependent on their concentration, P_O. DOM and the microbial loop are folded into a single fast-remineralization process, which is the product of P_O and the temperature dependent term

$$\mu_P = \mu_{PO}\, exp(T / T_b). \quad (5.21)$$

Diazotrophs die at a linear rate where half of the resulting detritus is included into the fast-remineralization process.

The grazing of phytoplankton by zooplankton formulation is unchanged from (Schmittner et al., 2005) as follows

$$G(P) = \frac{g\nu P^2}{g + \nu P^2} \quad (5.22)$$

where g is grazing rate, ν is prey-capture rate, and P is phytoplankton concentration (Table A1). Note prey-capture rate is reduced for diazotrophs relative to ordinary phytoplankton in these experiments (Table 1).

Detritus is generated from sloppy zooplankton feeding and mortality among the three classes of plankton, and is the only component of the ecosystem model to sink. It does so at a speed of

$$w_D = \left\{ \begin{array}{c} w_{D0} + m_w z, z \le 1000m \\ w_{D0} + m_w 1000m, z > 1000m \end{array} \right\}, \quad (5.23)$$

increasing linearly with depth z from w_{D0}=7 md^{-1} at the surface to 40 md^{-1} at 1 km depth and constant below that, consistent with observations (Berelson, 2001). The remineralization rate of detritus is temperature dependent and decreases by a factor of 2.5 in suboxic waters, as O_2 decreases from 10 μM to 0 μM:

$$\mu_D = \mu_{DO}\, exp(T / T_b)[0.75+0.25tanh(O_2 - 6)] \tag{5.24}$$

Remineralization transforms the N and P content of detritus to NO_3^- and PO_4^{3-}. Photosynthesis produces oxygen, while respiration consumes oxygen, at rates equal to the consumption and remineralization rates of PO_4, respectively, multiplied by the constant ratio $R_{O:P}$. Dissolved oxygen exchanges with the atmosphere in the surface layer (F_{sfc}) according to the OCMIP protocol.

Oxygen consumption in suboxic waters (O_2 < ~10 μM) is inhibited, according to

$$r_{sox}^{O2} = 0.5\left[\tanh\left(O_2 - 5\right)+1\right] \tag{5.25}$$

but is replaced by the oxygen-equivalent oxidation of nitrate,

$$r_{sox}^{NO3} = 0.5\left[1-\tanh\left(O_2 - 5\right)\right]. \tag{5.26}$$

Denitrification consumes nitrate at a rate of 80% of the oxygen equivalent rate, as NO_3 is a more efficient oxidant on a mol per mol basis (i.e. one mol of NO_3 can accept $5e^-$ while 1 mol of O_2 can accept only 4 e^-).

We include the benthic N-loss scheme of Bohlen et al. (2012, in review), which parameterizes benthic N-loss based on the labile carbon flux (F_c) into the sediments and bottom water oxygen and nitrate:

$$BN - l = \left(0.083 + 0.21 \times 0.98^{bwO_2 - bwNO_3^-}\right) \times RR_{POC} \tag{5.27}$$

BN-l is the rate at which nitrate is removed from the bottom water. We assume that the rain rate of carbon into the sediments occurs at a ratio of $R_{C:N} = 6.625$ of the nitrogen in the sinking organic detritus.

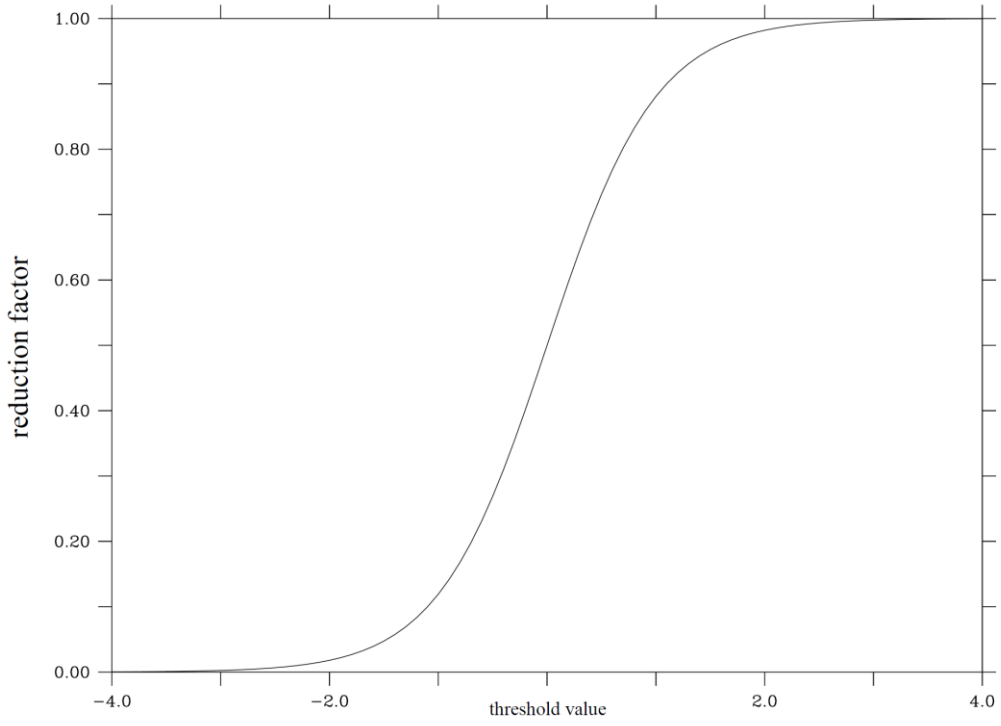

Figure 5.6 Reduction factor applied to water column N-loss for given NO_3^- concentration thresholds.

Since the continental shelves are not well resolved in the model, we use an additional sub-grid scale parameterization for them. The portion of each bottom ocean grid box that is covered by the real sea floor is calculated at each location from high resolution (1/5°) bathymetry. The rain rate of carbon that is included in the benthic N-loss function in this shelf parameterization is the amount of particulate organic carbon that sinks into the portion of the grid box covered by a shallower continental shelf. In the model, ~30% of the benthic denitrification occurs within this shelf parameterization. The remaining particulate organic matter continues to sink to greater depths. The coarse-resolution physical circulation model's

inability to fully resolve coastal systems generally underestimates primary production and sinking carbon fluxes on these continental shelves, which results in too low benthic N-loss rates there. To account for this deficiency, we arbitrarily multiply the benthic N-loss transfer function by a coefficient ($\alpha_{BN\text{-}l}$). This parameter is tuned to set the global deep ocean mean $\delta^{15}NO_3^-$ in the model to ~5‰ for each experiment. Figure 2 shows the spatial distribution of benthic denitrification.

Table 5.5: Marine ecosystem-biogeochemistry parameter list for experiment 3 (limWCD=32,$\varepsilon_{BN\text{-}l}$=0). See Table 2 for changes to parameters for other experiments.

Parameter	***Symbol***	***Value***	***Units***
Phytoplankton (P_O, P_D) Coefficients			
Initial slope of P-I curve	α	0.1	$(W\ m^{-2})^{-1}\ d^{-1}$
Photosynthetically active radiation	*PAR*	0.43	
Light attenuation in water	k_w	0.04	m^{-1}
Light attenuation through phytoplankton	k_c	0.03	$m^{-1}(mmol\ m^{-3})^{-1}$
Light attenuation through sea ice	k_i	5	m^{-1}
Half-saturation constant for N uptake	k_N	0.7	$mmol\ m^{-3}$
Phytoplankton specific mortality rate	v_{PO}	0.025	d^{-1}
Maximum growth rate (at 0°C)*	a_O	0.35	d^{-1}
Phytoplankton fast-recycling rate	μ_{P0}	0.014	d^{-1}
Diazotrophs' handicap	c_{Diaz}	0.13	d^{-1}
Diaztoroph specific mortality rate	v_{Diaz}	0.025	d^{-1}
Diazotroph fast-recycling rate	μ_{D0}	0.0016	d^{-1}
Zooplankton (Z) Coefficients			
Assimilation efficiency	γ	0.925	
Maximum grazing rate	g	1.575	d^{-1}
Phytoplankton prey-capture rate	ω_O	5.0	$(mmol\ m^{-3})^{-2}d^{-1}$
Diazotroph prey-capture rate	ω_{Diaz}	0.125	$(mmol\ m^{-3})^{-2}d^{-1}$
Mortality	μ_{Z0}	0.34	$(mmol\ m^{-3})^{-2}d^{-1}$
Excretion	v_Z	0.015	d^{-1}
Detritus (D) Coefficients			

Parameter	***Symbol***	***Value***	***Units***
Remineralization rate	μ_{D0}	0.065	d^{-1}
Sinking speed at surface	w_{D0}	13	m d^{-1}
Increase of sinking speed with depth	m_w	0.06	d^{-1}
E-folding temperature of biological rates	T_b	15.65	ºC
	Elemental Ratios		
Molar Oxygen:Nitrogen	$R_{O:N}$	10.6	
Molar Carbon:Nitrogen	$R_{C:N}$	6.625	
Phytoplankton Nitrogen:Phosphorus	$Phyt_{N:P}$	16	
Diazotroph Nitrogen:Phosphorus	$Diaz_{N:P}$	40	
Zooplankton Nitrogen:Phosphorus	$Zoop_{N:P}$	16	

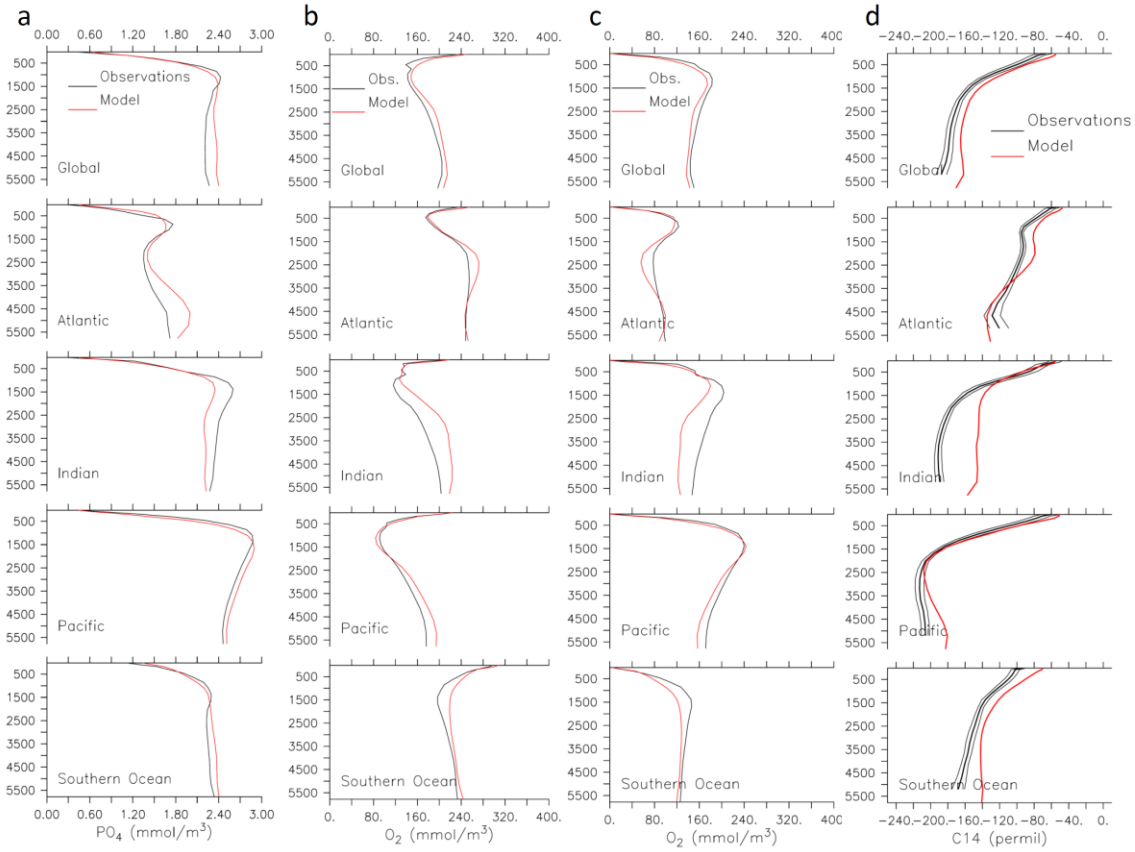

Figure 5.7 Basin-scale model-data comparison of (a) PO_4^-, (b) O_2, (c) apparent oxygen utilization (AOU), and (d) $\Delta^{14}C$ with limWCN-l=32, $\varepsilon_{BN\text{-}l}$=2 model experiment.

Acknowledgments. We thank the NICOPP group including Jan-Erik Tesdal and Markus Kienast for providing the seafloor $\delta^{15}N$ data. This work was conducted at IFM-GEOMAR and supported by the SFB754 project from the German Research Foundation (DFG).

6 Conclusions and Outlook

Nitrogen isotopes can be a valuable proxy to address processes critical to the oceanic nitrogen cycle. Some of the most important processes in the nitrogen cycle (e.g., N_2 fixation and N-loss processes) are rarely directly measured in the ocean, making it difficult quantify them. These processes all leave distinct imprints on the ratio of stable nitrogen isotopes, which make nitrogen isotopes an alternative constraint to infer these processes on spatial and temporal scales.

Changes in the nitrogen cycle in the past, as interpreted by sedimentary nitrogen isotope records, are linked with climate change (Galbraith et al., 2012, in review). Below the modern seafloor, the sediment compilation reveals isotopic shifts related to the climate swings of the last ice age and deglaciation. These coherent patterns of change are consistent with higher rates of N_2 fixation and N-loss processes during warmer climate regimes (e.g., interglacial periods). Although uncertainties in N-loss isotope effects, post-depositional alteration, and incomplete global coverage hamper quantification of these changes, our results confirm that the marine nitrogen cycle is sensitive to climate, and that an assemblage of globally-distributed sedimentary nitrogen isotope records can successfully document its response. This work confirms, from a global perspective, that the marine nitrogen cycle is intimately linked to climate. Improving the quantification of past changes will require improved spatial and temporal data coverage, as well as a better understanding of fractionation during N-loss (including anammox) in the water column and seafloor sediments.

Since many processes with different isotope effects influence the global patterns of $\delta^{15}N$, models are valuable tools to interpret these patterns (Somes et al., 2010b). The large degree of spatial variability in the signature of $\delta^{15}N$ made it a difficult tracer to interpret. This is due to the combination of processes (e.g., NO_3 assimilation, N_2 fixation, N-loss processes) that alter the $\delta^{15}N$ signature in different spatial scales. Models are useful to distinguish between these different isotope effects, which can be difficult to interpret with data alone. Although the spatial pattern of $\delta^{15}N$ is complicated, Somes et al. (2010b) showed this pattern can be

explained by the combination of isotope effects from phytoplankton NO_3^- assimilation, N_2 fixation, and N-loss processes.

While the strong (and opposite) isotope effects N_2 fixation and water column N-loss are well known, Somes et al. (2010b) showed that NO_3^- assimilation can also produce large variations in $\delta^{15}N$. The level of NO_3^- drawdown at the surface by phytoplankton strongly influences the $\delta^{15}N$ signature of the remaining surface nitrate. Phytoplankton preferentially incorporate ^{15}N-depleted nitrate leaving the residual oceanic NO_3^- pool will be ^{15}N-enriched when NO_3^- is significantly consumed. Since surface NO_3^- varies strongly across the surface ocean (most notably near the boundaries of HNLC regions), the $\delta^{15}N$ signature expresses sharp gradients as well. Although the fractionation factor associated with phytoplankton NO_3^- assimilation is much lower than water column N-loss (~5‰ vs. ~25‰, respectively), phytoplankton consume NO_3^- to lower levels compared to denitrifiers in suboxic zones and thus are able to produce large ranges $\delta^{15}NO_3^-$ values in some regions. This suggests changes is surface NO_3^- utilization must always be considered when interpreting $\delta^{15}N$.

Nitrogen isotopes can be a powerful constraint to infer patterns of N_2 fixation in the surface ocean (Somes et al., 2010a). The main habitat for N_2-fixing diazotrophs are the warm, oligotrophic NO_3^- depleted surface waters. These regions typically have high $\delta^{15}N$ values due to the high level of surface NO_3^- utilization there. N_2 fixation, on the other hand, introduces the ^{15}N-depleted ($\delta^{15}N_{NFIX} = -2 – 0$ ‰) values in the ocean. Thus if N_2 fixation was present in these regions, its influence on $\delta^{15}N$ would be evident.

Somes et al. (2010a) compared model versions with and without Fe limitation on diazotrophs with $\delta^{15}NO_3^-$ observations across the Pacific Ocean. Since diazotrophs have high Fe requirements, it has been suggested it is a key limiting factor regulating their habitat (Falkowski, 1997; Karl et al., 2002; Moore and Doney, 2007b). Indeed, Somet et al. (2010a) found that only the model version including Fe limitation of diazotrophs could reproduce the meridional trends of $\delta^{15}NO_3^-$ across the tropical central and western Pacific Ocean. When Fe limitation was not included, the simulated trends were anti-correlated with observations. This

model-data comparison suggests that atmospheric Fe limitation of diazotrophy is an important limiting factor for N_2 fixation.

We constrain global rates of N_2 fixation and N-loss using global mean $\delta^{15}NO_3^-$ in the pre-industrial ocean. Sensitivity experiments tested different assumptions for the isotope effect of N-loss in the water column and sediments, and how they affected the ratio of benthic to water column N-loss required to satisfy the mean $\delta^{15}NO_3^-$ assuming a balanced nitrogen budget. The ranges of rates for N_2 fixation and N-loss are estimated to vary by a factor of 2 given the current uncertainties for the isotope effect of N-loss.

The level of NO_3^- utilization within suboxic zones is an important process governing global mean $\delta^{15}NO_3^-$. This determines how high the local $\delta^{15}NO_3^-$ signature in suboxic zones that is removed by N-loss processes. The concentration of remaining nitrate in the suboxic zones also affects the influence of the high $\delta^{15}NO_3^-$ water from water column N-loss zones on global mean $\delta^{15}NO_3^-$. When this water mixes out of the suboxic zone, the mean $\delta^{15}NO_3^-$ value will be weighted towards the higher nitrate concentration, (i.e., dilution effect (Deutsch et al., 2004)). The model experiments performed here that test the range of uncertainty for NO_3^- utilization produce a range of benthic N-loss to water column N-loss ratios that vary by over a factor of 2. This suggests that the level of NO_3^- utilization in the suboxic zone is another crucial process that affects global mean $\delta^{15}NO_3^-$ and the rates of N-loss.

More observations of nitrogen isotopes in the water column are needed in the spatial and temporal scales to better quantify rates and isotope effects of N-loss processes. In water column suboxic zones, the role of canonical denitrification compared to anammox is not well known. Anammox consumes NH_4^+ and NO_2^- (rather than NO_3^-), two nitrogen species which the $\delta^{15}N$ signature is rarely measured. This adds uncertainty to understanding the most critical mechanisms important to the isotope effect of net N-loss in suboxic zones. A better understanding of the isotopes effect of anammox supported by $\delta^{15}N$ measurements of all species of nitrogen is needed to fully understand and quantify the fixed nitrogen removal in suboxic zones.

Measurements of ^{15}N-enriched ammonium overlying sites of benthic N-loss suggest that there may be a larger net fractionation associated with benthic N-loss ($\varepsilon_{BN\text{-}l}$ = 4–8 ‰) (Lehmann et al., 2004; Granger et al., 2011; Alkhatib et al., 2012) than previously thought ($\varepsilon_{BN\text{-}l}$ < 3 ‰) (Brandes and Devol, 2002; Lehmann et al., 2004). The net fractionation factor of benthic N-loss has an important role in determining the ratio benthic to water column N-loss needed to meet global mean $\delta^{15}NO_3^-$. If this high net fractionation is indeed validated on a global scale, this will require much higher ratios of benthic to water column N-loss rates than previously estimated. Model experiment conducted here suggest that increasing the net fractionation of benthic N-loss from 0 ‰ to 4 ‰ would then require more than double the benthic N-loss rate to balance global mean $\delta^{15}NO_3^-$ to observed level.

A new database of seafloor δ^{15}N measurements are used to constrain the distribution of δ^{15}N support high-end estimates for the net fractionation factor benthic N-loss. In the North Pacific, one of the largest basins for benthic N-loss in the ocean, only the model experiment with the high net fractionation factor for benthic N-loss ($\varepsilon_{BN\text{-}l}$=4‰) reproduces the trends of observations. Thses model experiments that best reproduce observations in the suboxic zone and seafloor sediments estimate rates of N_2 fixation, water column N-loss, and benthic N-loss are in the range 220–370, 70–90, and 150–280 Tg N yr^{-1}, respectively, assuming a balanced fixed nitrogen budget in the pre-industrial ocean. This model result suggests rates of N_2 fixation have been previously underestimated and the residence time of fixed nitrogen in the ocean is between 1,500 and 3,000 years.

In conclusion, this study found nitrogen isotopes to be a valuable tracer to constrain important nitrogen cycling processes in the global ocean. The nitrogen isotope model developed was able to reproduce the major trends of the δ^{15}N observations in the water column and seafloor sediments. It was a useful tool to distinguish between the different nitrogen isotope effects and constrain the important source (N_2 fixation) and sink (N-loss) processes in the oceanic fixed nitrogen budget. We identified key uncertainties involved with nitrogen isotope cycling that need to be better understood such as the level of nitrate utilization in suboxic zones and the associated impact of the dilution effect, as well as ^{15}N-cycling through all nitrogen species (e.g., nitrate, nitrite, ammonium, nitrous oxide,

dinitrogen, and organic N) in N-loss zones in the water column and seafloor sediments. Future work combining nitrogen isotope observations from all fixed nitrogen species with more sophisticated models that resolve all of these important physical and biogeochemical pathways will be able to further advance our understanding of the oceanic nitrogen cycle.

7 References

Alkhatib, M., Lehmann, M. F., and del Giorgio, P. A.: The nitrogen isotope effect of benthic remineralization-nitrification-denitrification coupling in an estuarine environment, Biogeosciences, 9, 1633-1646, 10.5194/bg-9-1633-2012, 2012.

Altabet, M. A., Deuser, W. G., Honjo, S., and Stienen, C.: Seasonal and depth-related changes in the source of sinking particles in the north atlantic, Nature, 354, 136-139, 10.1038/354136a0, 1991.

Altabet, M. A., and Francois, R.: Sedimentary nitrogen isotopic ratio as a recorder for surface ocean nitrate utilization, Global Biogeochem. Cycles, 8, 103-116, 10.1029/93GB03396, 1994.

Altabet, M. A., Francois, R., Murray, D. W., and Prell, W. L.: Climate-related variations in denitrification in the arabian sea from sediment 15n/14n ratios, Nature, 373, 506-509, 1995.

Altabet, M. A., Murray, D. W., and Prell, W. L.: Climatically linked oscillations in arabian sea denitrification over the past 1 m.Y.: Implications for the marine n cycle, Paleoceanography, 14, 732-743, 10.1029/1999PA900035 1999a.

Altabet, M. A., Pilskan, C., Thunell, R., Pride, C., Sigman, D., Chavez, F., and Francois, R.: The nitrogen isotope biogeochemistry of sinking particles from the margin of the eastern north pacific, Deep-Sea Res. I, 45, 655-679, 10.1016/S0967-0637(98)00084-3, 1999b.

Altabet, M. A.: Nitrogen isotopic evidence for micronutrient control of fractional no_3 utilization in the equatorial pacific, Limnology and Oceanogrphy, 46, 368-380, 2001.

Altabet, M. A., and Francois, R.: Nitrogen isotope biogeochemistry of the antarctic polar frontal zone at 170w, Deep-Sea Res. II, 48, 4247-4273, 10.1016/S0967-0645(01)00088-1, 2001.

Altabet, M. A.: Constraints on oceanic n balance/imbalance from sedimentary 15n records, Biogeosciences, 4, 75-86, 10.5194/bg-4-75-2007, 2007.

Antonov, J. I., Seidov, D., Boyer, T. P., Locarnini, R. A., Mishonov, A. V., Garcia, H. E., Baranova, O. K., Zweng, M. M., and Johnson, D. R.: World ocean atlas 2009, volume 2: Salinity, in: Noaa atlas nesdis 69, edited by: Levitus, S., U.S. Government Printing Office, Washington, D.C., 184, 2010.

Arrigo, K. R.: Marine microorganisms and global nutrient cycles, Nature, 437, 349-355, 2005.

Asner, G. P., Townsend, A. R., Riley, W. J., Matson, P. A., Neff, J. C., and Cleveland, C. C.: Physical and biogeochemical controls over terrestrial ecosystem responses to nitrogen deposition, Biogeochemistry., 54, 1-39, 2001.

Aumont, O., Maier-Reimer, E., Blain, S., and Monfray, P.: An ecosystem model of the global ocean including fe, si, p colimitations, Global Biogeochem. Cycles, 17, 1060, 10.1029/2001gb001745, 2003.

Berelson, W. M.: Particle settling rates increase wth depth in the ocean, Deep Sea Research Part II, 49, 237-251, 10.1016/S0967-0645(01)00102-3, 2001.

Bianchi, D., Dunne, J. P., Sarmiento, J. L., and Galbraith, E. D.: Data-based estimates of suboxia, denitrification, and n2o production in the ocean and their sensitivities to dissolved o2, Global Biogeochem. Cycles, 26, GB2009, 10.1029/2011gb004209, 2012.

Bigeleisen, J.: The effects of isotopic substitution on the rates of chemical reactions, The Journal of Physical Chemistry, 56, 823-828, 10.1021/j150499a002, 1952.

Bohlen, L., Dale, A. W., and Wallmann, K.: A simple transfer function for calculating benthic fixed nitrogen losses in global biogeochemical models, Global Biogeochem. Cycles, 2012, in review.

Bourbonnais, A., Lehmann, M. F., Waniek, J. J., and Schulz-Bull, D. E.: Nitrate isotope anomalies reflect n_2 fixation in the azores front region (subtropical ne atlantic), J. Geophys. Res., 114, 10.1029/2007JC004617, 2009.

Brandes, J. A., and Devol, A. H.: Isotopic fractionation of oxygen and nitrogen in coastal marine sediments, Geochim. Cosmochim. Acta, 61, 1793-1801, 10.1016/S0016-7037(97)00041-0, 1997.

Brandes, J. A., Devol, A. H., Yoshinari, T., Jayakumar, D. A., and Naqvi, S. W. A.: Isotopic composition of nitrate in the central arabian sea and eastern tropical north pacific: A tracer for mixing and nitrogen cycles, Limnol. Oceanogr., 43, 1680-1689, 1998.

Brandes, J. A., and Devol, A. H.: A global marine-fixed nitrogen isotopic budget: Implications for holocene nitrogen cycling, Global Biogeochem. Cycles, 16, 10.1029/2001GB001856, 2002.

Bridoux, M. C., Annenkov, V. V., Menzel, H., Keil, R. G., and Ingalls, A. E.: A new liquid chromatography/electrospray ionization mass spectrometry method for the analysis of underivatized aliphatic long-chain polyamines: Application to diatom-rich sediments, Rapid Communications in Mass Spectrometry, 25, 877-888, 10.1002/rcm.4931, 2011.

Brunelle, B. G., Sigman, D. M., Cook, M. S., Keigwin, L. D., Haug, G. H., Plessen, B., Schettler, G., and Jaccard, S. L.: Evidence from diatom-bound nitrogen isotopes for subarctic pacific stratification during the last ice age and a link to north pacific denitrification changes, Paleoceanography, 22, PA1215, 10.1029/2005pa001205, 2007.

Bryan, K., Manabe, S., and Pacanowski, R. C.: A global ocean-atmosphere climate model. Part ii. The oceanic circulation, J. Phys. Oceanogr., 5, 30-46, 10.1175/1520-0485(1975)005, 1975.

Bulow, S. E., Rich, J. J., Naik, H. S., Pratihary, A. K., and Ward, B. B.: Denitrification exceeds anammox as a nitrogen loss pathway in the arabian sea oxygen minimum zone, Deep Sea Research Part I: Oceanographic Research Papers, 57, 384-393, 2010.

Carpenter, E. J.: Nitrogen fixation by marine oscillatoria (*trichodesmium*) in the world's oceans, in: Nitrogen in the marine environment, edited by: Carpenter, E. J., and Capone, D. G., Academic, San Diego, California, 65-103, 1983.

Carpenter, E. J., Harvey, H. R., Fry, B., and Capone, D. G.: Biogeochemical tracers of the marine cyanobacterium *trichodesmium*, Deep Sea Research Part I: Oceanographic Research Papers, 44, 27-38, 10.1016/S0967-0637(96)00091-X, 1997.

Carpenter, E. J., and Foster, R. A.: Marine cyanobacterial symbioses cyanobacteria in symbiosis, in, edited by: Rai, A. N., Bergman, B., and Rasmussen, U., Springer Netherlands, 11-17, 2003.

Carpenter, E. J., and Capone, D. G.: Nitrogen fixation in the marine environment, in: Nitrogen in the marine environment, Second ed., edited by: Capone, D. G., Bronk, D. A., Mulholland, M. R., and Carpenter, E. J., Elsevier Inc., 141-198, 2008.

Church, M. J., Bjorkman, K. M., Karl, D. M., Saito, M. A., and Zehr, J. P.: Regional distributions of nitrogen-fixing bacteria in the pacific ocean, Limnol. Oceanogr., 53, 63-77, 2008.

Cline, J. D., and Kaplan, I. R.: Isotopic fractionation of dissolved nitrate during denitrification in the eastern tropical north pacific ocean, Marine Chemistry, 3, 271-299, 10.1016/0904-4203(75)90009-2, 1975.

Codispoti, L. A., and Richards, F. A.: An analysis of the horizontal regime of denitrification in the eastern tropical north pacific, Limnol. Oceanogr., 21, 379-388, 1976.

Codispoti, L. A., and Christensen, J. P.: Nitrification, denitrification and nitrous oxide cycling in the eastern tropical south pacific ocean, Marine Chemistry, 16, 277-300, 1985.

Codispoti, L. A., Brandes, J. A., Christensen, J. P., Devol, A. H., Naqvi, S. W. A., Paerl, H. W., and Yoshinari, T.: The oceanic fixed nitrogen and nitrous oxide budgets: Moving targets as we enter the anthropocene?, 2001.

Codispoti, L. A.: An oceanic fixed nitrogen sink exceeding 400 tg n a-1 vs the concept of homeostasis in the fixed-nitrogen inventory, Biogeosciences, 4, 233-253, 10.5194/bg-4-233-2007, 2007.

Delwiche, C. C., and Steyn, P. L.: Nitrogen isotope fractionation in soils and microbial reactions, Environmental Science and Technology, 4, 929-935, 1970.

Deutsch, C., Gruber, N., Key, R. M., Sarmiento, J. L., and Ganachaud, A.: Decreasing marine biogenic calcification: A negative feedback on rising atmospheric pco2, Global Biogeochem. Cycles, 15, 483-506, 10.1029/2000gb001291, 2001.

Deutsch, C., Sigman, D. M., Thunell, R. C., Meckler, A. N., and Haug, G. H.: Isotopic constraints on glacial/interglacial changes in the oceanic nitrogen budget, Global Biogeochem. Cycles, 18, GB4012, 10.1029/2003gb002189, 2004.

Deutsch, C., Sarmiento, J. L., Sigman, D. M., Gruber, N., and Dunne, J. P.: Spatial coupling of nitrogen inputs and losses in the ocean, Nature, 445, 163-167, http://www.nature.com/nature/journal/v445/n7124/suppinfo/nature05392_S1.html, 2007.

Deutsch, C., Brix, H., Ito, T., Frenzel, H., and Thompson, L.: Climate-forced variability of ocean hypoxia, Science, 333, 336-339, 10.1126/science.1202422, 2011.

DiFiore, P. J., Sigman, D. M., Trull, T. W., Lourey, M. J., Karsh, K., Cane, G., and Ho, R.: Nitrogen isotope constraints on subantarctic biogeochemistry, J. Geophys. Res., 111, 10.1029/2005JC003216, 2006.

Duce, R. A., LaRoche, J., Altieri, K., Arrigo, K. R., Baker, A. R., Capone, D. G., Cornell, S., Dentener, F., Galloway, J., Ganeshram, R. S., Geider, R. J., Jickells, T., Kuypers, M. M., Langlois, R., Liss, P. S., Liu, S. M., Middelburg, J. J., Moore, C. M., Nickovic, S., Oschlies, A., Pedersen, T., Prospero, J., Schlitzer, R., Seitzinger, S., Sorensen, L. L., Uematsu, M., Ulloa, O., Voss, M., Ward, B., and Zamora, L.: Impacts of atmospheric anthropogenic nitrogen on the open ocean, Science, 320, 893-897, 10.1126/science.1150369, 2008a.

Duce, R. A., LaRoche, J., Altieri, K., Arrigo, K. R., Baker, A. R., Capone, D. G., Cornell, S., Dentener, F., Galloway, J., Ganeshram, R. S., Geider, R. J., Jickells, T., Kuypers, M. M., Langlois, R., Liss, P. S., Liu, S. M., Middleburg, J. J., Moore, C. M., NIckovic, S., Oschlies, A., Pedersen, T., Prospero, J., Schlitzer, R., Seitzinger, S., Sorensen, L. L., Uematsu, M., Uloa, O., Voss, M., Ward, B., and Zamora, L.: Impacts of atmospheric anthropogenic nitrogen on the open ocean, Science, 320, 893-897, 10.1126/science.1150369, 2008b.

Eby, M., Zickfeld, K., Montenegro, A., Archer, D., Meissner, K. J., and Weaver, A. J.: Lifetime of anthropogenic climate change: Millennial time scales of potential co2 and surface temperature perturbations, Journal of Climate, 22, 2501-2511, 10.1175/2008jcli2554.1, 2009.

Eppley, R. W.: Temperature and phytoplankton growth in the sea, Fishery Bulletin, 70, 1972.

Falkowski, P. G.: Evolution of the nitrogen cycle and its influence on the biological sequestration of co2 in the ocean, Nature, 387, 272-275, 1997.

Farrell, J. W., Pedersen, T. F., Calvert, S. E., and Nielsen, B.: Glaciala-interglacial changes in nutrient utilization in the equatorial pacific ocean, Nature, 377, 514-517, 1995.

Foster, R. A., Kuypers, M. M. M., Vagner, T., Paerl, R. W., Musat, N., and Zehr, J. P.: Nitrogen fixation and transfer in open ocean diatom-cyanobacterial symbioses, ISME J, 5, 1484-1493, 2011.

Franois, R., Altabet, M. A., Yu, E.-F., Sigman, D. M., Bacon, M. P., Frank, M., Bohrmann, G., Bareille, G., and Labeyrie, L. D.: Contribution of southern ocean surface-water

stratification to low atmospheric co2 concentrations during the last glacial period, Nature, 389, 929-935, 1997.

Galbraith, E. D., Kienast, M., Jaccard, S. L., Pedersen, T. F., Brunelle, B. G., Sigman, D. M., and Kiefer, T.: Consistent relationship between global climate and surface nitrate utilization in the western subarctic pacific throughout the last 500 ka, Paleoceanography, 23, PA2212, 10.1029/2007pa001518, 2008.

Galbraith, E. D., Gnanadesikan, A., Dunne, J. P., and Hiscock, M. R.: Regional impacts of iron-light colimitation in a global biogeochemical model, Biogeosciences, 7, 1043-1064, 10.5194/bg-7-1043-2010, 2010.

Galbraith, E. D., Kienast, M., and group, N. w.: Coherent climate-driven changes in the global marine nitrogen cycle, Nature Geosci, 2012, in review.

Galbraith, E. G., Kienast, M., Pedersen, T. F., and Calvert, S. E.: Glacial-interglacial modulation of the marine nitrogen cycle by high-latitude o_2 supply to the global thermocline, Paleoceanography, 19, doi:10.1029/2003PA001000, 2004.

Galbraith, E. G.: Interactions between climate and the marine nitrogen cycle on glacial-interglacial timescales, Ph. D., Earth and Ocean Sciences, University of British Columbia, Vancouver, British Columbia, 2006.

Galloway, J. N., Dentener, F. J., Capone, D. G., Boyer, E. W., Howarth, R. W., Seitzinger, S. P., Asner, G. P., Cleveland, C. C., Green, P. A., Holland, E. A., Karl, D. M., Michaels, A. F., Porter, J. H., Townsend, A. R., and Vöosmarty, C. J.: Nitrogen cycles: Past, present, and future, Biogeochemistry, 70, 153-226, 10.1007/s10533-004-0370-0, 2004.

Ganeshram, R. S., Pedersen, T. F., Calvert, S. E., and Murray, J. W.: Large changes in oceanic nutrient inventories from glacial to interglacial periods, Nature, 376, 755-758, 1995.

Garcia, H. E., Locarnini, R. A., Boyer, T. P., Antonov, J. I., Baranov, O. K., Zweng, M. M., and Johnson, D. R.: World ocean atlas 2009, volume 3: Dissolved oxygen, apparent oxygen utilization, and oxygen saturation, in: Noaa atlas nesdis 70, edited by: Levitus, S., U.S. Government Printing Office, Washington, D.C., 344, 2010a.

Garcia, H. E., Locarnini, R. A., Boyer, T. P., Antonov, J. I., Zweng, M. M., Baranov, O. K., and Johnson, D. R.: World ocean atlas 2009, volume 4: Nutrients (phosphate, nitrate, silicate), in: Noaa atlas nesdis 71, edited by: Levitus, S., U.S. Government Printing Office, Washington, D. C., 398, 2010b.

Geider, R., and La Roche, J.: Redfield revisited: Variability of c:N:P in marine microalgae and its biochemical basis, European Journal of Phycology, 37, 1-17, 10.1017/s0967026201003456, 2002.

Gent, P. R., and Mcwilliams, J. C.: Isopycnal mixing in ocean circulation models, Journal of Physical Oceanography, 20, 150-155, doi:10.1175/1520-0485(1990)020<0150:IMIOCM>2.0.CO;2, 1990.

Giraud, X., Bertrand, P., Garc, on, V., and Dadou, I.: Modeling delta15n evolution: First palaeoceanographic applications in a coastal upwelling system, Journal of Marine Research, 58, 609-630, 2000.

Gnanadesikan, A., Dunne, J. P., and John, J.: Understanding why the volume of suboxic waters does not increase over centuries of global warming in an earth system model, Biogeosciences, 9, 1159-1172, 10.5194/bg-9-1159-2012, 2012.

Godfrey, L. V., and Falkowski, P. G.: The cycling and redox state of nitrogen in the archaean ocean, Nature Geosci, 2, 725-729, http://www.nature.com/ngeo/journal/v2/n10/suppinfo/ngeo633_S1.html, 2009.

Gottschalk, G.: Nutrition of bacteria
bacterial metabolism, in, Springer series in microbiology, Springer New York, 1-11, 1986.

Granger, J., Sigman, D. M., Needoba, J. A., and Harrison, P. J.: Coupled nitrogen and oxygen isotope fractionation of nitrate during assimilation by cultures of marine phytoplankton, Limnol. Oceanogr., 49, 1763-1773, 2004.

Granger, J., Prokopenko, M. G., Sigman, D. M., Mordy, C. W., Morse, Z. M., Morales, L. V., Sambrotto, R. N., and Plessen, B.: Coupled nitrification-denitrification in sediment of the eastern bering sea shelf leads to 15n enrichment of fixed n in shelf waters, J. Geophys. Res., 116, C11006, 10.1029/2010jc006751, 2011.

Großkopf, T., Mohr, W., and La Roche, J.: Global underestimation of of n2 fixation in the ocean, Nature, 2012, in review.

Gruber, N., and Sarmiento, J. L.: Global patterns of marine nitrogen fixation and denitrification, Global Biogeochem. Cycles, 11, 235-266, 1997.

Gruber, N.: The dynamics of the marine nitrogen cycle and its influence on atmospheric co_2 variations, in: The ocean carbon cycle and climate, IV ed., edited by: Follows, M., and Oguz, T., Nato science series, Kluwer Academics, Dordrecht, 97-148, 2004.

Gruber, N.: Chapter 1 - the marine nitrogen cycle: Overview and challenges, in: Nitrogen in the marine environment (2nd edition), Academic Press, San Diego, 1-50, 2008.

Gruber, N., and Galloway, J. N.: An earth-system perspective of the global nitrogen cycle, Nature, 451, 293-296, 2008.

Hamersley, M. R., Turk, K. A., Leinweber, A., Gruber, N., Zehr, J. P., Gunderson, T., and Capone, D. G.: Nitrogen fixation within the water column associated with two hypoxic basins in the southern california bight, Aquatic Microbial Ecology, 63, 193-205, 10.3354/ame01494, 2011.

Hedges, J. I., Baldock, J. A., Gélinas, Y., Lee, C., Peterson, M. L., and Wakeham, S. G.: The biochemical and elemental compositions of marine plankton: A nmr perspective, Marine Chemistry, 78, 47-63, 2002.

Higgins, M. B., Robinson, R. S., Carter, S. J., and Pearson, A.: Evidence from chlorin nitrogen isotopes for alternating nutrient regimes in the eastern mediterranean sea, Earth and Planetary Science Letters, 290, 102-107, 2010.

Holl, C. M., and Montoya, J. P.: Interactions between nitrate uptake and nitrogen fixation in continuous cultures of the marine diazotroph *trichodesmium* (cyanobacteria), J. Phycol., 41, 1178-1183, 10.1111/j.1529-8817.2005.00146.x, 2005.

Ito, T., and Follows, M. J.: Preformed phosphate, soft tissue pump and atmospheric co2, Journal of Marine Research, 63, 813-839, 2005.

Jaccard, S. L., and Galbraith, E. D.: Large climate-driven changes of oceanic oxygen concentrations during the last deglaciation, Nature Geosci, 5, 151-156, http://www.nature.com/ngeo/journal/v5/n2/abs/ngeo1352.html#supplementary-information, 2012.

Kalnay, E., Kanamitsu, M., Kistler, R., Collins, W., Deaven, D., Gandin, L., Iredell, M., Saha, S., White, G., Woollen, J., Zhu, Y., Leetmaa, A., Reynolds, R., Chelliah, M., Ebisuzaki, W., Higgins, W., Janowiak, J., Mo, K. C., Ropelewski, C., Wang, J., Jenne, R., and Joseph, D.: The ncep/ncar 40-year reanalysis project, Bulletin of the American Meteorological Society, 77, 437-471, 10.1175/1520-0477(1996)077<0437:tnyrp>2.0.co;2, 1996.

Karl, D., Michaels, A., Bergman, B., Capone, D., Carpenter, E., Letelier, R., Lipschultz, F., Paerl, H., Sigman, D., and Stal, L.: Dinitrogen fixation in the world's oceans, Biogeochemistry, 57-58, 47-98, 10.1023/a:1015798105851, 2002.

Karsh, K. L., Trull, T. W., Lourey, M. J., and Sigman, D. M.: Relationship of nitrgen isotope fractionation to phytoplankton size and iron availability during the southern ocean iron release experiment (soiree), Limnol. Oceanogr., 48, 1058-1068, 2003.

Kessler, W. S.: The circulation of the eastern tropical pacific: A review, Progress in Oceanography, 69, 181-217, 10.1016/j.pocean.2006.03.009, 2006.

Kienast, M., Lehmann, M. F., Timmermann, A., Galbraith, E., Bolliet, T., Holbourn, A., Normandeau, C., and Laj, C.: A mid-holocene transition in the nitrogen dynamics of the western equatorial pacific: Evidence of a deepening thermocline?, Geophysical Research Letter, 35, 10.1029/2008GL035464, 2008.

Kienast, S. S., Calvert, S. E., and Pedersen, T. F.: Nitrogen isotope productivity variations along the northeast pacific margin over the last 120 kyr: Surface and subsurface paleoceanography, Paleoceanography, 17, 10.1029/2001PA000650, 2002.

Kitajima, S., Furuya, K., Hashihama, F., Takeda, S., and Kanda, J.: Latitudinal distribution of diazotrophs and their nitrogen fixation in the tropical and subtropical western north pacific, Limnol. Oceanogr., 54, 537-547, 2009.

Klausmeier, C. A., Litchman, E., Daufresne, T., and Levin, S. A.: Optimal nitrogen-to-phosphorus stoichiometry of phytoplankton, Nature, 429, 171-174, http://www.nature.com/nature/journal/v429/n6988/suppinfo/nature02454_S1.html, 2004.

Knapp, A. N., Sigman, D. M., and Lipshultz, F.: N isotopic composition of dissolved organic nitrogen and nitrate at the bermuda atlatnic time-series study site, Global Biogeochem. Cycles, 19, 10.1029/2004GB002320, 2005.

Knapp, A. N., DiFiore, P. J., Deutsch, C., Sigman, D. M., and Lipshultz, F.: Nitrate isotopic composition between bermuda and puerto rico: Implications for n_2 fixation in the atlantic ocean, Global Biogeochem. Cycles, 22, 10.1029/2007GB003107, 2008.

Krauk, J. M., Villareal, T. A., Sohm, J. A., Montoya, J. P., and Capone, D. G.: Plasticity of n:P ratios in laboratory and field populations of trichodesmium spp., Aquat. Microb. Ecol., 42, 243-253, 2006.

Kuypers, M. M. M., Sliekers, A. O., Lavik, G., Schmid, M., Jorgensen, B. B., Kuenen, J. G., Sinninghe Damste, J. S., Strous, M., and Jetten, M. S. M.: Anaerobic ammonium oxidation by anammox bacteria in the black sea, Nature, 422, 608-611, 2003.

Kuypers, M. M. M., Lavik, G., Woebken, D., Schmid, M., Fuchs, B. M., Amann, R., Jørgensen, B. B., and Jetten, M. S. M.: Massive nitrogen loss from the benguela upwelling system through anaerobic ammonium oxidation, Proceedings of the National Academy of Sciences of the United States of America, 102, 6478-6483, 10.1073/pnas.0502088102, 2005.

Lam, P., Lavik, G., Jensen, M. M., van de Vossenberg, J., Schmid, M., Woebken, D., Gutiérrez, D., Amann, R., Jetten, M. S. M., and Kuypers, M. M. M.: Revising the nitrogen cycle in the peruvian oxygen minimum zone, Proceedings of the National Academy of Sciences, 106, 4752-4757, 10.1073/pnas.0812444106, 2009.

Large, W. G., Danabasoglu, G., McWilliams, J. C., Gent, P. R., and Bryan, F. O.: Equatorial circulation of a global ocean climate model with anisotropic horizontal viscosity, Journal of Physical Oceanography, 31, 518-536, doi:10.1175/1520-0485(2001)031<0518:ECOAGO>2.0.CO;2, 2001.

Le Quéré, C. L., Harrison, S. P., Colin Prentice, I., Buitenhuis, E. T., Aumont, O., Bopp, L., Claustre, H., Cotrim Da Cunha, L., Geider, R., Giraud, X., Klaas, C., Kohfeld, K. E., Legendre, L., Manizza, M., Platt, T., Rivkin, R. B., Sathyendranath, S., Uitz, J., Watson, A. J., and Wolf-Gladrow, D.: Ecosystem dynamics based on plankton functional types for global ocean biogeochemistry models, Global Change Biology, 11, 2016-2040, 10.1111/j.1365-2486.2005.1004.x, 2005.

Lehmann, M. F., Sigman, D. M., and Berelson, W. M.: Coupling the 15n/14n and 18o/16o of nitrate as a constraint on benthic nitrogen cycling, Marine Chemistry, 88, 1-20, 2004.

Lehmann, M. F., Sigman, D. M., McCorkle, D. C., Brunelle, B. G., Hoffmann, S., Kienast, M., Cane, G., and Clement, J.: Origin of the deep bering sea nitrate deficit: Constraints from the nitrogen and oxygen isotopic composition of water column nitrate and benthic nitrate fluxes, Global Biogeochem. Cycles, 19, 10.1029/2005GB00250, 2005.

Lehmann, M. F., Sigman, D. M., McCorkle, D. C., Granger, J., Hoffmann, S., Cane, G., and Brunelle, B. G.: The distribution of nitrate 15n/14n in marine sediments and the impact of benthic nitrogen loss on the isotopic composition of oceanic nitrate, Geochimica et Cosmochimica Acta, 71, 5384-5404, 2007.

Letelier, R. M., and Karl, D. M.: Role of trichodesmium spp. In the productivity of the subtropical north pacific ocean, Marine Ecology Progress Series, 133, 263-273, 10.3354/meps133263, 1996.

Letelier, R. M., and Karl, D. M.: *Trichodesmium* spp. Physiology and nutrient fluxes in the north pacific subtropical gyre, Aquatic Microbial Ecology, 15, 254-276, 10.3354/ame015265, 1998a.

Letelier, R. M., and Karl, D. M.: Trichodesmium spp. Physiology and nutrient fluxes in the north pacific subtropical gyre, Aquatic Microbial Ecology, 15, 265-276, 10.3354/ame015265, 1998b.

Lipshultz, F., Bates, N. R., Carlson, C. A., and Hansell, D. A.: New production in the sargasso sea: History and current status, Global Biogeochem. Cycles, 16, 10.1029/2000GB001319, 2002.

Liu, K.-K., and Kaplan, I. R.: The eastern tropical pacific as a source of ^{15}n-enriched nitrate in seawater off southern california, Limnol. Oceanogr., 34, 820-830, 1989.

Liu, K.-K., Su, M.-J., Hsueh, C.-R., and Gong, G.-c.: The nitrogen isotopic composition of nitrate in the kuroshio water northeast of taiwan: Evidence for nitrogen fixation as a source of isotopically light nitrate, Marine Chemistry, 54, 273-292, 1996.

Locarnini, R. A., Mishonov, A. V., Antonov, J. I., Boyer, T. P., Garcia, H. E., Baranova, O. K., Zweng, M. M., and Johnson, D. R.: World ocean atlas 2009, volume 1: Temperature, in: Noaa atlas nesdis 68, edited by: Levitus, S., U.S. Government Printing Office, Washington, D.C., 184, 2010.

Macko, S. A., Fogel, M. L., Hare, P. E., and Hoering, T. C.: Isotope fractionation of nitrogen and carbon in the synthesis of amino acids by microorganisms, Chemical Geology: Isotope Geoscience section, 65, 79-92, 10.1016/01689622(87)90064-9, 1987.

Mahaffey, C., Michaels, A. F., and Capone, D. G.: The conundrum of marine n2 fixation, American Journal of Science, 305, 546-595, 10.2475/ajs.305.6-8.546, 2005.

Mahowald, N. M., Baker, A. R., Bergametti, G., Brooks, N., Duce, R. A., Jickells, T. D., Kubilay, N., Prospero, J. M., and Tegen, I.: Atmospheric global dust cycle and iron inputs to the ocean, Global Biogeochem. Cycles, 19, 10.1029/2004GB002402, 2005a.

Mahowald, N. M., Baker, A. R., Bergametti, G., Brooks, N., Duce, R. A., Jickells, T. D., Kubilay, N., Prospero, J. M., and Tegen, I.: Atmospheric global dust cycle and iron inputs to the ocean, Global Biogeochem. Cycles, 19, GB4025, 10.1029/2004gb002402, 2005b.

Mahowald, N. M., Muhs, D. R., Levis, S., Rasch, P. J., Yoshioka, M., Zender, C. S., and Luo, C.: Change in atmospheric mineral aerosols in response to climate: Last glacial period, preindustrial, modern, and doubled carbon dioxide climates, J. Geophys. Res., 111, D10202, 10.1029/2005jd006653, 2006.

Mahowald, N. M., Engelstaedter, S., Luo, C., Sealy, A., Artaxo, P., Benitez-Nelson, C., Bonnet, S., Chen, Y., Chuang, P. Y., Cohen, D. D., Dulac, F., Herut, B., Johansen, A. M., Kubilay, N., Losno, R., Maenhaut, W., Paytan, A., Prospero, J. A., Shank, L. M., and Siefert, R. L.: Atmospheric iron deposition: Global distribution, variability, and human perturbations, in: Annual review of marine science, Annual review of marine science, Annual Reviews, Palo Alto, 245-278, 2009.

Mariotti, A., Germon, J., Hubert, P., Kaiser, P., Letolle, R., Tardieux, A., and Tardieux, P.: Experimental determination of nitrogen kinetic isotope fractionation: Some principles; illustration for the denitrification and nitrification processes, Plant and Soil, 62, 413-430, 10.1007/bf02374138, 1981.

Mark Moore, C., Mills, M. M., Achterberg, E. P., Geider, R. J., LaRoche, J., Lucas, M. I., McDonagh, E. L., Pan, X., Poulton, A. J., Rijkenberg, M. J. A., Suggett, D. J., Ussher, S. J., and Woodward, E. M. S.: Large-scale distribution of atlantic nitrogen fixation controlled by iron availability, Nature Geosci, 2, 867-871, http://www.nature.com/ngeo/journal/v2/n12/suppinfo/ngeo667_S1.html, 2009.

Martin, J. H.: Glacial-interglacial co2 change: The iron hypothesis, Paleoceanography, 5, 1-13, 10.1029/PA005i001p00001, 1990.

McCarthy, M. D., Benner, R., Lee, C., and Fogel, M. L.: Amino acid nitrogen isotopic fractionation patterns as indicators of heterotrophy in plankton, particulate, and dissolved organic matter, Geochimica et Cosmochimica Acta, 71, 4727-4744, 2007.

McElroy, M. B.: Marine biological controls on atmospheric co2 and climate, Nature, 302, 328-329, 1983.

Michaels, A. F., Olson, D., Sarmiento, J. L., Ammerman, J. W., Fanning, K., Jahnke, R., Knap, A. H., Lipshultz, F., and Prospero, J. M.: Inputs, losses and transformations of nitrogen and phosphorus in the pelagic north atlantic ocean, in: Nitrogen cycling in the north atlatnic ocean and its watersheds, edited by: Howarth, R. W., Kluwer Academic Publishers, Boston, MA, 181-226, 1996.

Middelburg, J. J., Soetaert, K., Herman, P. M. J., and Heip, C. H. R.: Denitrification in marine sediments: A model study, Global Biogeochem. Cycles, 10, 661-673, 10.1029/96gb02562, 1996.

Middleburg, J. J., Soetaert, K., Herman, P. M. J., and Heip, C. H. R.: Denitrification in marine sediments: A model study, Global Biogeochem. Cycles, 10, 661-673, 10.1029/96GB02562 1996.

Minagawa, M., and Wada, E.: Stepwise enrichment of ^{15}n along food chains: Further evidence and the relation between d^{15}n and animal age, Geochim. Cosmochim. Acta, 48, 1135-1140, 10.1016/0016-7037(84)90204-7, 1984.

Minagawa, M., and Wada, E.: Nitrogen isotope ratios of red tide organisms in the east china sea: A characterization of biological nitrogen fixation, Marine Chemistry, 19, 245-259, 10.1016/304-4203(86)90026-5, 1986.

Möbius, J., Gaye, B., Lahajnar, N., Bahlmann, E., and Emeis, K.-C.: Influence of diagenesis on sedimentary δ15n in the arabian sea over the last 130 kyr, Marine Geology, 284, 127-138, 2011.

Mohr, W., Großkopf, T., Wallace, D. W. R., and LaRoche, J.: Methodological underestimation of oceanic nitrogen fixation rates, PLoS ONE, 5, e12583, 2010.

Monteiro, F. M., Dutkiewicz, S., and Follows, M. J.: Biogeographical controls on the marine nitrogen fixers, Global Biogeochem. Cycles, 25, GB2003, 10.1029/2010gb003902, 2011.

Montoya, J. P., and McCarthy, J. J.: Isotopic fractionation during nitrate uptake by phytoplankton grown in continuous culture, J. Plankton Research, 17, 439-464, 1995.

Montoya, J. P., Holl, C. M., Zehr, J. P., Hansen, A., Villareal, T. A., and Capone, D. G.: High rates of n2 fixation by unicellular diazotrophs in the oligotrophic pacific ocean, Nature, 430, 1027-1032, 2004.

Montoya, J. P.: Nitrogen stable isotopes in marine environments, in: Nitrogen in the marine environment, Second ed., edited by: Capone, D. G., Bronk, D. A., Mulholland, M. R., and Carpenter, E. J., Elsevier Inc., 1277-1302, 2008.

Moore, J. K., Doney, S. C., and Lindsay, K.: Upper ocean ecosystem dynamics and iron cycling in a global three-dimensional model, Global Biogeochem. Cycles, 18, GB4028, 10.1029/2004gb002220, 2004.

Moore, J. K., and Doney, S. C.: Iron availability limits the ocean nitrogen inventory stabilizing feedbacks between marine denitrification and nitrogen fixation, in: Global Biogeochemical Cycles, April 4, 2007 ed., GB2001, 2007a.

Moore, J. K., and Doney, S. C.: Iron availability limits the ocean nitrogen inventory stabilizing feedbacks between marine denitrification and nitrogen fixation, Global Biogeochem. Cycles, 21, GB2001, 10.1029/2006gb002762, 2007b.

Moore, L. R., Post, A. F., Rocap, G., and Chisholm, S. W.: Utilization of different nitrogen sources by the marine cyanobacteria prochlorococcus and synechococcus, Limnnol. Oceanogr., 47, 989-996, 2002.

Mulder, A., van de Graaf, A. A., Robertson, L. A., and Kuenen, J. G.: Anaerobic ammonium oxidation discovered in a denitrifying fluidized bed reactor, FEMS Microbial Ecology, 16, 177-184, 10.1111/j.1574-6941.1995.tb00281.x, 1995.

Mulholland, M. R., Ohki, K., and Capone, D. G.: Nutrient controls on nitrogen uptake and metabolism by natural populations and cultures of *trichodesmium* (cyanobacteria), Journal of Phycology, 37, 1001-1009, 2001.

Mulholland, M. R.: The fate of nitrogen fixed by diazotrophs in the ocean, Biogeosciences, 4, 37-51, 10.5194/bg-4-37-2007, 2007.

Munk, W. H.: On the wind-driven ocean circulation, J. of Atmospheric Sciences, 7, 80-93, 10.1175/1520-0469(1950)007, 1950.

Naqvi, S. W. A.: The indian ocean, in: Nitrogen in the marine environment, Second ed., edited by: Capone, D. G., Bronk, D. A., Mulholland, M. R., and Carpenter, E. J., Elsevier Inc., 631-681, 2008.

Needoba, J. A., Waser, N. A., Harrison, P. J., and Calvert, S. E.: Nitrogen isotope fractionation in 12 species of marine phytoplankton during growth on nitrate, Marine Ecological Progressive Series, 255, 10.3354/meps255081, 2003.

Needoba, J. A., Foster, R. A., Sakamoto, C., Zehr, J. P., and Johnson, K. S.: Nitrogen fixation by unicellular diazotrophic cyanobacteria in the temperate oligotrophic north pacific ocean, Limnol. Oceanogr., 52, 1317-1327, 2007.

Nevison, C. D., Weiss, R. F., and Erickson, D. J., III: Global oceanic emissions of nitrous oxide, J. Geophys. Res., 100, 15809-15820, 10.1029/95jc00684, 1995.

Nier, A. O.: A redetermination of the relative abundances of the isotopes of carbon, nitrogen, oxygen, argon, and potassium, Physical Review, 77, 789-793, 1950.

Pandey, K. D., Shukla, S. P., Shukla, P. N., Giri, D. D., Singh, J. S., Singh, P., and Kashyap, A. K.: Cyanobacteria in antarctica: Ecology, physiology and cold adaptation, Cellular and molecular biology (Noisy-le-Grand, France), 50, 575-584, 2004.

Raven, J. A.: The iron and molybdenum use efficiencies of plant growth with different energy, carbon and nitrogen sources, New Phytologist, 109, 279-287, 1988.

Ravishankara, A. R., Daniel, J. S., and Portmann, R. W.: Nitrous oxide (n2o): The dominant ozone-depleting substance emitted in the 21st century, Science, 326, 123-125, 10.1126/science.1176985, 2009.

Redfield, A. C.: The biological control of chemical factors in the environment, Am. Sci., 46, 205-221, 1958.

Ren, H., Sigman, D. M., Meckler, A. N., Plessen, B., Robinson, R. S., Rosenthal, Y., and Haug, G. H.: Foraminiferal isotope evidence of reduced nitrogen fixation in the ice age atlantic ocean, Science, 323, 244-248, 2009.

Robinson, R. S., Sigman, D. M., DiFiore, P. J., Rohde, M. M., Mashiotta, T. A., and Lea, D. W.: Diatom-bound 15n/14n: New support for enhanced nutrient consumption in the ice age subantarctic, Paleoceanography, 20, PA3003, 10.1029/2004pa001114, 2005.

Robinson, R. S., and Sigman, D. M.: Nitrogen isotopic evidence for a poleward decrease in surface nitrate within the ice age antarctic, Quaternary Sciences Reviews, 27, 1076-1090, 10.1016/j.quascirev.2008.02.005, 2008.

Rütting, T., Boeckx, P., Müller, C., and Klemedtsson, L.: Assessment of the importance of dissimilatory nitrate reduction to ammonium for the terrestrial nitrogen cycle, Biogeosciences, 8, 1779-1791, 10.5194/bg-8-1779-2011, 2011.

Ryabenko, E., Kock, A., Bange, H. W., Altabet, M. A., and Wallace, D. W. R.: Contrasting biogeochemistry of nitrogen in the atlantic and pacific oxygen minimum zones, Biogeosciences, 9, 203-215, 10.5194/bg-9-203-2012, 2012.

Sanudo-Wilhelmy, S. A., Kustka, A. B., Gobler, C. J., Hutchins, D. A., Yang, M., Lwiza, K., Burns, J., Capone, D. G., Raven, J. A., and Carpenter, E. J.: Phophorus limitation of nitrogen fixation by *trichodesmium* in the central atlantic ocean, Nature, 411, 66-69, 10.1038/35075041, 2001.

Sanudo-Wilhelmy, S. A., Tovar-Sanchez, A., Fu, F.-X., Capone, D. G., Carpenter, E. J., and Hutchins, D. A.: The impact of surface-adsorbed phosphorus on phytoplankton redfield stoichiometry, Nature, 432, 897-901, http://www.nature.com/nature/journal/v432/n7019/abs/nature03125.html#supplementary-information, 2004.

Sarmiento, J. L., Hughes, T. M. C., Stouffer, R. J., and Manabe, S.: Simulated response of the ocean carbon cycle to anthropogenic climate warming, Nature, 393, 245-249, 1998.

Schmittner, A., Oschlies, A., Giraud, X., Eby, M., and Simmons, H. L.: A global model of the marine ecosystem for long-term simulations: Sensitivity to ocean mixing buoyancy forcing, particle sinking, and dissolved organic matter cycling, Global Biogeochem. Cycles, 19, 10.1029/2004GB002283, 2005.

Schmittner, A., Galbraith, E. D., Hostetler, S. W., Pedersen, T. F., and Zhang, R.: Large fluctuations of dissolved oxygen in the indian and pacific oceans during dansgaard-oeschger oscillations caused by variations of north atlantic deep water subduction, Paleoceanography, 22, PA3207, 10.1029/2006pa001384, 2007.

Schmittner, A., Oschlies, A., Matthews, H. D., and Galbraith, E. D.: Future changes in climate, ocean circulation, ecosystems, and biogeochemical cycling simulated for a business-as-usual co2 emission scenario until year 4000 ad, Global Biogeochem. Cycles, 22, GB1013, 10.1029/2007gb002953, 2008.

Seitzinger, S. P., Mayorga, E., Bouwman, A. F., Kroeze, C., Beusen, A. H. W., Billen, G., Van Drecht, G., Dumont, E., Fekete, B. M., Garnier, J., and Harrison, J. A.: Global river nutrient export: A scenario analysis of past and future trends, Global Biogeochem. Cycles, 24, GB0A08, 10.1029/2009gb003587, 2010.

Shakun, J. D., and Carlson, A. E.: A global perspective on last glacial maximum to holocene climate change, Quaternary Science Reviews, 29, 1801-1816, 2010.

Shakun, J. D., Clark, P. U., He, F., Marcott, S. A., Mix, A. C., Liu, Z., Otto-Bliesner, B., Schmittner, A., and Bard, E.: Global warming preceded by increasing carbon dioxide concentrations during the last deglaciation, Nature, 484, 49-54, http://www.nature.com/nature/journal/v484/n7392/abs/nature10915.html#supplementary-information, 2012.

Sherwood, O. A., Lehmann, M. F., Schubert, C. J., Scott, D. B., and McCarthy, M. D.: Nutrient regime shift in the western north atlantic indicated by compound-specific δ15n of deep-sea gorgonian corals, Proceedings of the National Academy of Sciences, 108, 1011-1015, 10.1073/pnas.1004904108, 2011.

Sigman, D. M., Altabet, M. A., Michener, R., McCorkle, D. C., Fry, B., and Holmes, R. M.: Natural abundance-level measurment of the nitrogen isotopic composition of oceanic nitrate: An adaptiation of the ammonia diffusion method, Marine Chemistry, 57, 227-242, 10.1016/S0304-4203(97)00009-1, 1997.

Sigman, D. M., Altabet, M. A., McCorkle, D. C., Francois, R., and Fischer, G.: The $\delta^{15}\nu$ of nitrate in the southern ocean: Consumption of nitrate in surface waters, Global Biogeochem. Cycles, 13, 1149-1166, 1999.

Sigman, D. M., Robinson, R., Knapp, A. N., van Green, A., McCorkle, D. C., Brandes, J. A., and Thunell, R. C.: Distinguishing between water column and sedimentary denitrification in the santa barbara basin using the stable isotopes of nitrate, Geochem. Geophys. Geosyst., 4, doi:10.1029/2002GC000384, 2003.

Sigman, D. M., Granger, J., DiFiore, P. J., Lehmann, M. F., Ho, R., Cane, G., and Green, A. v.: Coupled nitrogen and oxygen isotope measurements of nitrate along the eastern north pacific margin, Global Biogeochem. Cycles, 19, GB4022, 10.1029/2005GB002458, 2005.

Simmons, H. L., Jayne, S. R., Laurent, L. C. S., and Weaver, A. J.: Tidally driven mixing in a numerical model of the ocean general circulation, Ocean Modelling, 6, 245-263, 10.1016/S1463-5003(03)00011-8, 2004.

Somes, C. J., Schmittner, A., and Altabet, M. A.: Nitrogen isotope simulations show the importance of atmospheric iron deposition for nitrogen fixation across the pacific ocean, Geophys. Res. Lett., 37, L23605, 10.1029/2010gl044537, 2010a.

Somes, C. J., Schmittner, A., Galbraith, E. D., Lehmann, M. F., Altabet, M. A., Montoya, J. P., Letelier, R. M., Mix, A. C., Bourbonnais, A., and Eby, M.: Simulating the global

distribution of nitrogen isotopes in the ocean, Global Biogeochem. Cycles, 24, GB4019, 10.1029/2009gb003767, 2010b.

Sterner, R. W., and Elser, J. J.: Ecological stoichiometry: The biology of elements from molecules to the biosphere, Princeton University Press, 429 pp., 2002.

Strohm, T. O., Griffin, B., Zumft, W. G., and Schink, B.: Growth yields in bacterial denitrification and nitrate ammonification, Applied and Environmental Microbiology, 73, 1420-1424, 10.1128/aem.02508-06, 2007.

Tesdal, J. E., Galbraith, E. D., and Kienast, M.: The marine sedimentary nitrogen isotope record, Biogeosciences Discuss., 9, 4067-4097, 10.5194/bgd-9-4067-2012, 2012.

Teske, A., Alm, E., Regan, J. M., Toze, S., Rittmann, B. E., and Stahl, D. A.: Evolutionary relationships among ammonia- and nitrite-oxidizing bacteria, Journal of Bacteriology, 176, 6623-6630, 1994.

Thamdrup, B., and Dalsgaard, T.: Production of n(2) through anaerobic ammonium oxidation coupled to nitrate reduction in marine sediments, Appl Environ Microbiol, 68, 1312-1318, citeulike-article-id:1557343, 2002.

Tiedje, J. M.: Ecology of denitrification and dissimilatory nitrate reduction to ammonium, in: Biology of anaerobic microorganisms, edited by: Zehnder, A. J. B., John Wiley & Sons, New York, USA, 179-244, 1988.

Tyrrell, T.: The relative influences of nitrogen and phosphorus on oceanic primary production, Nature, 400, 525-531, 10.1038/22941, 1999a.

Tyrrell, T.: The relative influences of nitrogen and phosphorus on oceanic primary production, Nature, 400, 525-531, http://www.nature.com/nature/journal/v400/n6744/suppinfo/400525a0_S1.html, 1999b.

Voss, M., Dippner, J. W., and Montoya, J. P.: Nitrogen isotope patterns in the oxygen-deficient waters of the eastern tropical north pacific ocean, Deep Sea Research Part I: Oceanographic Research Papers, 48, 1905-1921, 2001a.

Voss, M., Dippner, J. W., and Montoya, J. P.: Nitrogen isotope patterns in the oxygen-deficient waters of the eastern tropical north pacific, Deep-Sea Res. I, 48, 1905-1921, 10.1016/S097-0637(00)00110-2, 2001b.

Wada, E., and Hattori, A.: Nitrogen isotope effects in the assimilation of inorganic nitrogenous compounds by marine diatoms, Geomicrobiology 1, 85-101, 10.1080/01490457809377725 1978.

Wada, E.: Nitrogen isotope fractionation and its significance in biogeochemical processes occurring in marine environments, in: Isotope marine chemistry, edited by: Goldberg, E. D., Horibe, Y., and Saruhashi, K., Uchida-Rokakuho, Tokyo, 375-398, 1980.

Ward, B. B., Capone, D. G., and Zehr, J. P.: What's new in the nitrogen cycle?, Oceanography, 20, 101-109, 2007.

Ward, B. B., Devol, A. H., Rich, J. J., Chang, B. X., Bulow, S. E., Naik, H., Pratihary, A., and Jayakumar, A.: Denitrification as the dominant nitrogen loss process in the arabian sea, Nature, 461, 78-81, http://www.nature.com/nature/journal/v461/n7260/suppinfo/nature08276_S1.html, 2009.

Waser, N. A. D., Harrison, P. J., Nielsen, B., Calvert, S. E., and Turpin, D. H.: Nitrogen isotope fractionation during the uptake and assimilation of nitrate, nitrite, ammonium, and urea by a marine diatom, Limnol. Oceanogr., 43, 215-224, 1998.

Weaver, A. J., Eby, M., Wiebe, E. C., Bitz, C. M., Duffy, P. B., Ewen, T. L., Fanning, A. F., Holland, M. M., MacFadyen, A., Matthews, H. D., Meissner, K. J., Saenko, O., Schmittner, A., Wang, H., and Yoshimori, M.: The uvic earth system climate model: Model description, climatology, and applications to past, present and future climates, Atmosphere-Ocean, 39, 361 - 428, 2001.

White, A. E., Spitz, Y. H., and Karl, D. M.: Flexible elemental stoichiometry in trichodesmium spp. And its ecological implications, Limnology and Oceanogrphy, 51, 1777-1790, 2006.

Wu, J., Sunda, W., Boyle, E. A., and Karl, D. M.: Phosphate depletion in the western north atlantic ocean, Science, 289, 759-762, 10.1126/science.289.5480.759, 2000.

Yoshikawa, C., Yamanaka, Y., and Nakatsuka, T.: Nitrate-nitrogen isotopic patterns in surface waters of the western an central equatorial pacific, J. Oceanogr., 62, 511-525, 2006.

Zehr, J. P., Waterbury, J. B., Turner, P. J., Montoya, J. P., Omoregie, E., Steward, G. F., Hansen, A., and Karl, D. M.: Unicellular cyanobacteria fix n_2 in the subtropical north pacific ocean, Nature, 412, 635-638, 10.1038/35088063, 2001.

Zehr, J. P., and Ward, B. B.: Nitrogen cycling in the ocean: New perspectives on processes and paradigms, Applied and Environmental Microbiology, 68, 1015-1024, 10.1128/aem.68.3.1015-1024.2002, 2002.

Zehr, J. P.: Nitrogen fixation by marine cyanobacteria, Trends in Microbiology, 19, 162-173, 2011.

List of Tables

List of Figures

Acknowledgements - Danksagung

I express sincere appreciation to Andreas Oschlies for his guidance during this journey. Your positive attitude , encouragement, and wisdom has been invaluable for my growth as a scientist and has made it a pleasure to come in to work every day.

I would also like to thank Andreas Schmittner for his continued support and input into my research.

I am grateful to the Biogeochemical Modelling Group for their friendly faces around the office and during lunch, as well as helpful comments on my results.

I am thankful for the never-ending support from my family, who always raise my spirits through the toughest of times.

Last but not least, I express heartfelt appreciation to Nazgol Emrani, who every day inspires me to become a better person and scientist. You made this tough journey a pleasant one for me.

Erklärung

Die vorgelegte Dissertation mit dem Titel "Nitrogen Isotopes in the Global Ocean", abgesehen von der Beratung durch meine Betreuer - nach Inhalt und Form meine eigene Arbeit. Sie hat weder ganz noch in Teilen bereits an anderer Stelle im Rahmen eines Prüfungsverfahrens vorgelegen.

Ich versichere auβerdem, dass die Arbeit unter Einhaltung der Regeln guter wissenchaftlicher Praxis der Deutschen Forschungsgemeinschaft entstanden ist.

_____

Christopher J. Somes
Kiel, den März 2013